A DATA-DRIVEN APPROACH TO DEPARTURE AND ARRIVAL NOISE ABATEMENT FLIGHT PROCEDURE DEVELOPMENT

Ara Mahseredjian, Jacqueline L. Huynh, and R. John Hansman

This report is based on the Master's Thesis of Ara Mahseredjian submitted to the Department of Aeronautics and Astronautics in partial fulfillment of the requirements for the degree of Master of Science at the Massachusetts Institute of Technology.

Report No. ICAT-2022-01
May 2022

MIT International Center for Air Transportation (ICAT)
Department of Aeronautics & Astronautics
Massachusetts Institute of Technology
Cambridge, MA 02139 USA

[Page Intentionally Left Blank]

A DATA-DRIVEN APPROACH TO DEPARTURE AND ARRIVAL NOISE ABATEMENT FLIGHT PROCEDURE DEVELOPMENT

by

Ara Mahseredjian, Prof. Jacqueline L. Huynh, and Prof. R. John Hansman

ABSTRACT

An aircraft noise modeling framework is presented and used to perform a data-driven exploration of factors correlating with measured aircraft community noise and a model-based validation of the variables found to have the greatest noise impact. Aggregate departure and arrival noise and flight procedures were examined so that factors correlating with measured noise could be isolated. Operational flights at Seattle-Tacoma International Airport were examined using a framework that includes ADS-B data, a force balance kinematics model to estimate aircraft performance, and noise monitor recordings. Variation in measured noise within the network was examined as a function of observed data, including aircraft type, aircraft trajectory, airline, wind, temperature, and relative humidity; and inferred variables, including aircraft configuration, weight, and thrust. Airline-specific departure procedures were shown to impact noise measurements. Departure procedures with higher thrust and higher initial climb gradients were observed to have lower measured noise. Arrival procedures that delayed their deceleration were observed to have lower measured noise in some cases. Ambient environmental conditions, including wind, temperature, and relative humidity, were found to impact noise variation. A model-based evaluation of the factors correlating with aircraft noise followed the data-driven exploration. The delayed deceleration approach, a procedure in which aircraft maintain higher speeds, remain cleanly configured, and fly with lower thrust levels for a longer period of time, was identified as having noise reduction potential beyond 8 nm from the airport. Noise from operational Boeing 737, Airbus A320, and Embraer E190 flights at Boston Logan and Seattle Tacoma airports was modeled using the NASA Airplane Noise Prediction Program and was compared with ground noise monitor measurements. When corrected for atmospheric conditions, modeled noise results were consistent with noise monitor readings under reasonable flap deployment assumptions during various early, intermediate, and delayed deceleration approach procedures. Measured noise results indicated that compared to aircraft that decelerated early, aircraft performing delayed deceleration approaches reduced noise by an average of 3-6 dB across different aircraft types.

ACKNOWLEDGEMENTS

This work was sponsored by the Federal Aviation Administration (FAA) under ASCENT Center of Excellence Project 44. Opinions, interpretations, conclusions, and recommendations are those of the authors and are not necessarily endorsed by the United States Government. The author acknowledges the support of Chris Dorbian, Joseph DiPardo, and Bill He of the FAA Office of Environment and Energy as well as Thomas Fagerstrom and Stan Shepherd of the Port of Seattle.

Contents

List of Figures

List of Tables

Chapter 1

Introduction

1.1 The Aircraft Community Noise Problem

Noise due to aircraft departures and arrivals is a significant environmental impact of commercial aviation. Mitigating noise exposure is a key sustainability objective within the aviation industry and will grow in significance as a larger portion of the global population begins to fly. There are two primary strategies to reducing airplane noise. One is to develop quieter aircraft and engines. However, it will take decades for quieter aircraft to replace existing louder aircraft operating within the global fleet. The second strategy is to implement noise abatement procedures, which are operational procedures designed to reduce the community noise impact of departing and arriving aircraft. The advantage of noise abatement procedures is that they can be flown by aircraft already operating around the world. Therefore, noise abatement procedures will likely have a more immediate community noise reduction impact than new aircraft or engines.

1.2 Thesis Objective

This thesis took a data-driven approach to identifying the factors that correlate with aircraft noise to determine the factors that influence community noise. These findings may be useful in developing new noise abatement flight procedures. Aggregate

departure and arrival flight procedures, and their corresponding noise measurements, were examined so that factors that correlate with measured noise could be isolated. Operational flights at Seattle-Tacoma International Airport were examined using a framework that includes ADS-B data, a force balance kinematics model to estimate aircraft performance, and noise monitor recordings from the Port of Seattle Aircraft Noise Monitoring System. Variation in measured departure and arrival noise at various monitors was examined as a function of observed data, including aircraft type, aircraft trajectory, airline, wind, temperature, and relative humidity; and inferred variables, including aircraft configuration, weight, and thrust. For departures, altitude was shown to have the strongest effect on community noise exposure. Airline-specific departure procedures were shown to impact noise measurements. Departure procedures with higher thrust and higher initial climb gradients were observed to have lower measured noise. For arrivals, aircraft that delayed their deceleration to the final approach speed were observed to have lower measured noise. This finding was consistent with previous assessments of the delayed deceleration approach [17]. Aircraft weight was also found to correlate with measured noise for both departures and arrivals. Ambient environmental conditions, including wind, temperature, and relative humidity, were found to impact noise variation for both departures and arrivals.

Once the factors correlating with noise were identified, a model-based approach to validating advanced operational flight procedures designed to reduce community noise exposure was taken. Delayed-deceleration approaches were identified as having potential to reduce noise due to arriving aircraft and were modeled using a framework that used the NASA Airplane Noise Prediction Program (ANOPP), a component-based aircraft noise model. The impacts of aircraft weight and relative humidity were also modeled since they impact both departure and arrival noise. Current noise models do not include the impacts of wind on noise, so this impact was not modeled.

In summary, the thesis objective was to:

- Present a framework to model aircraft noise using open-source surveillance data, source component-based models, and aircraft performance parameters.

- Perform a data-based exploration of the various factors that correlate with departure and arrival noise.
- Perform a model-based validation of the factors identified in the data-based exploration using the aircraft noise modeling framework.

Chapter 2

Aircraft Noise Sources, Metrics, Models, and Noise Abatement Procedures

2.1 Sources of Aircraft Noise

Aircraft noise can be categorized into two primary categories, each with its own sub-categories. The two main categories are airframe noise and engine noise.

Airframe noise refers to the noise generated by an aerodynamic body moving through a fluid, causing the flow to become turbulent. Noise arises from this turbulent flow and is an energy loss. Airframe noise typically occurs in areas where there are sharp geometry changes or where non-aerodynamic bodies are exposed to the oncoming free-stream flow. Sources of airframe noise include:

- **Landing Gear**, whose cylindrical struts, linkages, exposed wires, and tires lead to periodic vortex shedding and represent a dissipation of energy;
- **Slats**, designed to increase the stall angle of attack by changing the geometry of the wing leading edge;
- **Flaps**, which increase lift coefficient at a given angle of attack by increasing

wing camber (and for most jet transport category aircraft, wing area), increasing airframe noise. Flaps may be slotted to further increase lift coefficient, which may further increase noise; and

- **Wing and Tail Trailing Edge**, where turbulent boundary layers on the top and bottom surfaces of the mix and interact with the surrounding flow [8].

Engine noise depends on the type of engine architecture. Turbofan engines are assumed in this thesis, but noise due to open-rotor turboprop engines remains an active area of research given the potential fuel-burn reduction from aircraft with higher bypass-ratio engines. Sources of turbofan engine noise include:

- **Fan Noise**, where shocks form due to supersonic tip mach numbers and turbulent flow interacts with fan blades and stator vanes;

- **Core Noise**, which refers to the noise due to the high-pressure and low-pressure compressors, combustor, and turbine, in addition to the noise from air combusting within the core; and

- **Jet Noise**, which refers to turbulent, high-speed flow exiting the compressor and mixing with the slower ambient fluid or bypass stream

While each component of engine and airframe noise contributes to the total aircraft noise, perceived noise is characterized by a dominant noise source, which refers to the loudest component. The dominant noise source may vary with flight state, meaning that in some cases, the engine noise may dominate the airframe noise, and in other cases, the airframe noise may dominate the engine noise. Engine noise typically dominates during departure, where the aircraft is in a high-thrust state and slats and flaps are only partially deployed. Airframe noise typically dominates during arrival, where the landing gear is exposed to the oncoming flow, flaps and slats are fully (or almost fully) deployed, and the aircraft is in a low-thrust state.

2.2 Aircraft Noise Metrics

Noise propagates due to a compression and rarefaction of ambient air molecules [25]. This means that noise can be modeled by a sinusoidal function with characteristic amplitude and a frequency. Amplitude corresponds to loudness, and frequency to pitch. Amplitude is measured in decibels and is defined as a ratio of two sound pressures, and is expressed as the Sound Pressure Level (SPL) in Equation 2.1.

$$\text{Sound Pressure Level [dB]} = 20\log(\mathrm{P}_1/\mathrm{P}_2) \tag{2.1}$$

Various noise metrics are defined as functions of sound pressure level. The two most relevant to this thesis are given below and shown in Figure 2-1.

- $\mathbf{L}_{A,MAX}$: $\mathrm{L}_{A,MAX}$ is the maximum A-weighted sound pressure level measured during an overflight event. A-weighting reduces the decibel values of low-frequency sounds and is applied because the human ear is more sensitive to high-frequency sounds than to low frequency sounds [20].
- **Sound Exposure Level (SEL)**: SEL is a time-integration of the A-weighted sound pressure level over all SPL values within 10 dB of $\mathrm{L}_{A,MAX}$.

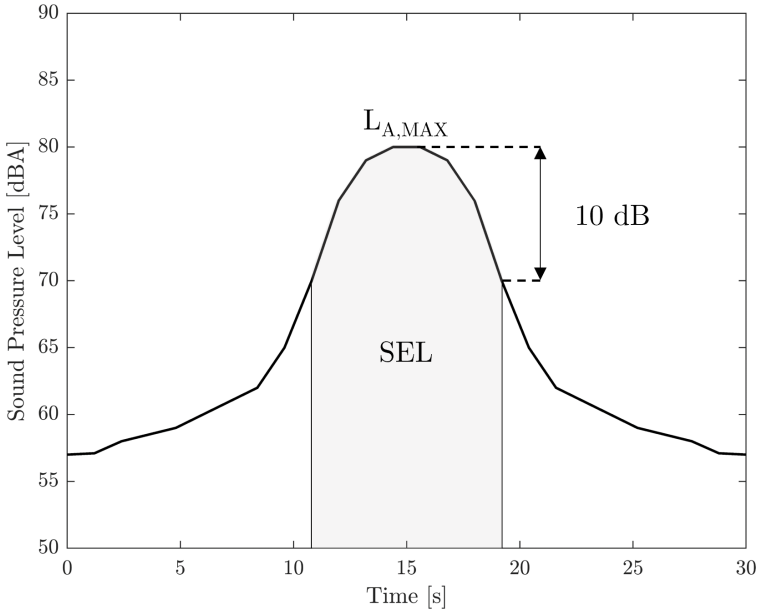

Figure 2-1: Noise Metric Definitions

2.3 Aircraft Noise Modeling Methodologies

Two common aircraft noise models are Noise-Power Distance (NPD) Models and Component-Based Models. Noise-Power Distance methods model aircraft noise as interpolations of airframe and engine noise data produced by manufacturers or obtained during certification flight tests. NPD models assume that airframe and engine noise correlate with thrust. NPD models are used in the Federal Aviation Administration (FAA) Aviation Environmental Design Tool (AEDT) [7] and offer users the ability obtain quick estimates of aircraft noise. More detailed source component-based noise models, such as NASA Airplane Noise Prediction Program (ANOPP) [26], use a combination of physics-based and semi-empirical modules that simulate aircraft noise based on individual aircraft components. Individual sources of aircraft noise can be modeled and isolated, and comparisons between various aircraft noise sources can be made. Source component-based noise models are computationally expensive but offer much more detailed estimates of aircraft noise than NPD-based methods.

2.4 Noise Abatement Procedures

Noise abatement procedures are an operational means of reducing community noise exposure due to departing and arriving aircraft. Noise abatement departure procedures (NADPs) are designed to reduce noise due to aircraft departures. NADP1 and NADP2 were set out by the International Civil Aviation Organization (ICAO) and were designed to reduce departure noise at varying distances from the airport. NADP1 is intended to reduce departure noise close to the airport, while NADP2 is intended to reduce departure noise far from the airport. Aircraft flying NADP1 depart at a prescribed takeoff thrust, reduce their thrust at the cutback altitude, retract flaps, and accelerate to 250 knots. Upon reaching 250 knots, the aircraft climb at constant airspeed to 10,000 ft. Aircraft flying NADP2 depart at a prescribed takeoff thrust, reduce thrust at the cutback altitude, and climb at V2 + 20 KIAS with flaps deployed until reaching an altitude of 3000 ft. V2 is the single-engine out climb

speed calculated prior to departure. At 3000 ft, the aircraft retract flaps, accelerate to 250 knots, and then climb at constant airspeed until reaching 10000 ft. NADP1 and NADP2 are shown in Figure 2-2.

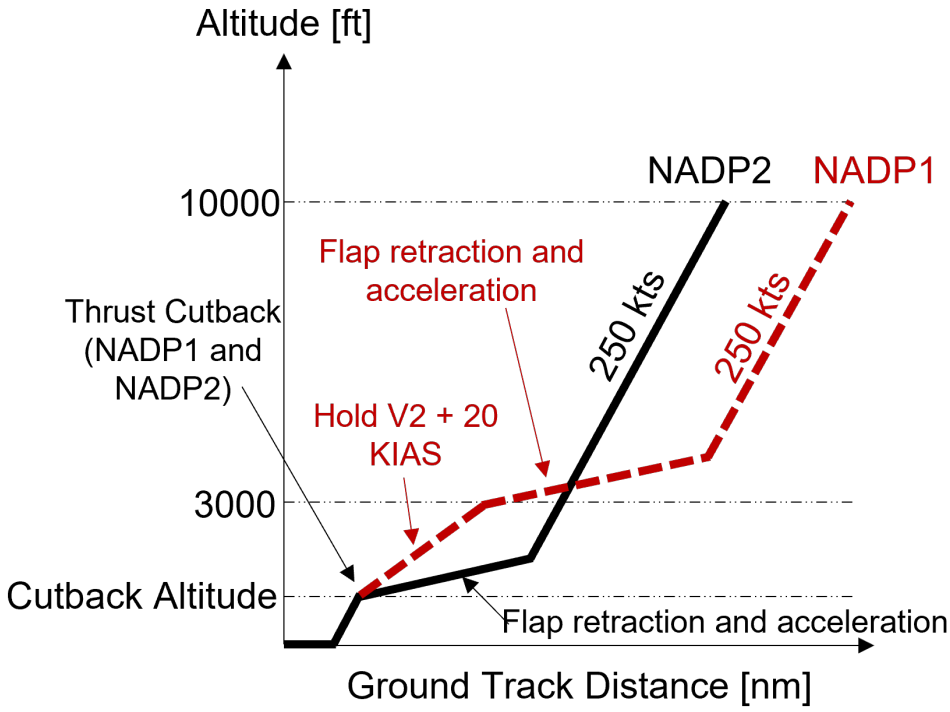

Figure 2-2: Noise Abatement Departure Procedure (NADP) 1 and 2 [22]

The delayed deceleration approach (DDA) has been proposed to reduce community noise due to aircraft arrivals far ($>$ 8 nm) from the airport. Delaying deceleration delays slat and flap deployment to the final approach stabilization point, potentially reducing airframe noise during the portion of the flight for which the aircraft remains cleanly configured. There is also potential for aircraft performing DDAs to produce less engine noise during the portions of the flight where flaps and slats remain retracted. This is because aircraft flying at higher airspeeds in a clean configuration produce less drag, lowering thrust requirements on approach. The delayed deceleration approach concept is illustrated in Figure 2-3.

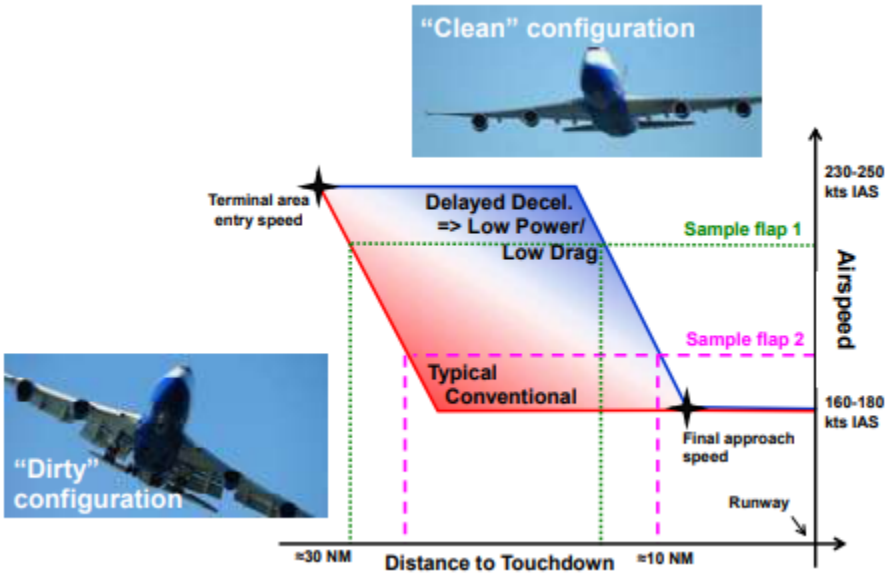

Figure 2-3: Delayed Deceleration Approach. Figure from [17]

Chapter 3

Methodology

This chapter presents the framework used to model aircraft performance and noise, and the sources used to acquire the data used by the framework. Modeling aircraft performance was required to obtain estimates for aircraft weight and thrust given assumptions about aircraft landing gear, slat, and flap configuration. Weight and thrust were used in the data-driven exploration of factors contributing to aircraft noise as described in Chapter 4, and were also required for the model-based validation of noise described in Chapter 5.

3.1 Noise Modeling Framework

The noise modeling framework used aircraft surveillance (ASDE-X or ADS-B) data and weather data to model aircraft performance. Performance estimates from the framework were used to model noise in the NASA Airplane Noise Prediction Program [26]. Aircraft groundspeed provided by aircraft surveillance data was converted to true airspeed using wind data from the NOAA Rapid Refresh numerical weather model [3]. True airspeed was converted to indicated airspeed using atmospheric pressure and density. Slat, flap, and landing gear configuration assumptions were made based on indicated airspeed for both departures and arrivals. Configuration assumptions are detailed in Chapter 4. True airspeed was used in combination with lift and drag coefficients from Eurocontrol Base of Aircraft Data (BADA) [16] to estimate weight

and thrust. Thrust estimates were fed into TASOPT (Transport Aircraft System OPTimization) [4] to obtain internal engine states. Internal engine states and aircraft geometry were fed into NASA ANOPP, which provided noise estimates at the monitor locations of interest. Modeled noise was compared to SEL measurements taken by noise monitors. A summary of the framework defined in this section follows in Figure 3-1.

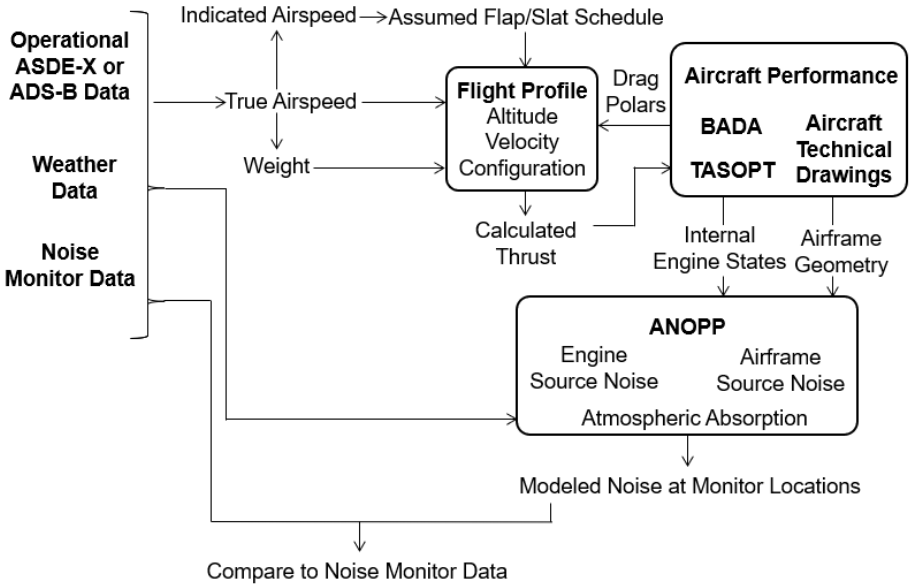

Figure 3-1: Aircraft Performance and Noise Modeling Framework used for the Data-Driven Exploration and Model-Based Validation of Factors Correlating with Aircraft Noise

3.2 Data Sources

3.2.1 Noise Monitor Data

Noise monitor data from the Port of Seattle Noise Monitoring System was used to obtain flyover noise measured in SEL for aircraft departing and arriving from Seattle. The Port of Seattle Noise Monitoring System is shown in Figure 3-2.

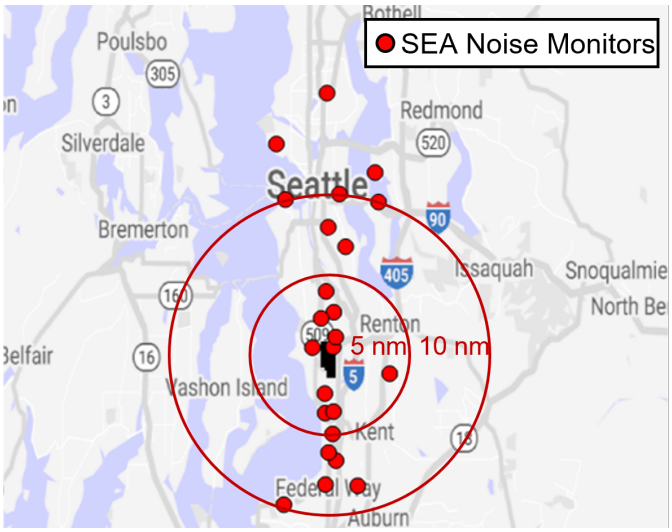

Figure 3-2: Port of Seattle Noise Monitoring System

Noise data measured in SEL from monitors placed along the flight path to the RNAV 22L approach at Boston Logan International Airport was used to examine arrival noise at Boston. The monitors examined at Boston Logan International Airport are shown in Figure 3-3.

Figure 3-3: Boston Logan International Airport Noise Monitor Network. Monitor examined are shown in red

3.2.2 Aircraft Data

Aircraft Trajectory and Operator Data

ASDE-X Data was used to obtain aircraft data at Boston including aircraft type, aircraft operator, altitude, lateral position, and groundspeed. ADS-B Data from the OpenSky Network [19] was used to obtain aircraft the same data at Seattle.

Aircraft Performance Data

The Eurocontrol Base of Aircraft Data (BADA), a database of performance parameters from commercial aircraft manufacturers [16], was used to obtain drag data for the aircraft examined in Chapters 4 and 5. Drag data was used to calculate thrust for each aircraft type.

3.2.3 Weather Data

Weather data including wind, temperature, and relative humidity was obtained from NOAA Rapid Refresh (RAP) [3]. NOAA Rapid Refresh is a grid-based numerical model updated hourly, with grid points placed laterally every 13 nautical miles across the Continental United States. Data was reported as a function of altitude, lateral position, and time of flight. The grid point closest to the noise monitor being examined was used to obtain weather data. For the data-driven exploration of factors correlating with noise, all weather data except relative humidity was averaged between the surface and the aircraft altitude. Relative humidity was averaged between the surface and 1000 ft above field elevation. For the model-based validation, weather data was interpolated in altitude. This allowed weather data at each lateral position, altitude, and time to be estimated. An example of wind, temperature and relative humidity at various noise monitor locations at Boston Runway 22L for a sample flight time is shown in Fig. 3-4.

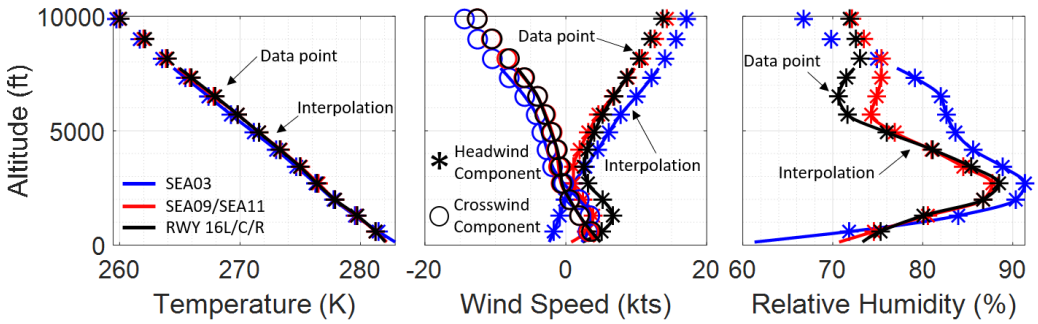

Figure 3-4: Example wind speed, temperature, and relative humidity as functions of altitude

3.3 Aircraft Performance Modeling

3.3.1 Weight Prediction

Departures

Departure weight was modeled as a function of true airspeed and altitude 10 nautical miles from the runway, which has been shown to correlate with FDR data [18]. This method was chosen because it allowed departure weight to be modeled using only surveillance and weather data.

Arrivals

Aircraft weight was estimated from the stable final approach speed from the wind-corrected surveillance data using the method from [18]. In this method, the true airspeed on final approach was assumed to be the reference landing speed $1.23V_{stall}$ in the landing configuration plus a safety factor b, as defined in 14 CFR 25.125. Weight was inferred using Equation 3.1, where, S is the wing surface area, $C_{L,max}$ is the maximum lift coefficient, and ρ is the air density. Thrust was modeled based on this weight estimate and drag from BADA that corresponds to assumed configuration settings.

$$V_{approach} = 1.23V_{stall} + b[kts] = 1.23\sqrt{\frac{2W}{\rho S C_{L,max}}} + b[kts] \tag{3.1}$$

$C_{L,max}$ was obtained from BADA and the air density ρ from NOAA Rapid Refresh. Figure 3-5 depicts the predicted weights of of 260 Boeing 737-800 and 330 Airbus A320 flights at BOS from November 2015-January 2016. A safety factor b of 7 knots was used to be consistent with the methodology defined in [18]. Flaps 30 was assumed for the 737-800, and Flaps Full was assumed for the A320. The predicted weight for most flights was within the maximum landing weight and operating empty weight of this aircraft, indicating that the assumption was reasonable.

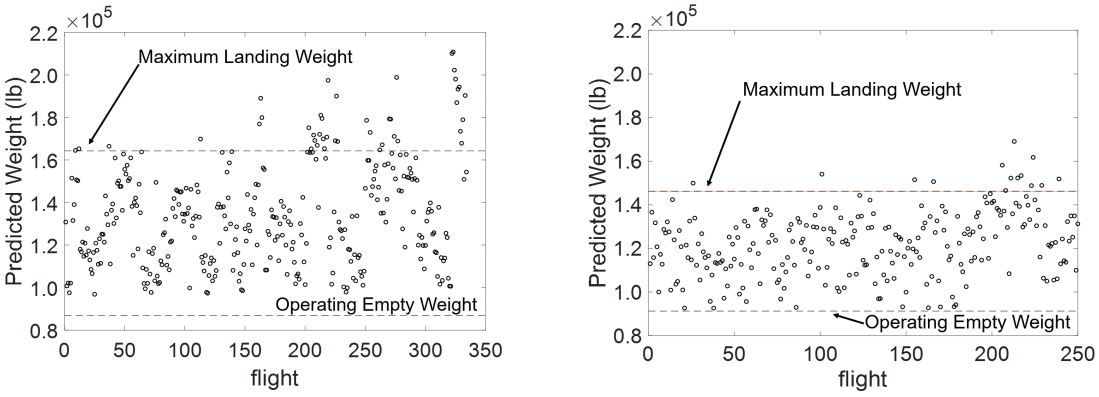

(a) A320 (b) B737-800

Figure 3-5: Predicted weight of Airbus A320s (Flaps Full), Boeing 737-800s (Flaps 30) from final approach velocity at BOS, 2015-2016.

3.3.2 Flight Profile Modeling

Flight profiles were generated for each flight being examined. A flight profile included aircraft altitude, velocity, configuration, thrust, and lateral position as functions of time. Altitude and velocity were provided in surveillance data. Landing gear, slat, and flap configuration for departures and arrivals were inferred for each aircraft. The specific configuration assumptions for each aircraft are given in Chapters 4 for both departures and arrivals. Thrust was modeled using a force-balance kinematics model that calculated thrust based on flight path angle and velocity obtained from surveillance (ASDE-X/ADS-B) data, and using the drag coefficients from BADA. The flight profile generation model is summarized in Figure 3-6.

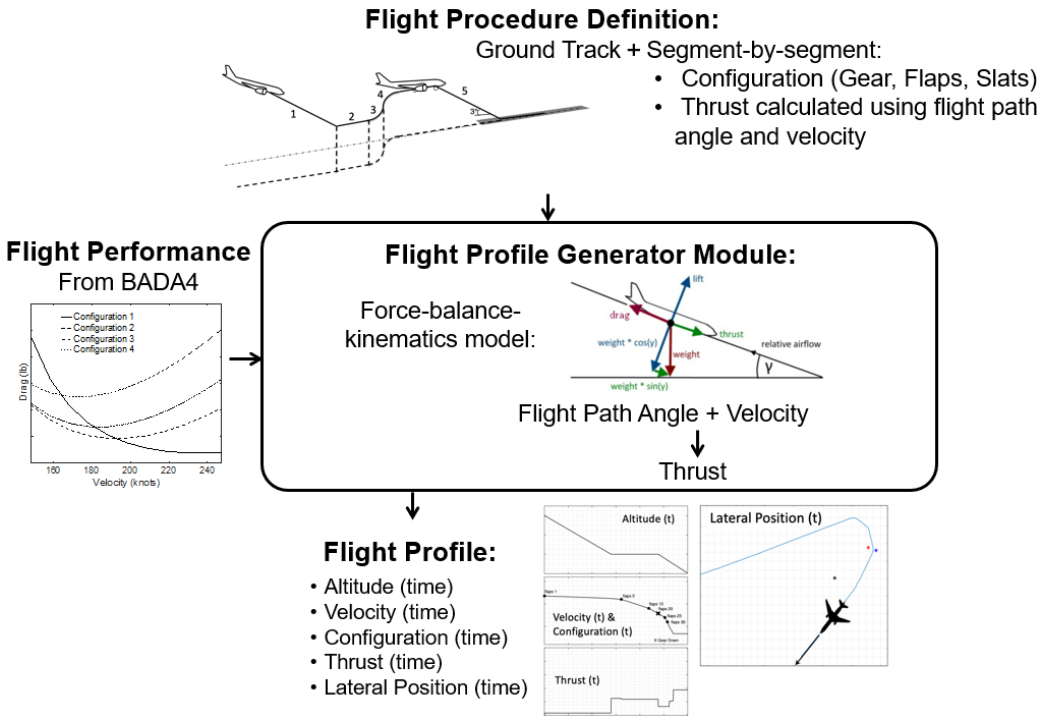

Figure 3-6: Flight Profile Generation Model. Figure adapted from [22]

3.3.3 Internal Engine State Modeling

TASOPT (Transport Aircraft System OPTimization 2.16) [4] was used to estimate internal engine states for each aircraft type using thrust estimates. The internal engine states were required by the engine noise components in NASA ANOPP and were obtained from a work-balance based, engine component-matching formulation [14]. TASOPT provides a mapping of the internal engine performance states as a function of off-design thrusts and velocities given the engine design conditions, such as bypass ratio, turbine entry temperature and overall pressure ratio. The velocity and modeled thrust were used to determine the engine states at a given segment in the flight procedure from the TASOPT engine maps. These engine states, along with the airframe geometry from publicly available geometry data [13], were inputs to ANOPP and determined source noise for each flight segment. Finally, the propagation of the source noise to the desired location on the ground where noise received was assessed based on a defined atmosphere.

3.3.4 Noise Modeling

NASA ANOPP was used to model airframe noise, engine noise, and atmospheric attenuation of noise propagating from the aircraft. NASA ANOPP employs various modules to model the noise from each component. For this thesis, airframe noise due to the extension of slats, flaps, and landing gear was modeled by the Boeing Airframe Noise Model [9] [10], and noise due to the wing and tail trailing edges was modeled by the Fink Airframe Noise Model [8]. Engine noise due to the turbulent jet exhaust was modeled using the Stone Jet Noise Model [21], noise due to the engine core was modeled using the ANOPP Combusion Noise Model [26], and engine fan noise was modeled using the Heidmann Large Fan Method [12]. Atmospheric attenuation was modeled using the ANSI S1.26-2014 method [2].

Chapter 4

Data-Driven Analysis of Community Departure and Arrival Noise Exposure Variation Using Seattle Noise Monitors and operational ADS-B data

4.1 Motivation

A data-driven exploration of factors that contribute to the variation in noise monitor measurements seen at Seattle-Tacoma International Airport (SEA) is presented in this chapter. The causes of variation in airport noise monitor network measurements of departing and arriving aircraft remain a source of uncertainty which must be understood in order to improve existing noise models [15] and develop new noise abatement procedures. Variation in departure noise was of specific interest because it was found to be up to 15 dB when aircraft type and departure procedure were held constant. Understanding the potential contributors to this variation was therefore the aim of this chapter.

The variables which potentially contributed to this variation included those that arose as a result of flight procedures, including operator-specific practices relating to thrust, airspeed, and configuration management; those that arose as a result of the environment, including ambient wind, relative humidity, and temperature; and those that were specific to individual flights, including weight. The Port of Seattle Noise Monitoring System was chosen for this study because of the extensive placement of monitors ranging from those at the airport boundary to those further from the airport than monitors at other airports. Noise monitor recording data for Airbus A320 and Boeing 737NG aircraft taken in March and August of 2019 was used for this study. March and August were chosen to increase the range of measured ambient temperature and relative humidity. Operational ADS-B data from SEA for the same time periods was taken from the OpenSky Network [19] and was matched with flyovers triggering noise monitor recordings. Weather data, including wind, relative humidity, and temperature, was taken from the NOAA Rapid Refresh numerical weather model [3] and was treated both as a raw variable potentially impacting monitor recordings and as a variable in modeling flight performance. The purpose of this study was to measure how noise measurements may correlate with raw data, but variables not included in surveillance data, including weight, thrust, and configuration, were modeled by necessity.

The impact of both raw and modeled variables on sound exposure level (SEL) recordings at various monitors throughout the SEA noise monitoring network was demonstrated. Trends that consistently appeared at monitors at distances varying between 3-12 nautical miles from SEA were illustrated using data from the network. Data suggesting that specific airline operational techniques impacted community noise exposure was shown, and areas for future work and model refinement were identified. While data that may explain some of the variation in the recordings was presented, they may not be the only contributors. Future model refinement or analysis using flight data recorder (FDR) data for multiple flights may help address this ambiguity. The causes of variation in departure and arrival noise may be used to improve noise models and contribute to the development of future noise abatement procedures.

4.2 Departure Noise Data Exploration using Operational Flights and Ground Noise Measurements

4.2.1 Identification of Variables with Potential Departure Noise Variation Impact

The parameters investigated were organized into three categories: observed aircraft data, environmental data, and aircraft performance parameters. Observed aircraft data included the data that characterized the aircraft type, position, and velocity. Environmental data characterized the ambient wind, temperature, and relative humidity. Performance parameters included takeoff weight; landing gear, slat and flap configuration; flight path angle; and takeoff thrust. Noise data, measured in Sound Exposure Level (SEL) at discrete monitor locations and correlated with specific flights, was provided by the Port of Seattle. The noise, aircraft, and environmental data were observed, while performance parameters were modeled using observed data. The parameters investigated in this study are listed in Table 4.1.

Table 4.1: Departure Noise Parameters Investigated

Noise Data	**Aircraft Data**	**Environmental Data**	**Aircraft Performance**
SEL at Monitor Locations	Aircraft Type	Relative Humidity	Takeoff Weight
	Aircraft Operator	Northward Wind	Aircraft Configuration
	Altitude	Eastward Wind	Takeoff Thrust
	Lateral Position	Temperature	
	Groundspeed		
	Flight Path Angle		

4.2.2 Data Sources and Seattle Noise Monitoring Network

Noise Data

Noise data from Seattle Tacoma International Airport, shown in Figure 4-1, was used for departures. There are three runways. Aircraft departing to the north and arriving from the south used runways 34L, 34C, and 34R. Aircraft departing to the south and arriving from the north used runways 16L, 16C, and 16R.

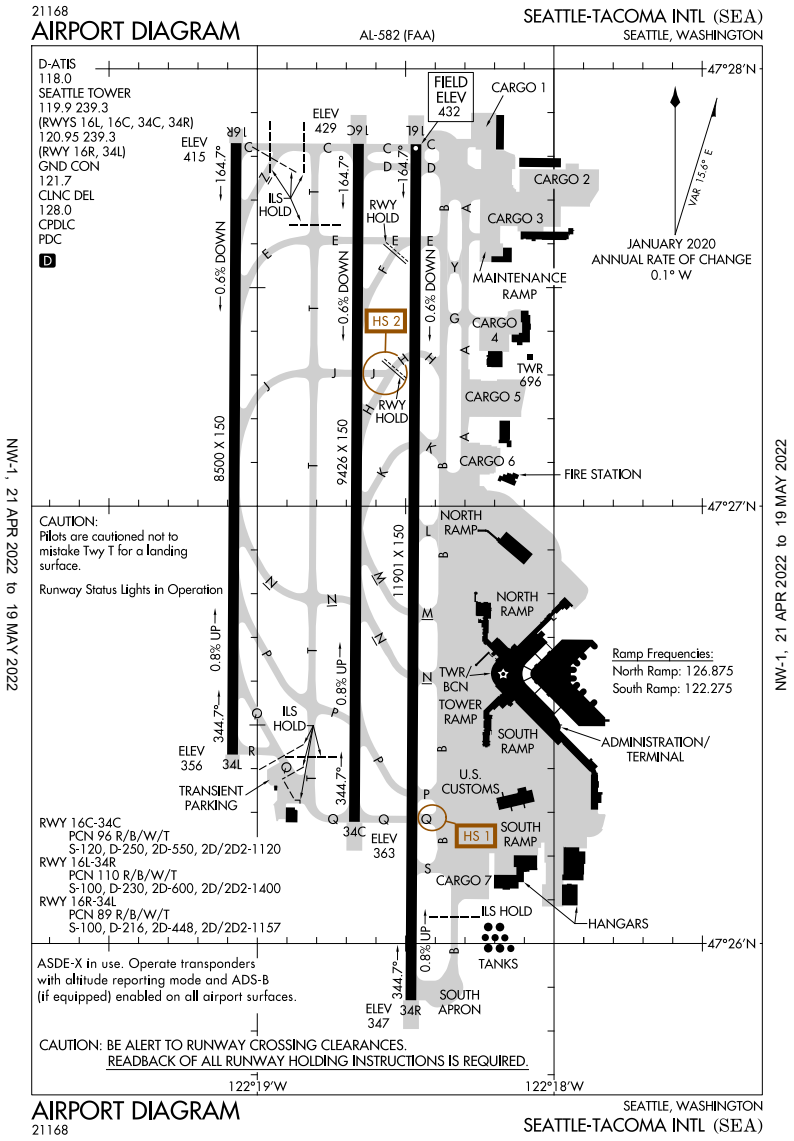

Figure 4-1: Seattle-Tacoma International Airport Diagram [1]

Noise data from the Port of Seattle Noise Monitoring System was used to obtain flyover noise measured in SEL. Each flyover was correlated with a specific flight. The noise monitoring system is shown in Figure 4-2. The south monitors measured noise from aircraft departing to the south. The north monitors measured noise from aircraft departing to the north. The six monitors chosen for this study were highlighted green. These monitors recorded sufficient data for both Airbus A320 and Boeing 737NGs.

Close, medium-distance, and far monitors were examined because the variation at each monitor may depend on its proximity to the airport.

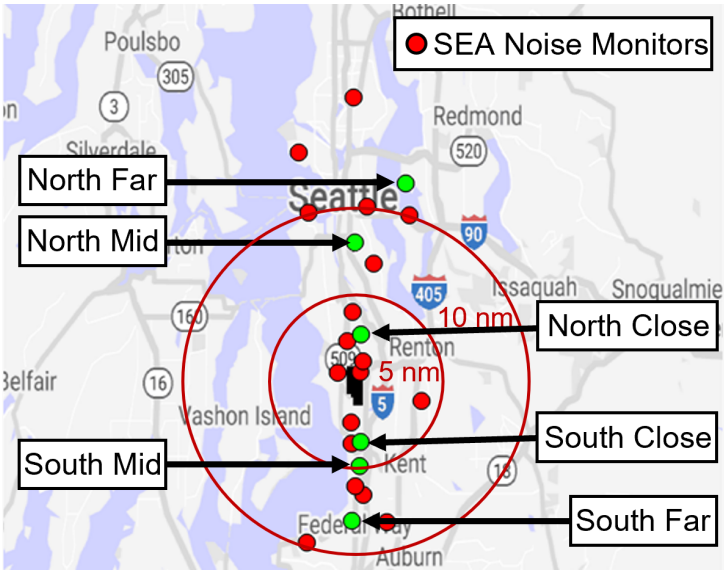

Figure 4-2: Port of Seattle noise monitor network. Monitors analyzed for departures shown in green

The lateral tracks of departures to the south and north are shown in Figure 4-3 (a) and (b), respectively. Aircraft departed from all three runways.

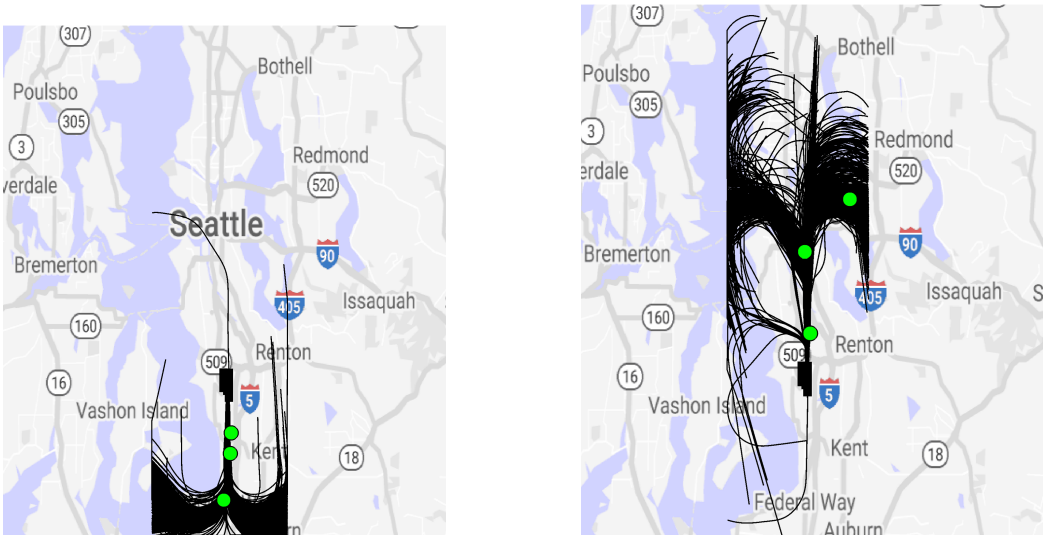

(a) South departures

(b) North departures

Figure 4-3: Lateral tracks of Seattle departures

Flights were filtered so that only aircraft that flew within a 0.25 nautical mile lateral

track distance of the monitor being analyzed were considered. This filtering was done as a means of holding flyover distance approximately constant.

Aircraft Data

ADS-B data from the OpenSky Network [19] was correlated with the flights that generated noise monitor recordings and was used to obtain data including aircraft type, aircraft operator, altitude, lateral position, and groundspeed. Flight path angle was estimated using the change in altitude and lateral position at two successive ADS-B data points. Flight path angle was sensitive to noise in ADS-B data. Aircraft operator was used to determine whether any airline-specific operational practices impacted measured noise.

Environmental Data

Environmental data was obtained from the NOAA Rapid Refresh numerical model [3]. Weather data taken at the time closest to the aircraft flyover was used. Temperature, northward wind, and eastward wind were averaged between the surface and the aircraft altitude at the point of closest approach to the monitor. Relative humidity was averaged between the surface and 1000 ft above ground level.

4.2.3 Departure Flight Performance Modeling Assumptions

Operational ADS-B and weather data were used to model flight performance as described in Chapter 3. The thrust modeling required assumptions about aircraft landing gear, slat, and flap configuration to be established. Landing gear retraction was assumed to occur 0.25 nautical miles after liftoff. Flaps and slats were assumed to be extended from the takeoff roll up until 10 knots below the maximum flap extension speed. Airbus A320s were assumed to take off with a slats and flaps extended to

CONF2, and Boeing 737NGs were assumed to take off with slats and flaps extended to Flaps 5. Flap and slat retraction thus occurred at 190 KIAS and 200 KIAS for the A320 and 737NG, respectively. Thrust was calculated based on configuration assumptions.

4.3 Observed Variation in Aircraft Departure Noise Measurements using Seattle ADS-B and Noise Monitor Measurement Data

4.3.1 Boeing 737NG Departure Noise Trends at South Monitors

The noise impact of each variable for the B737NG at the south close, mid, and far monitors is given in Figures 4-4, 4-5, and 4-6, respectively. Altitude, thrust per engine, true airspeed, and flight path angle were taken at the point of closest approach to the monitor. Environmental data was averaged as described in Section 4.2.2. Plots were color-coded by airline so that the noise impact of airline-specific operating procedures could be seen. The correlation coefficient between SEL and each variable, as well as the slope of the linear regression between SEL and each variable were included.

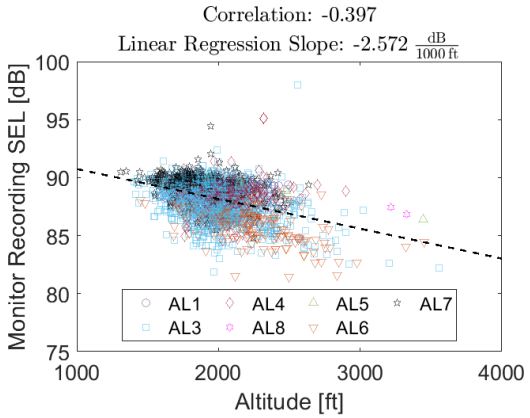

(a) Altitude impact, south close monitor

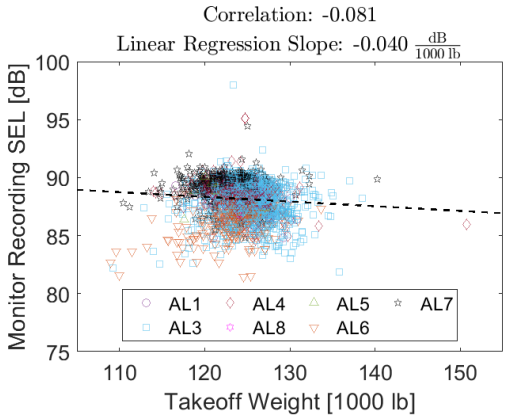

(b) Weight impact, south close monitor

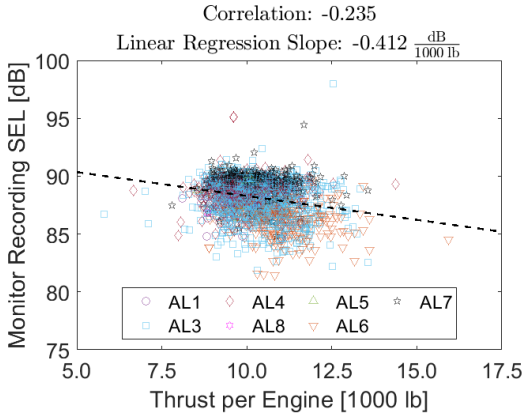

(c) Thrust impact, south close monitor

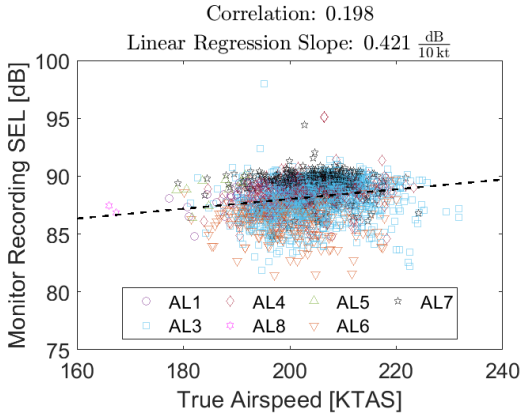

(d) True airspeed impact, south close monitor

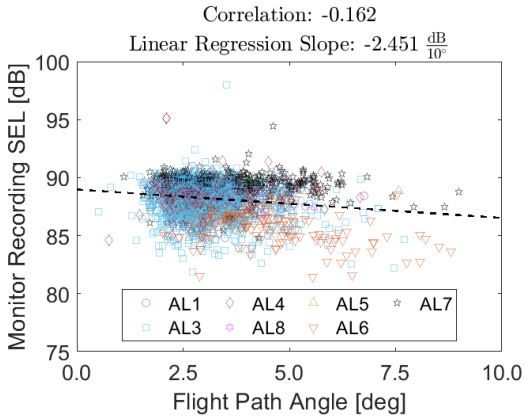

(e) Flight path angle impact, south close monitor

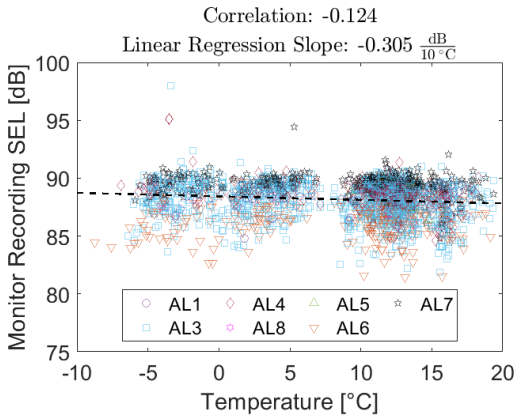

(f) Temperature impact, south close monitor

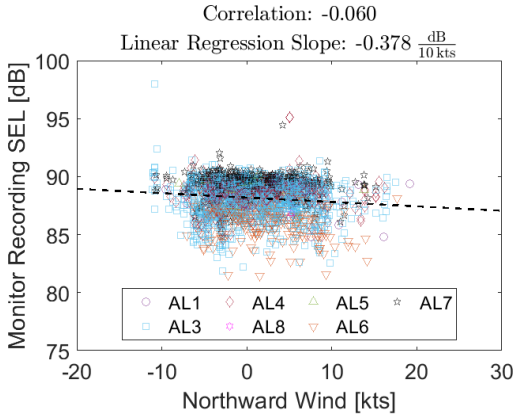

(g) Northward wind (headwind) impact, south close monitor. Northward wind positive to the north

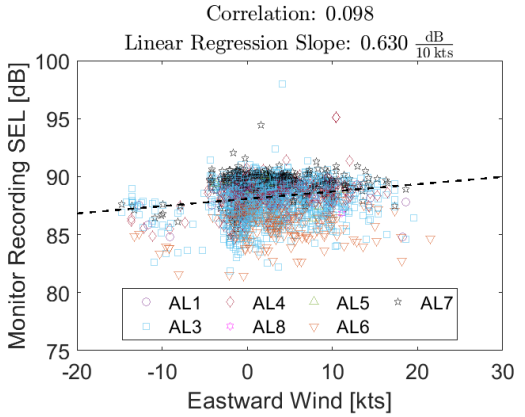

(h) Eastward wind (crosswind) impact, south close monitor. Eastward wind positive to the east

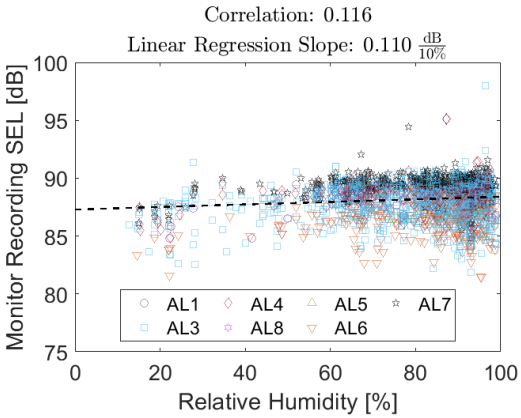

(i) Relative humidity wind impact, south close monitor

Figure 4-4: Trends for departing Boeing 737NGs at the south close monitor

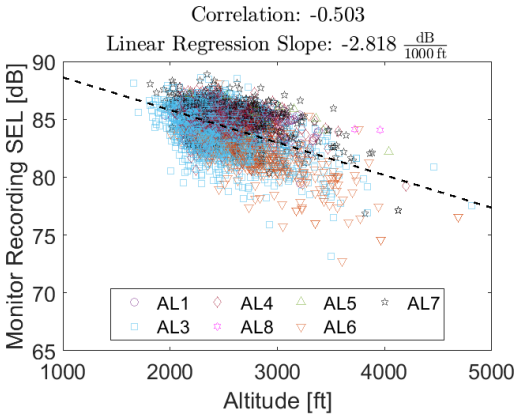

(a) Altitude impact, south mid monitor

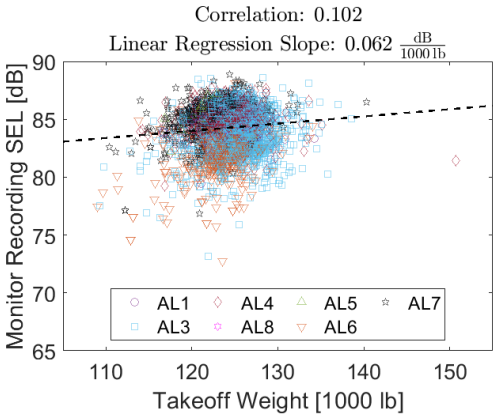

(b) Weight impact, south mid monitor

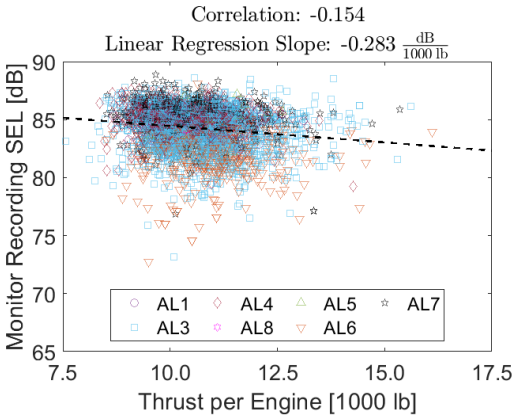

(c) Thrust impact, south mid monitor

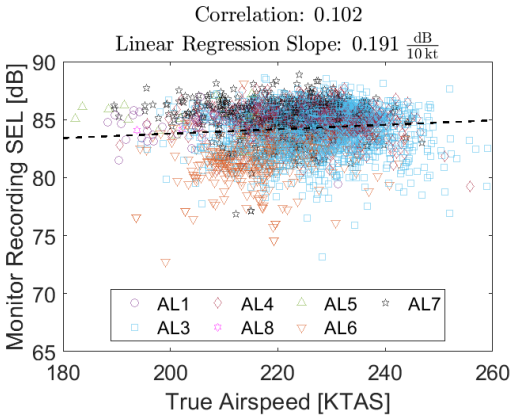

(d) True airspeed impact, south mid monitor

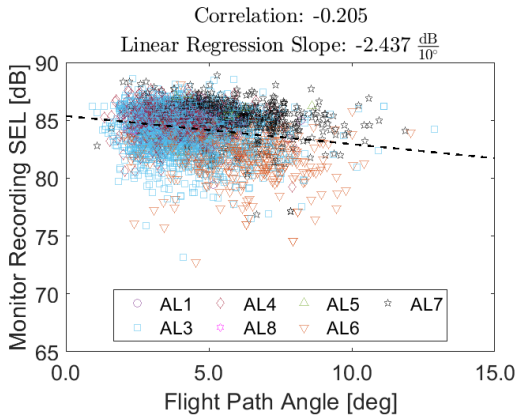

(e) Flight path angle impact, south mid monitor

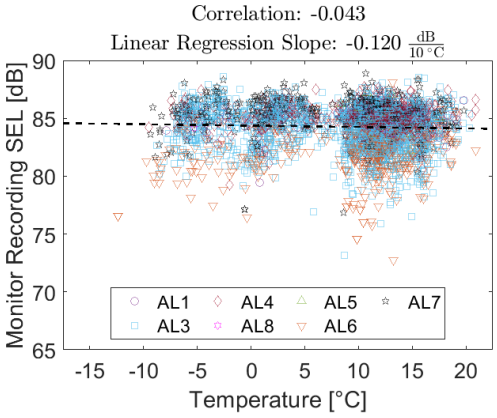

(f) Temperature impact, south mid monitor

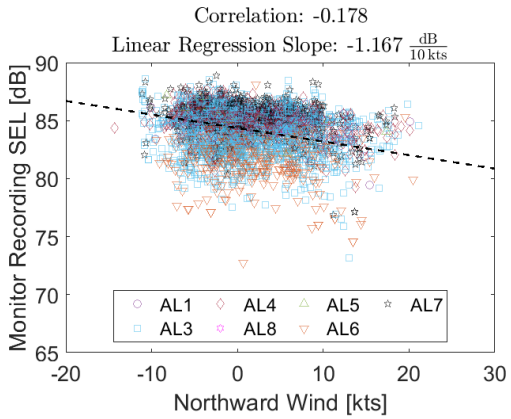

(g) Northward wind (headwind) impact, south mid monitor. Northward wind positive to the north

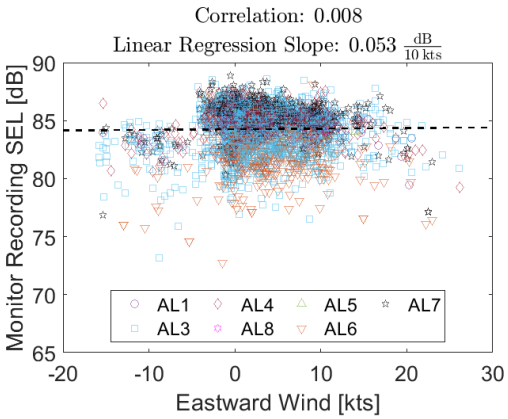

(h) Eastward wind (crosswind) impact, south mid monitor. Eastward wind positive to the east

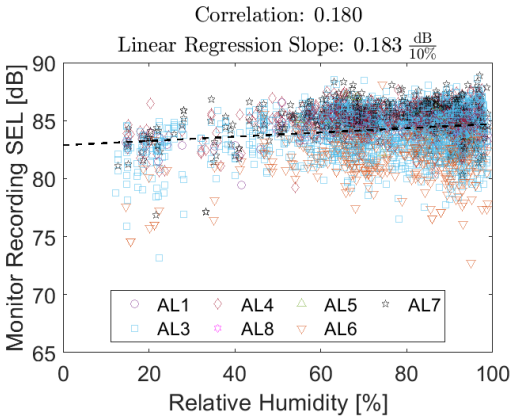

(i) Relative humidity wind impact, south mid monitor

Figure 4-5: Trends for departing Boeing 737NGs at the south mid monitor

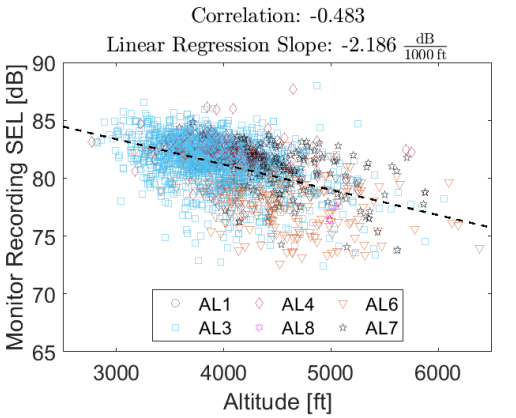

(a) Altitude impact, south far monitor

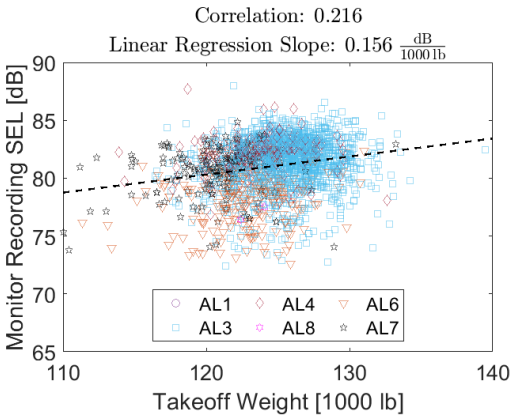

(b) Weight impact, south far monitor

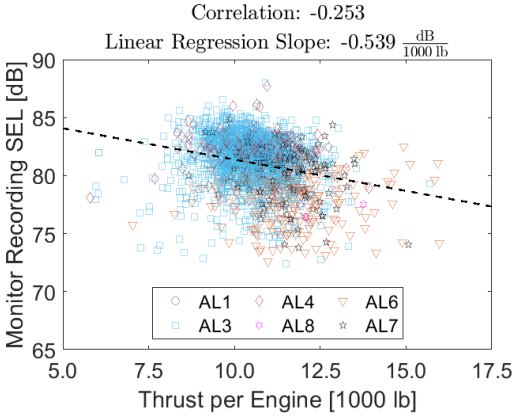

(c) Thrust impact, south far monitor

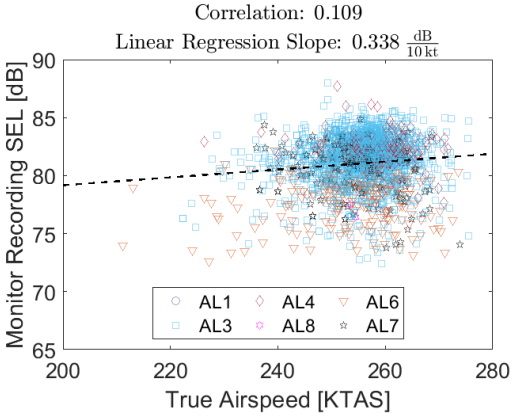

(d) True airspeed impact, south far monitor

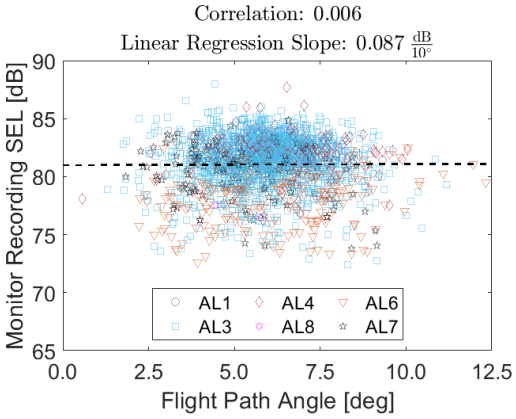

(e) Flight path angle impact, south far monitor

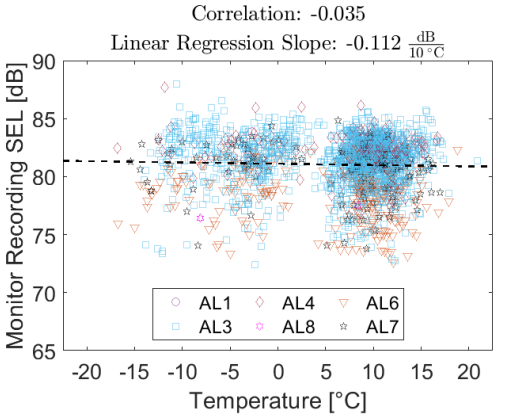

(f) Temperature impact, south far monitor

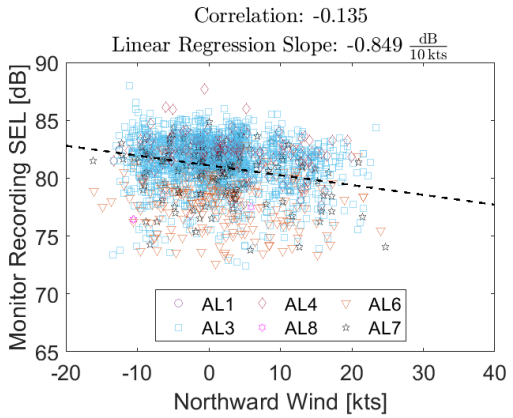

(g) Northward wind (headwind) impact, south far monitor. Northward wind positive to the north

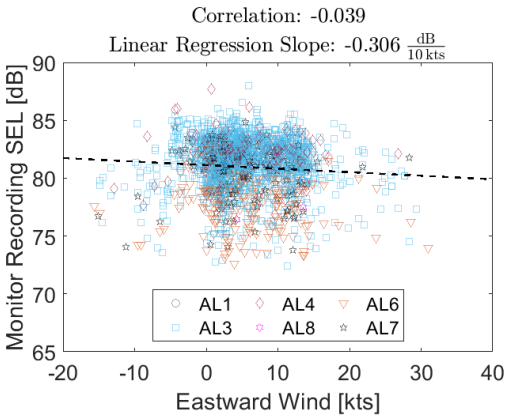

(h) Eastward wind (crosswind) impact, south far monitor. Eastward wind positive to the east

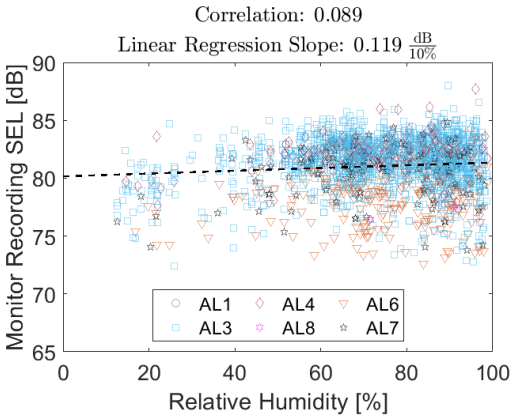

(i) Relative humidity wind impact, south far monitor

Figure 4-6: Trends for departing Boeing 737NGs at the south far monitor

Noise measurements for the B737NG at the north monitors were consistent with the results at the south monitors, with the exception that noise measurements increase with the northward wind for northbound departures. This was likely because tailwinds decreased climb performance. Results for northbound B737NG departures are given in Appendix A.

4.3.2 Analysis of Boeing 737NG Departure Noise Trends at South Monitors

The variables correlating with departure noise at the three south monitor locations were examined in order of strongest impact to weakest impact. Impact was determined by averaging the absolute value of the correlation coefficients at the close, mid, and far monitors. The variable with the highest impact had the highest average correlation coefficient, and the variable with the lowest impact had the lowest average correlation coefficient.

Effect 1: Altitude

Altitude was observed to have the strongest impact on measured noise at all three monitor locations, with lower noise at higher altitude. Noise decreased by approximately 2-3 dB for each 1000 ft altitude gained. There was a spread in altitude of approximately 2000 ft at each monitor. This meant that approximately 4-6 dB variation in measured noise may have been attributable to variation in altitude, although there may have been confounding factors. This trend is shown in Figure 4-7 and is is consistent with spherical spreading and attenuation losses.

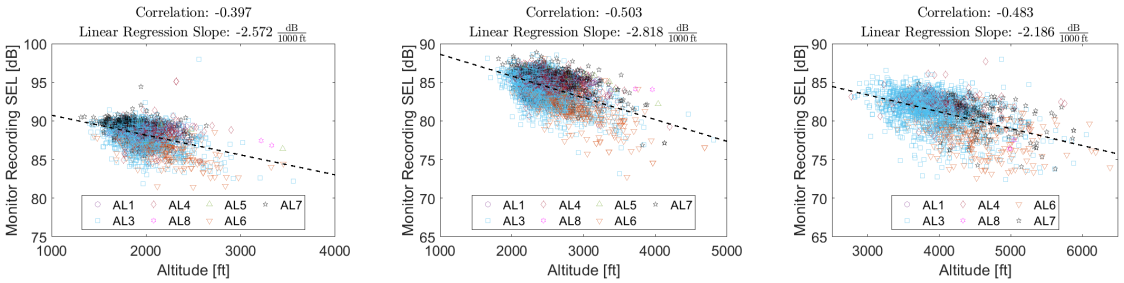

(a) South close monitor (b) South mid monitor (c) South far monitor

Figure 4-7: Altitude Impact on Noise from Departing B737NG Aircraft

Effect 2: Thrust

Next, the impact of thrust on measured noise at all three monitor locations is shown in Figure 4-8. Measured noise decreased by approximately 0.3-0.5 dB for each 1000 lb of increased thrust per engine. There was a spread of approximately 5000 lb thrust

per engine over each monitor. This meant that approximately 1.5-2.5 dB variation in measured noise may have been attributable to variation in thrust, although there may have been confounding factors. This trend was observed because aircraft that flew with higher thrust levels achieved higher average altitude.

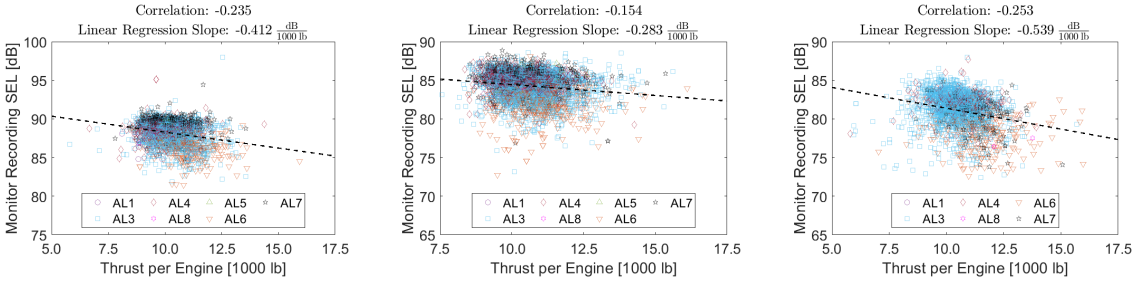

(a) South close monitor (b) South mid monitor (c) South far monitor

Figure 4-8: Thrust Impact on Noise from Departing B737NG Aircraft

Effect 3: True Airspeed

The impact of true airspeed on measured noise at all three monitor locations is shown in Figure 4-9. Measured noise increased by approximately 0.2-0.4 dB for each additional 10 knots of true airspeed. There was a spread in true airspeed of approximately 40 knots at monitor. This meant that approximately 0.8-1.6 dB variation in measured noise may have been attributable to variation in true airspeed, although there may have been confounding factors. This trend was expected, since aircraft climbing at steeper climb gradients typically fly at lower true airspeeds. Airframe noise is also known to increase with true airspeed, so flying at lower true airspeed may have had an impact on measured noise in cases where airframe noise dominated engine noise on departure.

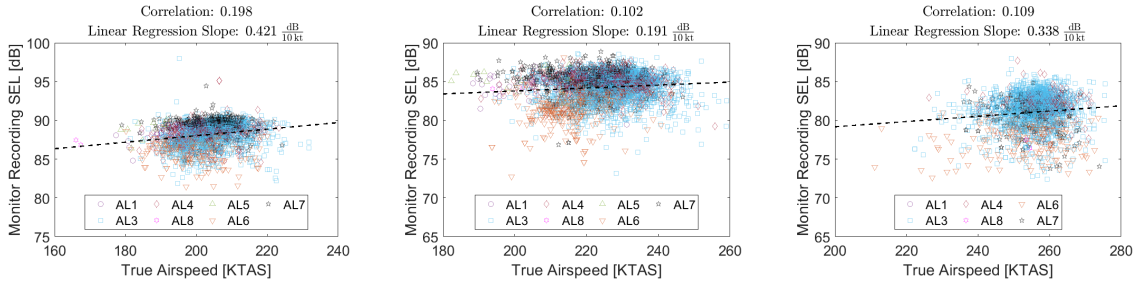

(a) South close monitor (b) South mid monitor (c) South far monitor

Figure 4-9: True Airspeed Impact on Noise from Departing B737NG Aircraft

Effect 4: Takeoff Weight

The impact of takeoff weight on measured noise at all three monitor locations is shown in Figure 4-10. Measured noise was observed to decrease with higher departure weight at the close monitor. The trend was reversed at the mid and far monitors: measured noise was observed to increase with higher departure weight. Heavier aircraft typically climb more slowly and with more thrust than light aircraft, so the trend at the mid and far monitors was expected. At these monitors, measured noise increased by approximately 0.06-0.15 dB for each additional 1000 lb of takeoff weight. Takeoff weight varied by approximately 20,000 lb. This meant that approximately 1.2-3.0 dB variation in measured noise may have been attributable to variation in takeoff weight, although there may have been confounding factors. The trend at the close monitor may be explained airline-specific operational practices, such as policies regarding de-rated thrust, in the early phases of the climb.

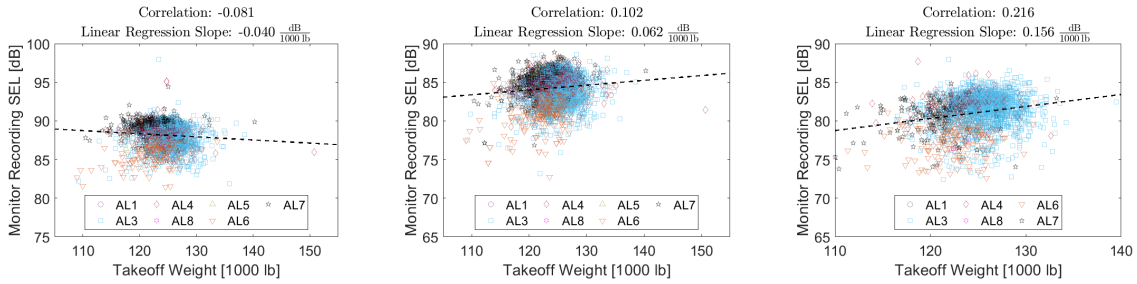

(a) South close monitor (b) South mid monitor (c) South far monitor

Figure 4-10: Weight Impact on Noise from Departing B737NG Aircraft

Effect 5: Flight Path Angle

The impact of flight path angle on measured noise at all three monitor locations is shown in Figure 4-11. Measured noise decreased by approximately 0.09-2.5 dB for each additional 10 degrees of flight path angle. Flight path angle was observed to vary by approximately 7.5 degrees over each monitor. This meant that up to 1.9 dB variation in noise may have been attributable to variation in flight path angle, although there may have been confounding factors. Aircraft flying with higher climb gradients overflew the monitors at higher altitudes, generating lower average noise measurements.

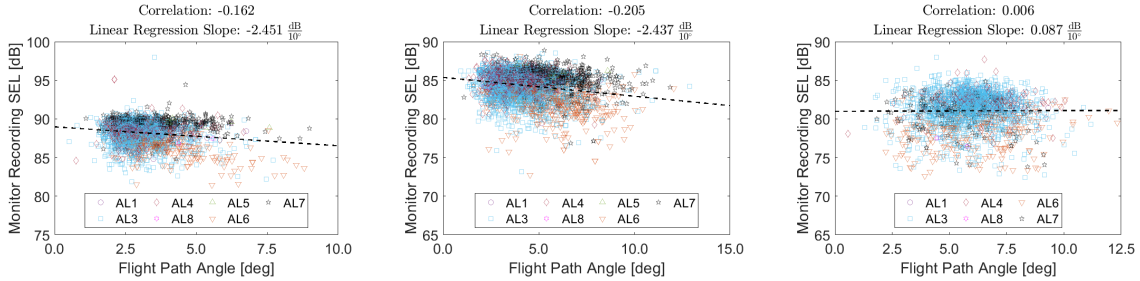

(a) South close monitor (b) South mid monitor (c) South far monitor

Figure 4-11: Flight Path Angle Impact on Noise from Departing B737NG Aircraft

Next, the impact of environmental variables on measured noise was demonstrated at all three monitor locations. The environmental variables correlating with departure noise at all three monitor locations were examined in order of strongest impact to weakest impact. Impact was determined by averaging the absolute value of the correlation coefficients at the close, mid, and far monitors. The environmental variable with the highest impact had the highest average correlation coefficient, and the variable with the lowest impact had the lowest average correlation coefficient.

Environmental Effect 1: Relative Humidity

As shown in Figure 4-12, noise increased by approximately 0.11-0.18 dB for each additional 10% increase in relative humidity. Relative humidity was observed to vary by up to 80% at all three monitors. This meant that up to 0.9-1.4 dB variation in measured noise may have been attributable to variation in relative humidity, although

there may have been confounding factors. This trend was consistent with the findings in [11], which demonstrated lower noise attenuation for increased relative humidity values above 20 percent.

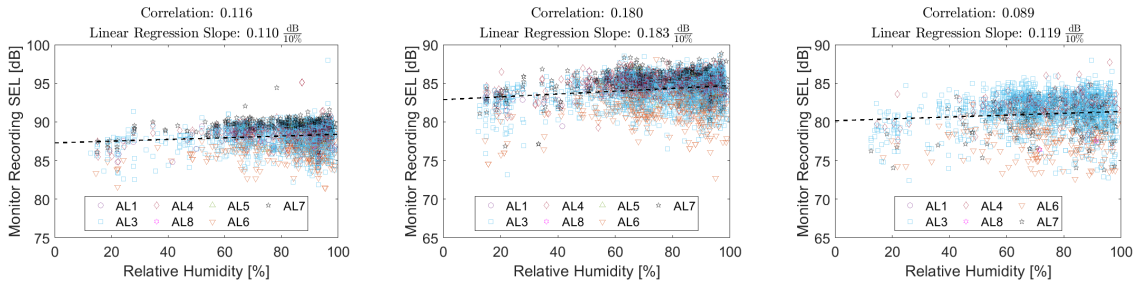

(a) South close monitor (b) South mid monitor (c) South far monitor

Figure 4-12: Relative Humidity Impact on Noise from Departing B737NG Aircraft

Environmental Effect 2: Headwind (Northward Wind)

As shown in Figure 4-13, measured noise decreased by approximately 0.4-1.2 dB for each additional 10 knots of headwind (northward wind). Headwinds were expected to increase climb gradients, so this trend was expected. Headwind was observed by vary by approximately 30 knots at each monitor. This meant that up to 1.2-3.6 dB variation in noise may have been attributable to variation in headwind, although there may have been confounding factors. Note that the correlation was stronger at the mid and far monitors than at the close monitor. This was likely because the difference in altitude achieved by climbing with a strong headwind grew as a function of distance from the airport, so the effect of the headwind was magnified as the aircraft flew further from the airport.

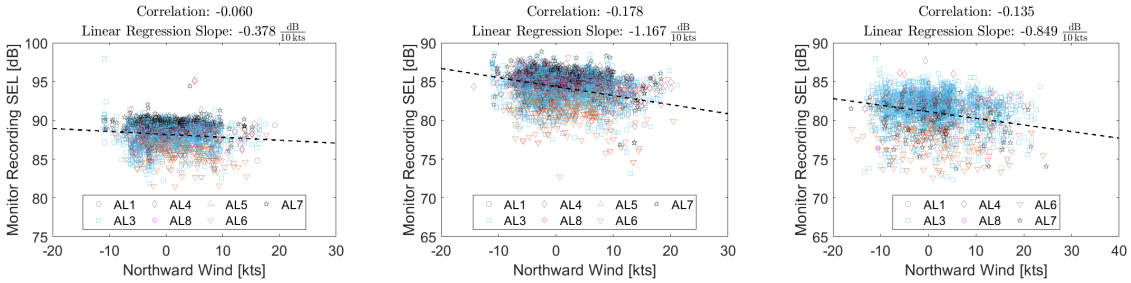

(a) South close monitor (b) South mid monitor (c) South far monitor

Figure 4-13: Northward Wind (Headwind) Impact on Noise from Departing B737NG Aircraft

Environmental Effect 3: Temperature

The impact of temperature on measured noise at all three monitor locations is shown in Figure 4-14. Measured noise was observed to correlate weakly with temperature. Measured noise decreased by approximately 0.1-0.3 dB for each additional 10°C at the three monitor locations. Temperature was observed to vary by approximately 30°C at each monitor location. This meant that 0.3-0.9 variation in measured noise may have been attributable to temperature, although there may have been confounding factors. This trend was not expected, given that attenuation is known to decrease as temperature increases. This trend may have resulted from of airline-specific takeoff thrust corrections as functions of temperature.

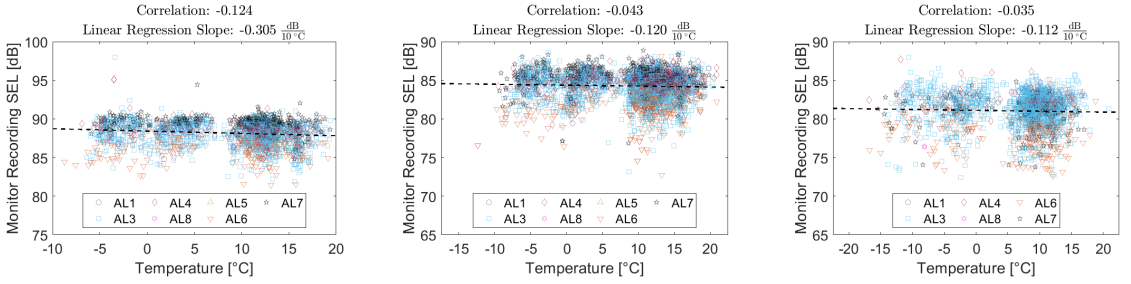

(a) South close monitor (b) South mid monitor (c) South far monitor

Figure 4-14: Temperature Impact on Noise from Departing B737NG Aircraft

Environmental Effect 4: Crosswind (Eastward Wind)

The impact of the crosswind (eastward) component at all three monitor locations is shown in Figure 4-15. Measured noise varied by up to 0.6 dB for each additional 10 knots of crosswind. The crosswind component was observed by vary by approximately 30 knots. This meant that up to 1.8 dB variation in measured noise may have been attributable to variation in the crosswind component, although there may have been confounding factors. This observation may be explained by advection. Noise advected towards or away from the monitors depending on the direction of the eastward wind and the location of the airplane relative to the monitor being examined. The south close monitor was offset east of the departure path, so a positive crosswind component to the east caused the noise to advect towards the monitor, increasing measured noise close to the airport. The mid and far monitors were more closely aligned with the departure path, so the impact of the crosswind component was weaker.

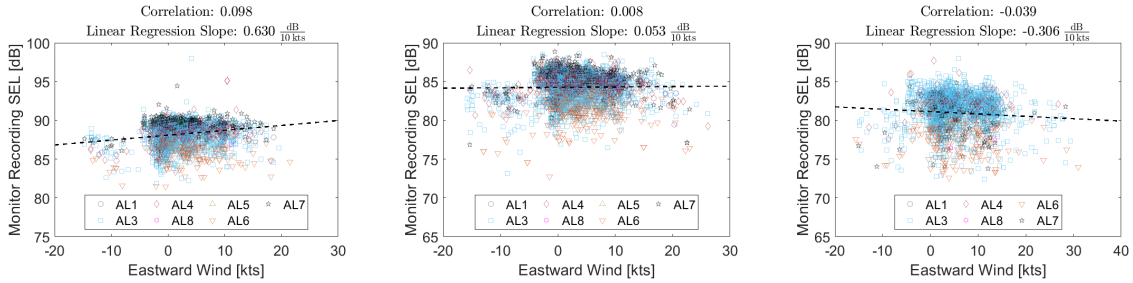

(a) South close monitor (b) South mid monitor (c) South far monitor

Figure 4-15: Eastward Wind (Crosswind) Impact on Noise from Departing B737NG Aircraft

4.3.3 Impact of Airline-Specific Departure Procedures on Measured B737NG Noise

Figure 4-16 shows how departure performance parameters for each airline varied relative to the average B737NG flyover. The difference between the average airline parameter and the average overall parameter was then normalized by the maximum difference so that all values fell between -1 and 1. Airlines that registered more than 10 noise measurements were included. The average performance parameter values for

each airline are given in Appendix C.

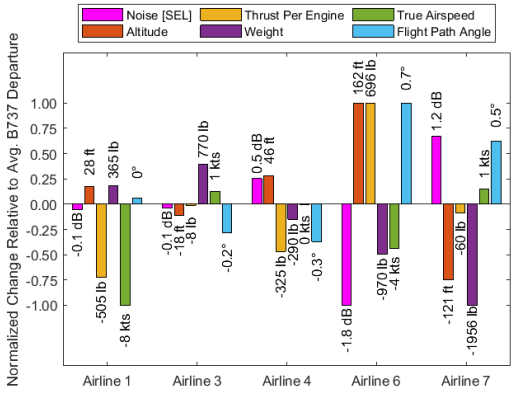

(a) South close monitor

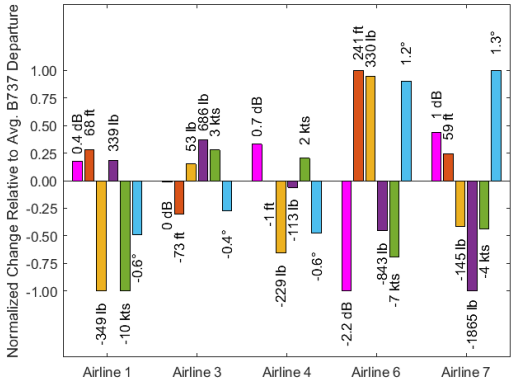

(b) South mid monitor

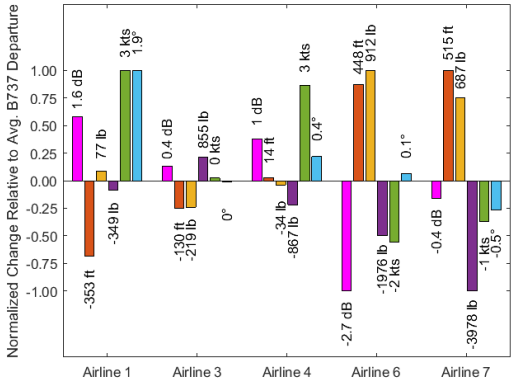

(c) South far monitor

Figure 4-16: B737NG Departure Performance Parameter Averages by Airline Relative to Average B737NG Southbound Departure

Significant differences between noise recordings produced by different airlines were

seen in the noise monitor data. Airline 6 was observed to generate the lowest average noise measurements at all three monitors, and was quieter than the average Boeing 737 by 2-3%. On average, Airline 6 overflew the three monitors with the highest thrust (approximately 11,000-11,500 lb thrust, or equivalently, 3-9% higher thrust compared to the average B737NG). Airline 6 also overflew the close and mid monitors at the highest altitudes, approximately 8-11% higher than the average B737NG. Its aircraft overflew the monitors with flight path angles that were up to 25% higher than the average. Airline 6 also departed with lower true airspeed (up to 3% below average). The procedure flown by Airline 6 appears similar to NADP1, where aircraft climb with higher thrust and flight path angle until reaching 3000 ft altitude, at which point they retract slats and flaps and accelerate to 250 knots [22]. Airline 6 overflew over the south close monitor with the highest average flight path angle, but by the time its aircraft reached the mid and far monitors, they climbed with the second and third highest flight path angles, respectively. Furthermore, by the time the aircraft flown by Airline 6 overflew the far monitor, they had climbed to a lower average altitude than those operated by Airline 7. This is further evidence that Airline 6 climbed with higher initial thrust and climb gradient close to the airport before accelerating, similar to the procedure defined by NADP1.

Airline 7 was observed to generate the highest average noise measurements at the close and mid monitors, louder than the average by approximately 1%. By the time its aircraft overflew the far monitor, they generated the second quietest noise measurements on average, quieter than the average by approximately 0.6%. Airline 7 overflew the close monitor at the lowest average altitude (6% below the average B737NG), but had reached the highest average altitude (12.7% higher than average) by the time it overflew the far monitor. The procedure flown by Airline 7 appears similar to NADP2, where aircraft retract slats and flaps and accelerate to 250 knots early and then increase their climb gradient further from the airport. This may explain why the aircraft flown by Airline 7 were at the lowest average altitudes close to the airport and the highest average altitudes far from the airport, and why they were observed to generate the highest average noise measurements at the close monitor

and the second lowest average noise measurements at the far monitor.

4.3.4 Airbus A320 Departure Noise Trends at South Monitors

The noise impact of each variable for the A320 at the south close, mid, and far monitors is given in Figures 4-17, 4-18, and 4-19, respectively. Altitude, thrust per engine, true airspeed, and flight path angle were taken at the point of closest approach to the monitor. Environmental data was averaged as described in Section 4.2.2. Plots were color-coded by airline so that the noise impact of airline-specific operating procedures could be seen. The correlation coefficient between SEL and each variable, as well as the slope of the linear regression between SEL and each variable were included.

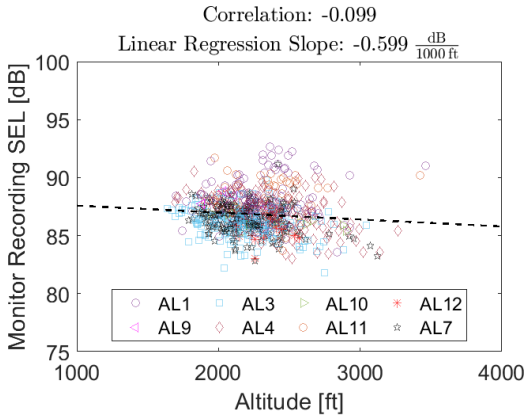

(a) Altitude impact, south close monitor

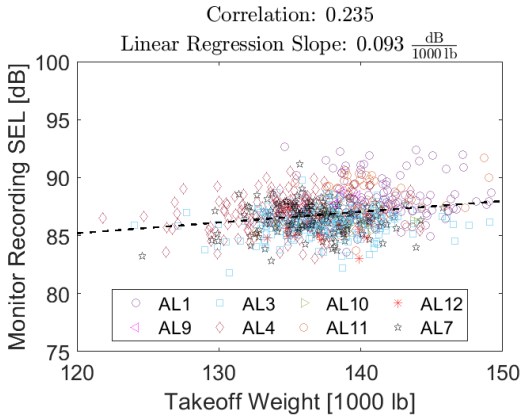

(b) Weight impact, south close monitor

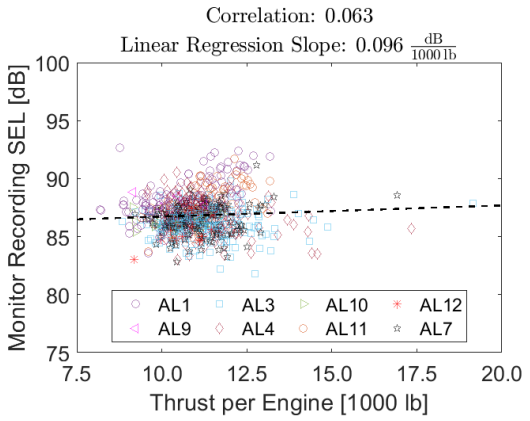

(c) Thrust impact, south close monitor

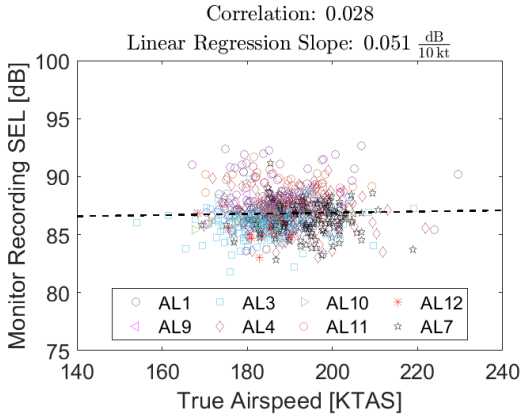

(d) True airspeed impact, south close monitor

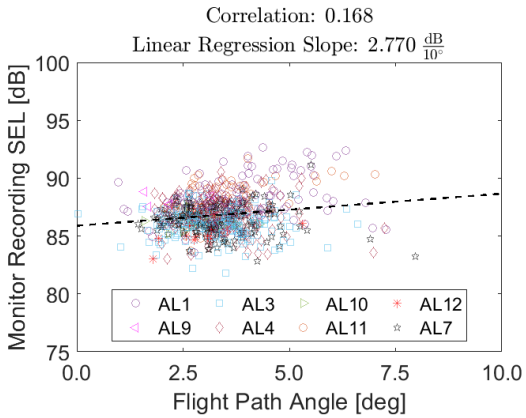

(e) Flight path angle impact, south close monitor

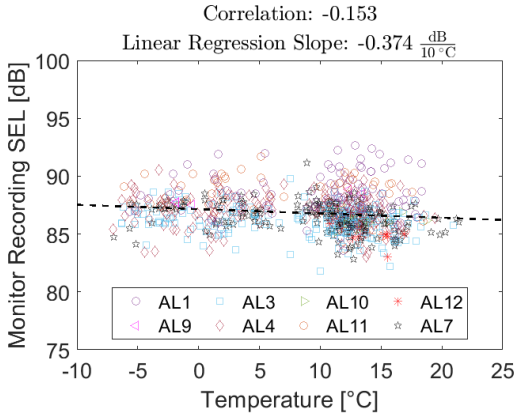

(f) Temperature impact, south close monitor

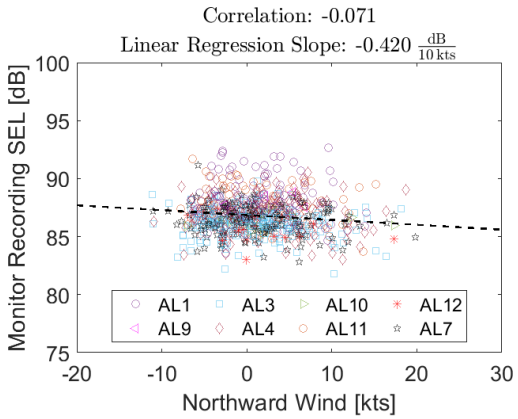

(g) Northward wind (headwind) impact, south close monitor. Northward wind positive to the north

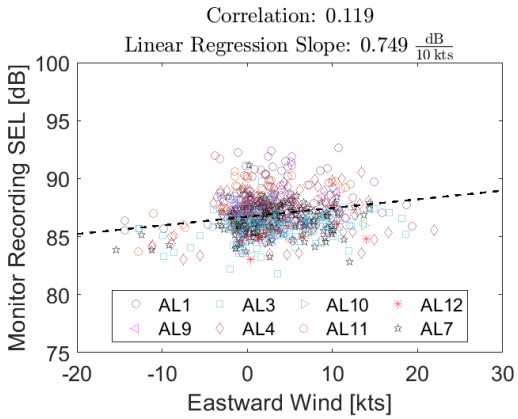

(h) Eastward wind (crosswind) impact, south close monitor. Eastward wind positive to the east

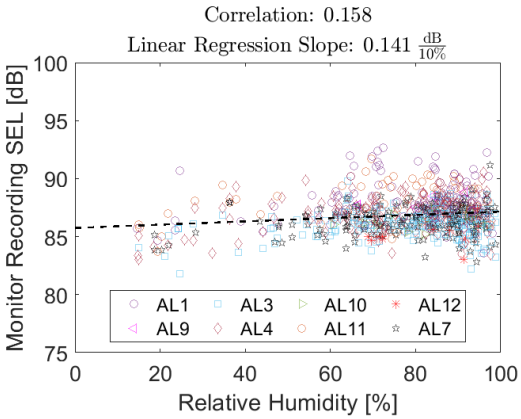

(i) Relative humidity wind impact, south close monitor

Figure 4-17: Trends for departing Airbus A320s at the south close monitor

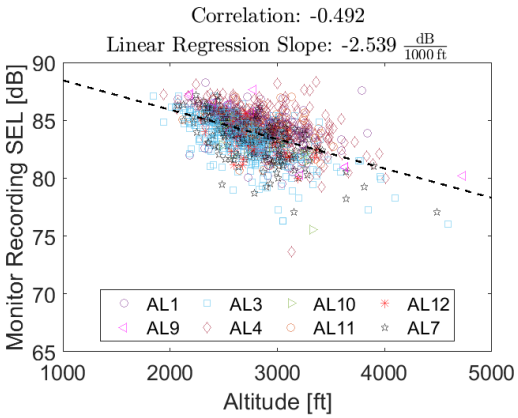

(a) Altitude impact, south mid monitor

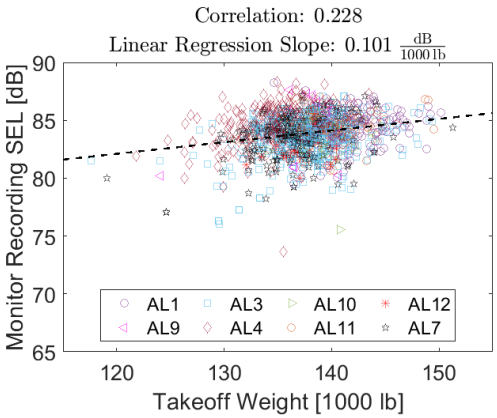

(b) Weight impact, south mid monitor

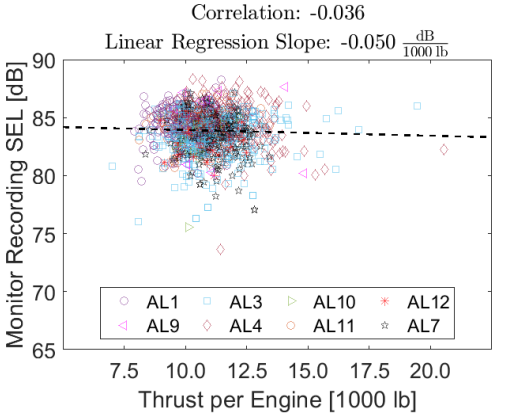

(c) Thrust impact, south mid monitor

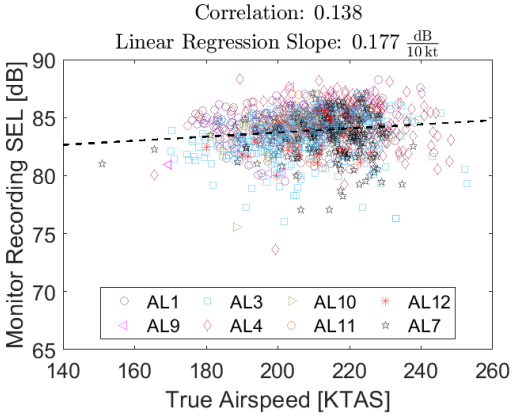

(d) True airspeed impact, south mid monitor

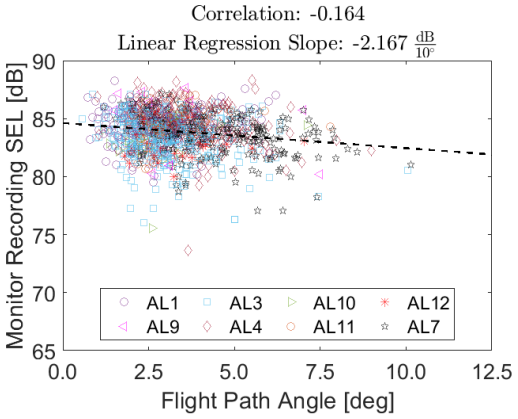

(e) Flight path angle impact, south mid monitor

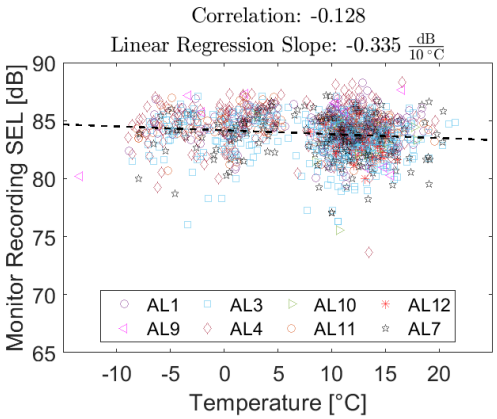

(f) Temperature impact, south mid monitor

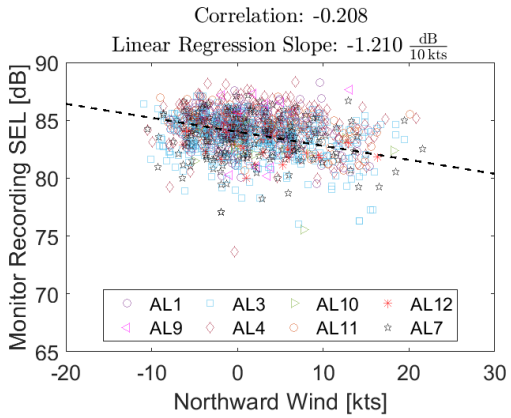

(g) Northward wind (headwind) impact, south mid monitor. Northward wind positive to the north

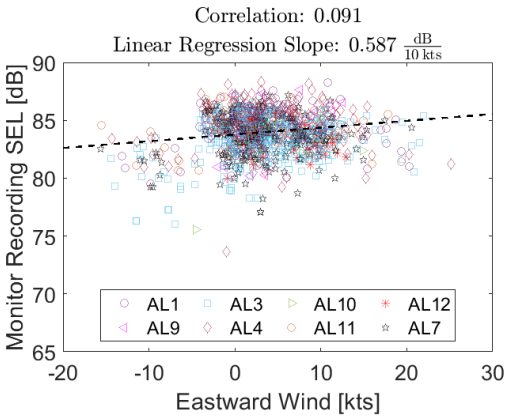

(h) Eastward wind (crosswind) impact, south mid monitor. Eastward wind positive to the east

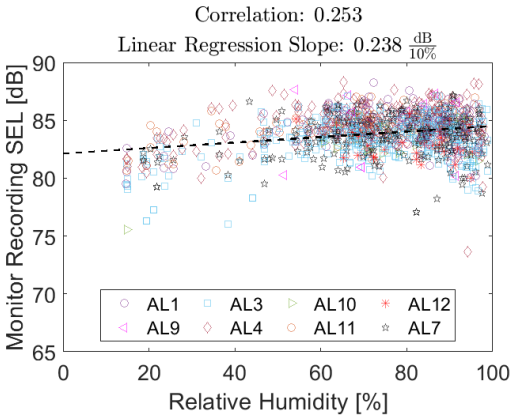

(i) Relative humidity wind impact, south mid monitor

Figure 4-18: Trends for departing Airbus A320s at the south mid monitor

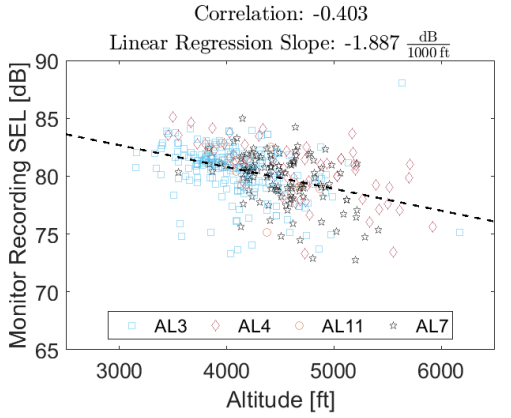

(a) Altitude impact, south far monitor

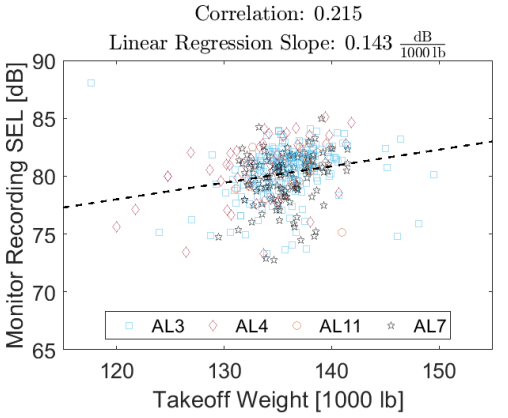

(b) Weight impact, south far monitor

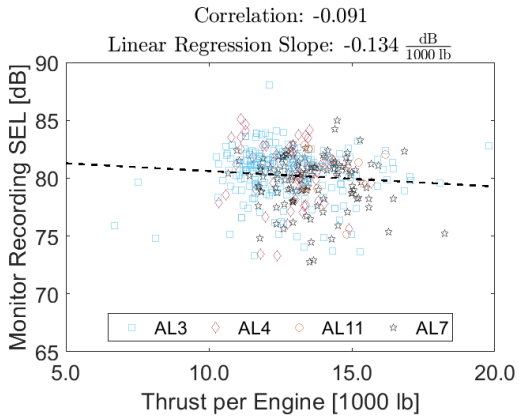

(c) Thrust impact, south far monitor

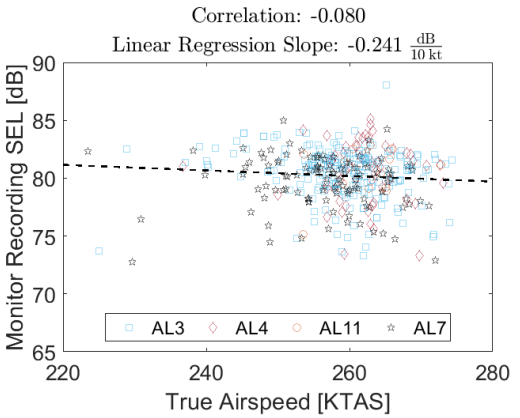

(d) True airspeed impact, south far monitor

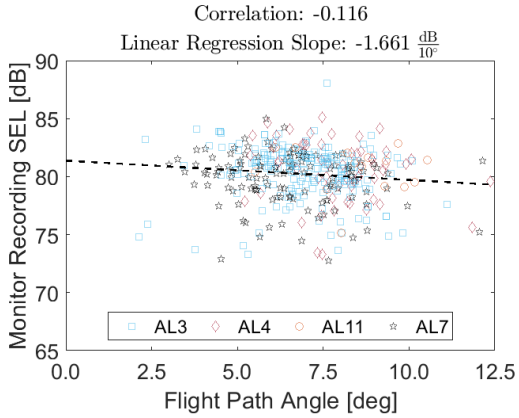

(e) Flight path angle impact, south far monitor

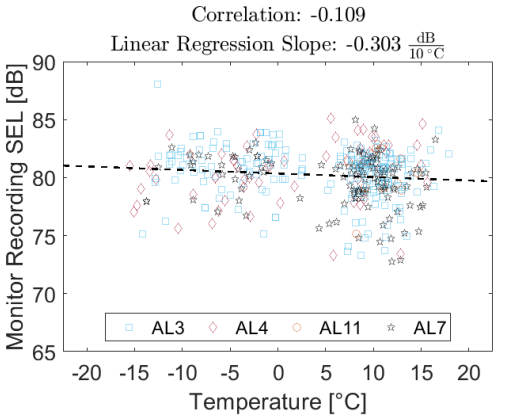

(f) Temperature impact, south far monitor

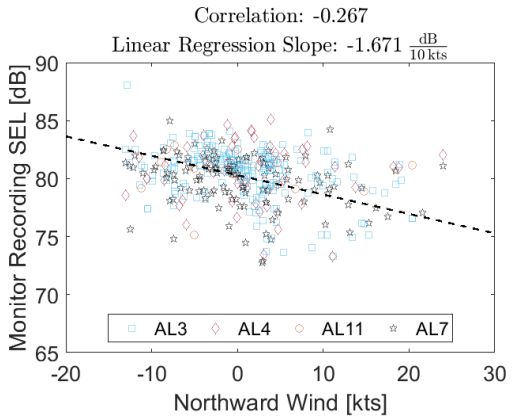

(g) Northward wind (headwind) impact, south far monitor. Northward wind positive to the north

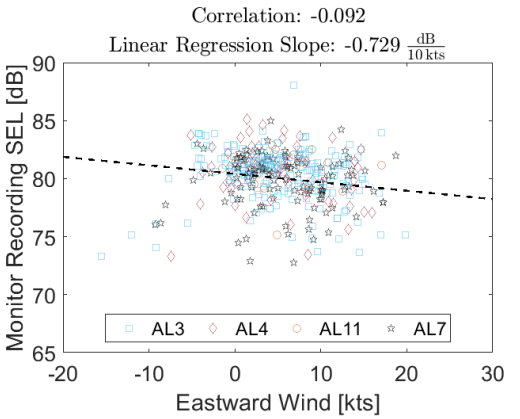

(h) Eastward wind (crosswind) impact, south far monitor. Eastward wind positive to the east

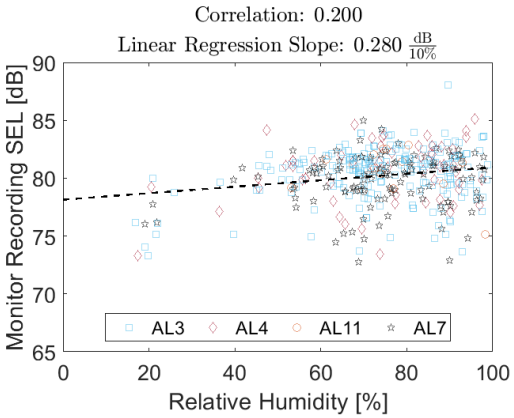

(i) Relative humidity wind impact, south far monitor

Figure 4-19: Trends for departing Airbus A320s at the south far monitor

Noise measurements for the A320 at the north monitors are consistent with the results at the south monitors, with the exception that noise measurements increase with the northward wind for northbound departures. This is likely because tailwinds decrease climb performance, increasing noise exposure on the ground. Results for northbound A320 departures are given in Appendix B.

4.3.5 Analysis of Airbus A320 Departure Noise Trends at South Monitors

The variables correlating with departure noise at the three south monitor locations were examined in order of strongest impact to weakest impact. Impact was determined by averaging the absolute value of the correlation coefficients at the close, mid, and far monitors. The variable with the highest impact had the highest average correlation coefficient, and the variable with the lowest impact had the lowest average correlation coefficient.

Effect 1: Altitude

Altitude was observed to have the strongest impact on measured noise at the mid and far monitors, with lower noise at higher altitude. Altitude was observed to have

a weaker impact at the close monitor, although this may be because the variation in altitude at the close monitor was approximately 1500 ft while the variation in altitude at the mid and far monitors was approximately 2000 ft and 2500 ft, respectively. Measured noise decreased by approximately 0.6-2.6 dB for each additional 1000 ft altitude gained. Altitude was observed to vary by up to 2500 ft. This meant that up to 1.5-6.5 dB variation in measured noise may have been attributable to variation in altitude, although there may have been confounding factors. This trend is shown in Figure 4-20 and is is consistent with spherical spreading and attenuation losses.

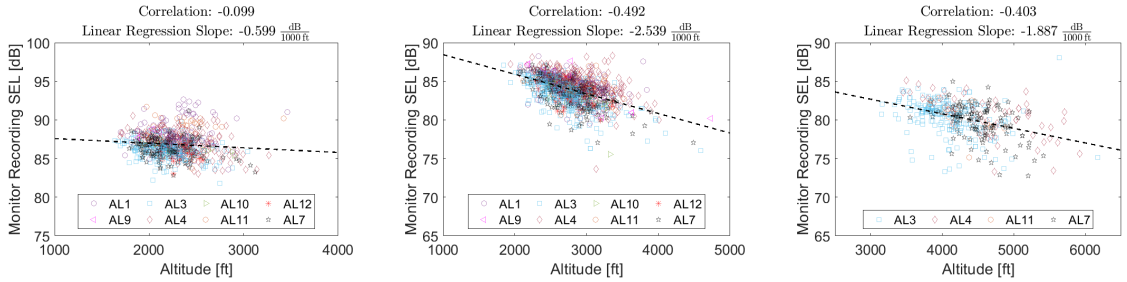

(a) South close monitor (b) South mid monitor (c) South far monitor

Figure 4-20: Altitude Impact on Noise from Departing A320 Aircraft

Effect 2: Takeoff Weight

Next, the impact of takeoff weight on measured noise at all three monitor locations is shown in Figure 4-21. Measured noise was observed to increase by approximately 0.1 dB for each additional 1000 lb increase in departure weight. Departure weight was observed to vary by approximately 15,000 lb. This meant that up to 1.5 dB variation in measured noise may have been attributable to variation in departure weight, although there may have been confounding factors. Heavier aircraft typically climb more slowly and with more thrust than light aircraft, so the trend was expected.

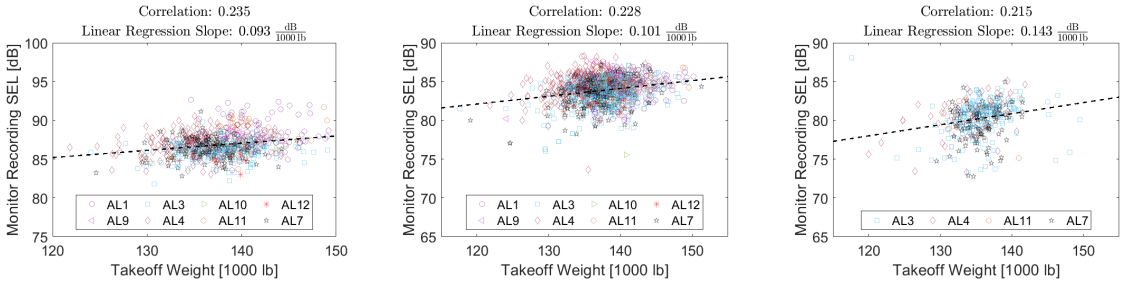

(a) South close monitor (b) South mid monitor (c) South far monitor

Figure 4-21: Weight Impact on Noise from Departing A320 Aircraft

Effect 3: Flight Path Angle

The impact of flight path angle on measured noise at all three monitor locations is shown in Figure 4-22. Measured noise was observed to decrease with higher flight path angle at the mid and far monitors, but decreased with lower flight path angle at the close monitor. The behavior at the mid and far monitors was expected given that aircraft flying with higher climb gradients overflew the monitors at higher altitudes, generating lower average noise measurements. At these monitors, measured noise decreased by 1.6-2.2 dB for each additional 10°of increased flight path angle. Flight path angle was observed to vary by approximately 5°at the mid and far monitors. This meant that up to 0.8-1.1 dB variation in measured noise may have been attributable to variation in flight path angle, although there may have been confounding factors. The behavior at the close monitor was not expected, but may be alleviated by using multiple ADS-B data points to calculate an average flight path angle value instead of using an instantaneous estimate.

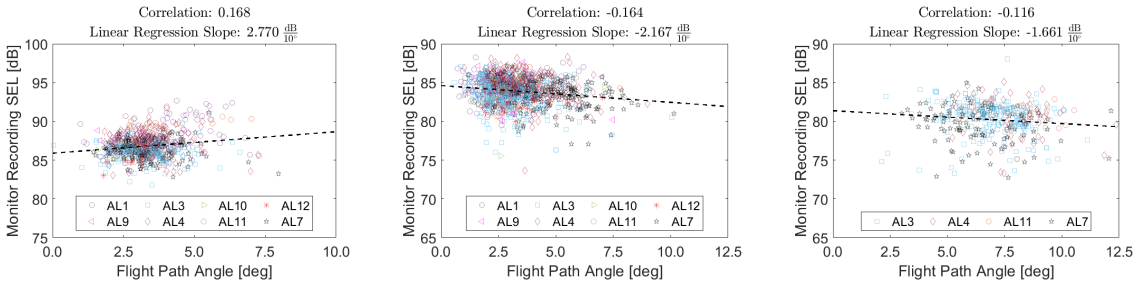

(a) South close monitor (b) South mid monitor (c) South far monitor

Figure 4-22: Flight Path Angle Impact on Noise from Departing A320 Aircraft

Effect 4: True Airspeed

The impact of true airspeed on measured noise at all three monitor locations is shown in Figure 4-23. Measured noise was observed to increase with true airspeed at the close and mid monitors by up to 0.18 dB for each additional 10 knots true airspeed. True airspeed was observed to vary by approximately 60 knots at these monitors. This meant that approximately 1 dB variation in measured noise may have been attributable to variation in true airspeed at the close and mid monitors, although there may have been confounding factors. This trend was expected, since aircraft climbing at steeper climb gradients typically fly at lower true airspeeds. Airframe noise also increases with true airspeed, so flying at lower true airspeed may have had an impact on measured noise in cases where airframe noise dominated engine noise on departure. Measured noise was observed to decrease as true airspeed increased at the far monitor. This could potentially be because aircraft overflying the far monitor were accelerating to climb speed at reduced climb thrust with slats and flaps retracted, although flight data recorder data would be required to validate this prediction.

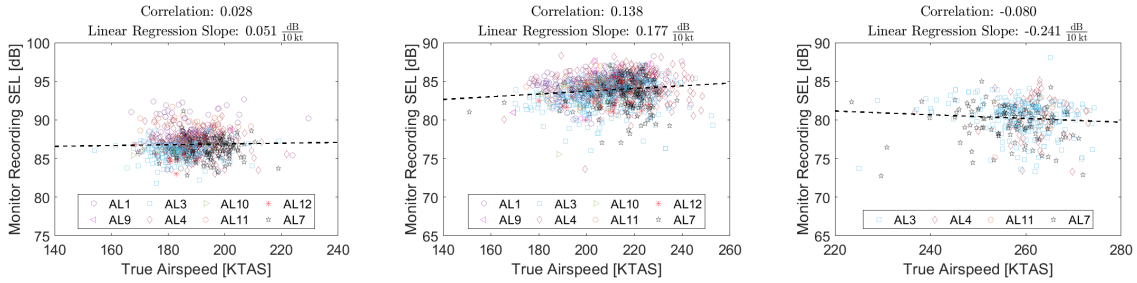

(a) South close monitor (b) South mid monitor (c) South far monitor

Figure 4-23: True Airspeed Impact on Noise from Departing A320 Aircraft

Effect 5: Thrust

Next, the impact of thrust on measured noise at all three monitor locations is shown in Figure 4-24. Measured noise was observed to increase with higher thrust at the close monitor, and decrease with higher thrust at the mid and far monitors. This trend was consistent with the modeled results in Thomas 2020 [22], which demonstrated that aircraft departing with higher thrust generated higher modeled noise near the airport,

and lower modeled noise at the equivalent mid and far distances from the airport. Measured noise varied by 0.05-0.13 dB for each additional 1000 lb increase in thrust. Modeled thrust varied by approximately 5000 lb at each monitor. This meant that approximately 0.2-0.7 dB dB variation in measured noise may have been attributable to variation in thrust, although there may have been confounding factors.

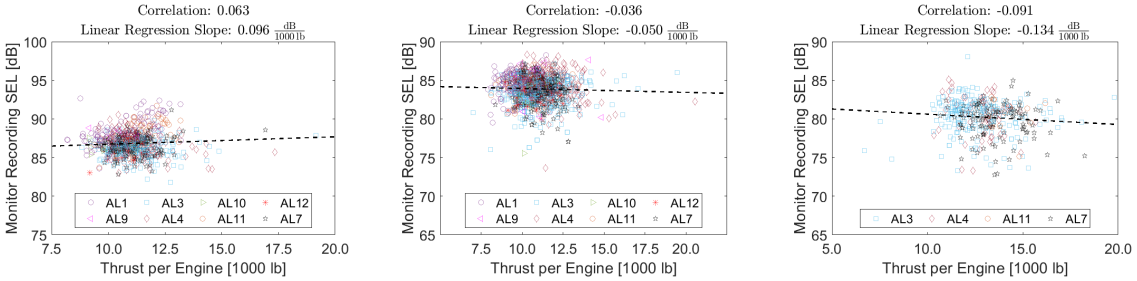

(a) South close monitor (b) South mid monitor (c) South far monitor

Figure 4-24: Thrust Impact on Noise from Departing A320 Aircraft

Next, the impact of environmental variables on measured noise was demonstrated at all three monitor locations. The environmental variables correlating with departure noise at all three monitor locations were examined in order of strongest impact to weakest impact. Impact was determined by averaging the absolute value of the correlation coefficients at the close, mid, and far monitors. The environmental variable with the highest impact had the highest average correlation coefficient, and the variable with the lowest impact had the lowest average correlation coefficient.

Environmental Effect 1: Relative Humidity

As shown in Figure 4-25, noise increased with relative humidity at all three monitor locations by approximately 0.14-0.28 dB for each additional 10% increase in relative humidity. Relative humidity was observed to vary by up to 80% at the three monitor locations. This meant that approximately 1-2 dB variation in measured noise may have been attributable to variation in relative humidity, although there may have been confounding factors. This trend was consistent with the findings in [11], which demonstrated lower noise attenuation for increased relative humidity values above 20 percent.

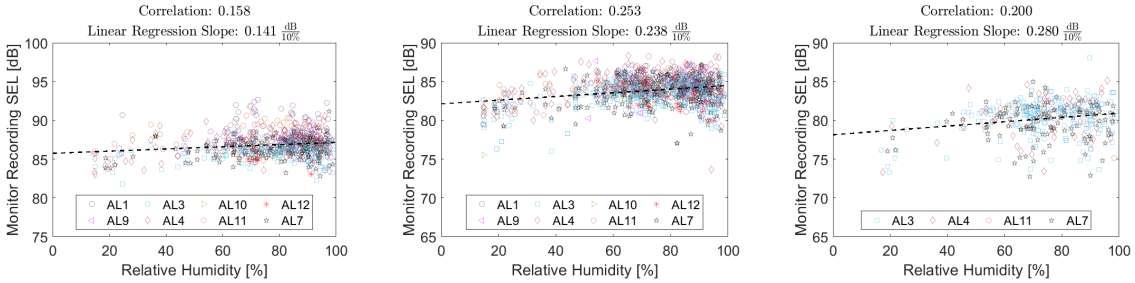

(a) South close monitor (b) South mid monitor (c) South far monitor

Figure 4-25: Relative Humidity Impact on Noise from Departing A320 Aircraft

Environmental Effect 2: Headwind (Northward Wind)

As shown in Figure 4-26, noise was observed to decrease with headwinds (the north wind component). Measured noise decreased by 0.4-1.7 dB for each additional 10 knot increase in headwind. Headwind was observed to vary by approximately 30 knots at the three monitor locations. This meant that approximately 1-5 dB variation in measured noise may have been attributable to variation in headwind, although there may have been confounding factors. Headwinds were expected to increase climb gradients, so this trend was expected. Note that the correlation was stronger at the mid and far monitors than at the close monitor. This was likely because the difference in altitude achieved by climbing with a strong headwind grew as a function of distance from the airport, so the effect of the headwind was magnified as the aircraft flew further from the airport.

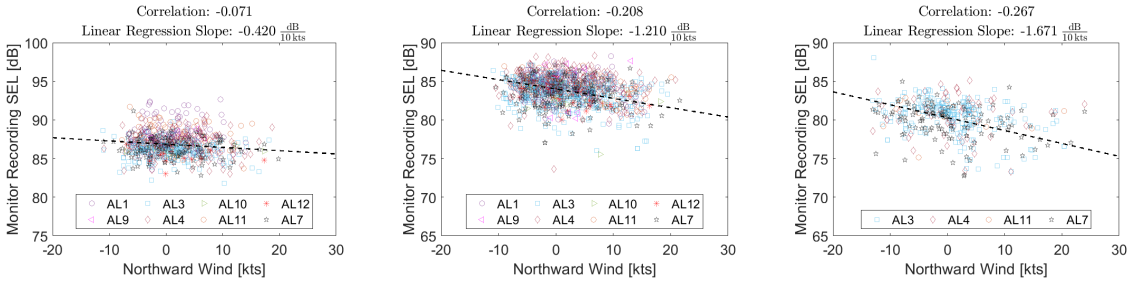

(a) South close monitor (b) South mid monitor (c) South far monitor

Figure 4-26: Northward Wind (Headwind) Impact on Noise from Departing A320 Aircraft

Environmental Effect 3: Temperature

The impact of temperature on measured noise at all three monitor locations is shown in Figure 4-27. Measured noise was observed to correlate weakly with temperature. Measured noise decreased by approximately 0.30-0.38 dB for each additional 10°C increase in temperature. Temperature was observed to vary by approximately 30°C at the three monitor locations. This meant that approximately 1 dB variation in measured noise may have been attributable to variation in temperature, although there may have been confounding factors. This trend was not expected, given that attenuation is known to decrease as temperature increases. This trend may be a result of airline-specific takeoff thrust corrections as functions of temperature.

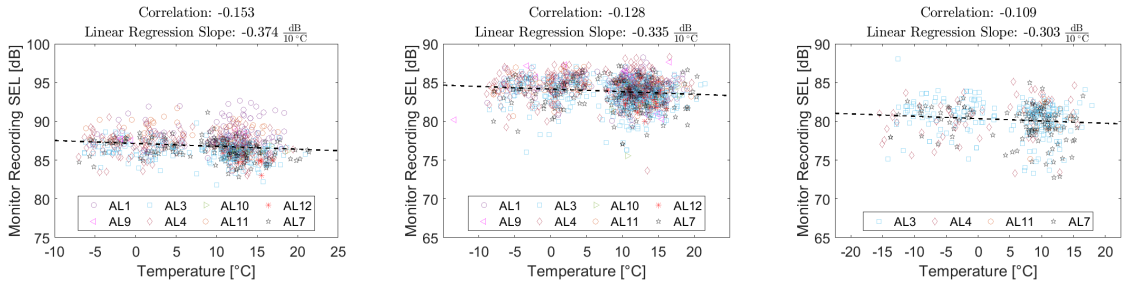

(a) South close monitor (b) South mid monitor (c) South far monitor

Figure 4-27: Temperature Impact on Noise from Departing A320 Aircraft

Environmental Effect 4: Crosswind (Eastward Wind)

The impact of the crosswind (eastward) component at all three monitor locations is shown in Figure 4-28. Measured noise was observed to vary by 0.6-0.7 dB for each additional 10 knot increase in crosswind component. The crosswind component was observed to vary by approximately 20 knots. This meant that 1.2-1.4 dB variation in measured noise may have been attributable to variation in the crosswind component, although there may have been confounding factors. Noise advected towards or away from the monitors depending on the direction of the eastward wind and the location of the airplane relative to the monitor being examined. The south close monitor was offset east of the departure path, so a positive crosswind component to the east caused the noise to advect towards the monitor, increasing measured noise close to

the airport. The mid and far monitors were more closely aligned with the departure path. Aircraft more directly overflew the south far monitor than the close and mid monitors, which may explain why the trend is reversed at the far monitor.

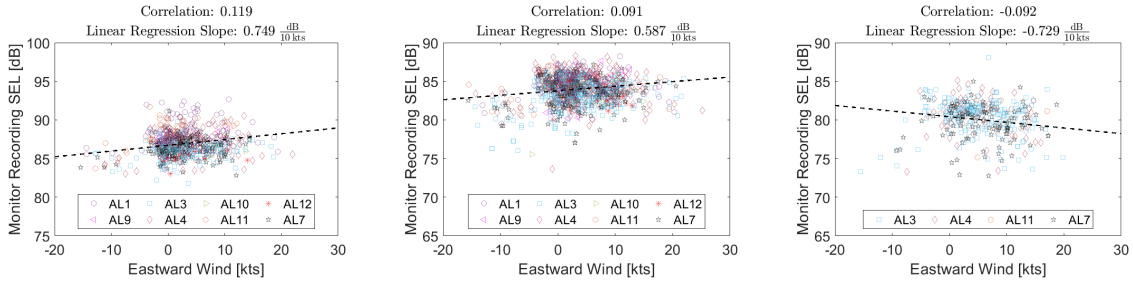

(a) South close monitor (b) South mid monitor (c) South far monitor

Figure 4-28: Eastward Wind (Crosswind) Impact on Noise from Departing A320 Aircraft

4.3.6 Impact of Airline-Specific Departure Procedures on Measured A320 Noise

Figure 4-29 shows how departure performance parameters for each airline varied relative to the average A320 flyover. The difference between the average airline parameter and the average overall parameter was then normalized by the maximum difference so that all values fell between -1 and 1. The average performance parameter values for each airline are given in Appendix C.

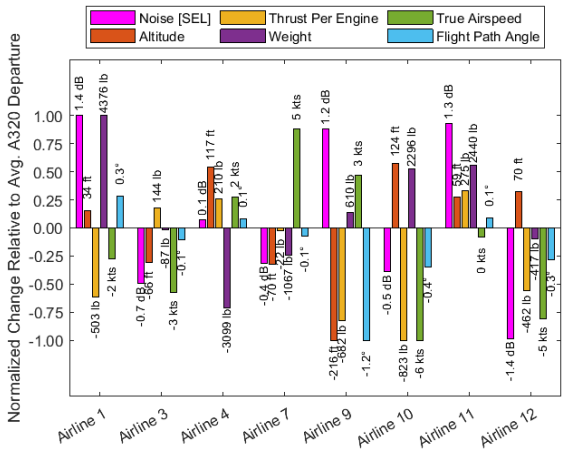

(a) South close monitor

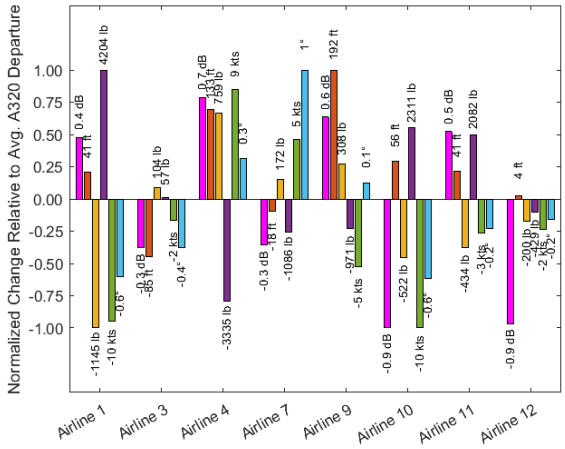

(b) South mid monitor

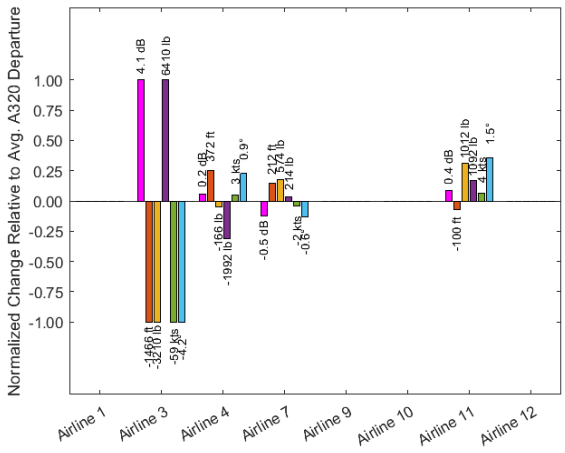

(c) South far monitor

Figure 4-29: A320 Departure Performance Parameter Averages by Airline Relative to Average A320 Southbound Departure

Noise measurements due to aircraft operated by each of the airlines were consistent for Airbus A320s; noise was not as distinguished by operator for the A320 as it was for the B737NG. However, a trend that was observed for B737NGs operated by Airline 7 is also apparent for A320s operated by Airline 7: aircraft operated by Airline 7 were quieter relative to aircraft operated by other airlines the farther the aircraft flew from the airport. At the close monitor, A320s operated by Airline 7 on average generated a noise measurement of 86.4 dB, 1.8 dB quieter than the loudest A320s at the close monitor. However, at the far monitor, A320s operated by Airline 7 generated an average noise measurement of 79.7 dB, 4.6 dB quieter than the loudest A320s at the far monitor and 0.6% quieter than the average A320 at the far monitor. Furthermore, operated by Airline 7 overflew the close monitor at the second lowest average altitude, but by the time they overflew the far monitor, they did so with the second highest average altitude. This finding suggests that Airline 7 operated using a procedure similar to NADP2, intended to reduce community noise far from the airport, with both the B737NG and A320.

4.3.7 Departure Noise Data Summary

Variation in departure noise can be attributed to operator-specific climb procedures, aircraft weight, and environmental factors. Altitude was shown to have the strongest effect on community noise exposure. Airline-specific procedures with higher thrust and higher initial climb gradients were observed to have lower noise exposure. This finding may help inform the development of new noise abatement departure procedures. Future validation studies may examine the impact of specific airline standard operating procedures on aircraft noise. Data from flight data recorders can also be used to obtain precise configuration and weight data.

Environmental factors including ambient wind and relative humidity were shown to have impacts on climb performance (headwind), advection of noise (crosswind), and attenuation of noise (relative humidity).

4.4 Arrival Noise Data Exploration using Operational Flights and Ground Noise Measurements

4.4.1 Identification of Variables with Potential Arrival Noise Variation Impact

As with departures, the parameters investigated were categorized into three groups: observed aircraft data, environmental data, and aircraft performance parameters. The parameters investigated for arrivals are listed in Table 4.2.

Table 4.2: Arrival Noise Parameters Investigated

Noise Data	**Aircraft Data**	**Environmental Data**	**Aircraft Performance**
SEL at Monitor Locations	Aircraft Type	Relative Humidity	Landing Weight
	Aircraft Operator	Northward Wind	Aircraft Configuration
	Altitude	Eastward Wind	Landing Thrust
	Lateral Position	Temperature	
	Groundspeed		
	Flight Path Angle		

4.4.2 Arrival Flight Performance Modeling Assumptions

Operational ADS-B and weather data were used to model flight performance as described in Chapter 3. The thrust modeling required assumptions about aircraft landing gear, slat, and flap configuration to be established. Landing gear deployment was

assumed to occur at the final approach fix for the RNAV 22L at Boston and ILS 16L/C/R at Seattle. Flaps and slats were assumed to be deployed 10 knots below the maximum flap extension speed. Airbus A320s were assumed to land with flaps set to CONF FULL, and Boeing 737s were assumed to land with flaps set to Flaps 30. Thrust was calculated based on configuration assumptions. Assumed flap extension speeds are given in Table 4.3 for the B737NG and Table 4.4 for the A320.

Table 4.3: B737-800 Flap Extension Speeds

Flap Setting	Flaps 1	Flaps 5	Flaps 10	Flaps 15	Flaps 25	Flaps 30
Extension Speed [KIAS]	230	210	200	190	180	165

Table 4.4: A320 Flap Extension Speeds

Flap Setting	CONF 1	CONF 2	CONF 3	FULL
Extension Speed [KIAS]	220	190	175	167

4.4.3 Monitors Examined for Aircraft Arrivals

Three monitors north of Seattle-Tacoma International Airport were chosen to perform the data-driven analysis of arrival noise. Arrivals from the north were chosen because monitors extended further from the airport to the north than to the south, allowing for trends at far, medium-distance, and close monitors to be identified. The far, mid, and close monitors chosen are showin in Figure 4-30.

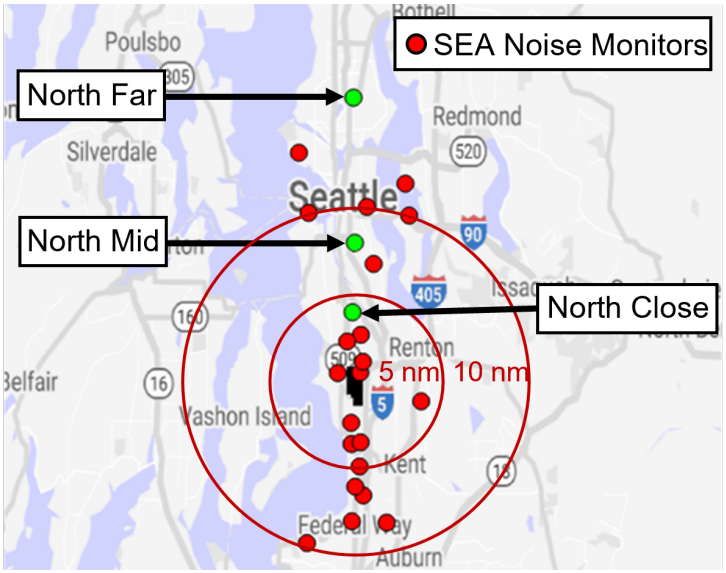

Figure 4-30: Port of Seattle noise monitor network. Monitors analyzed for arrivals shown in green

The lateral tracks of arrivals from the north are shown in Figure 4-31. Aircraft land on all three runways. As with departures, flights were filtered so that only aircraft that flew within a 0.25 nautical mile lateral track distance of the monitor being analyzed were considered.

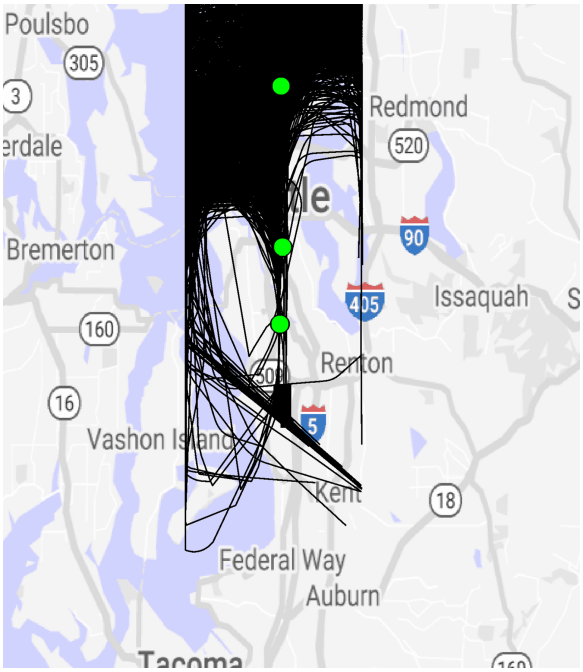

Figure 4-31: Lateral Tracks of Seattle arrivals

4.5 Observed Variation in Aircraft Arrival Noise Measurements using Seattle ADS-B and Noise Monitor Measurement Data

4.5.1 Boeing 737NG Arrival Noise Trends

The noise impact of each variable for the B737NG at the north far monitor is given in Figure 4-32. Note that available data for aircraft arrivals was limited at the north far monitor. Data from the north mid and north close monitors follows in Figures 4-33 and 4-34, respectively.

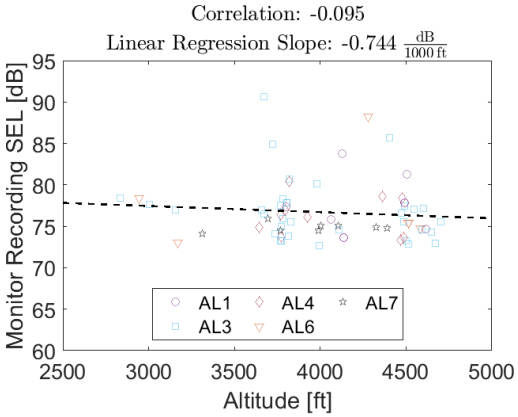

(a) Altitude impact, north far monitor

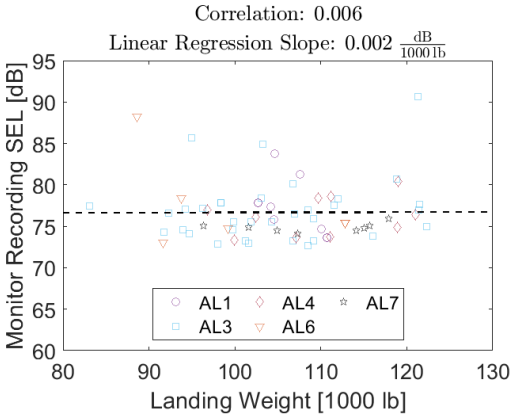

(b) Weight impact, north far monitor

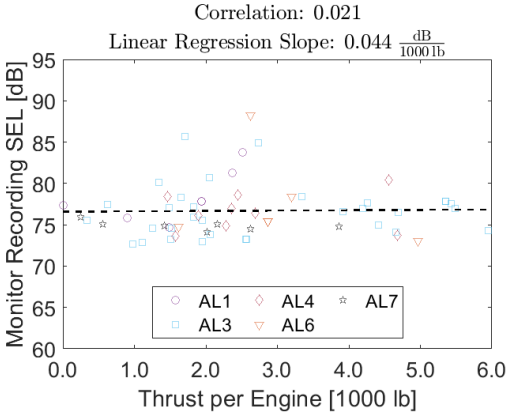

(c) Thrust impact, north far monitor

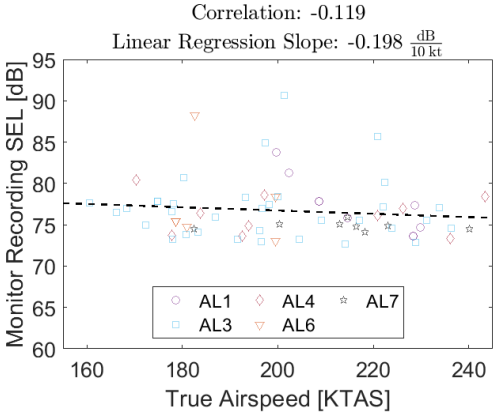

(d) True airspeed impact, north far monitor

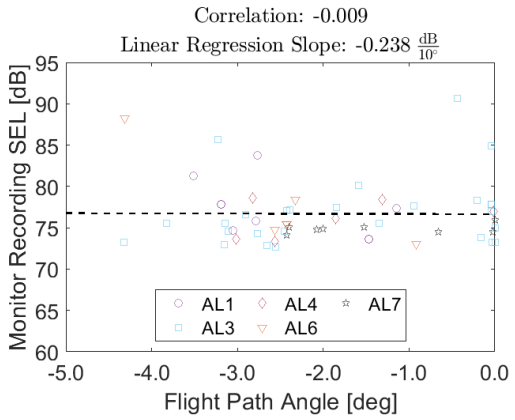

(e) Flight path angle impact, north far monitor

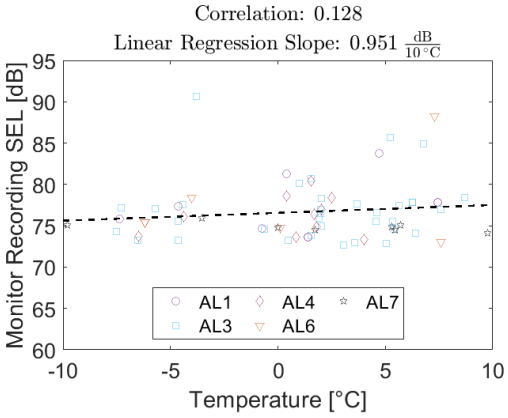

(f) Temperature impact, north far monitor

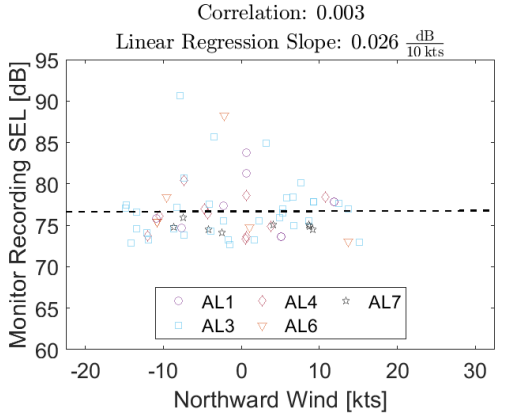

(g) Northward wind (headwind) impact, north far monitor. Northward wind positive to the north

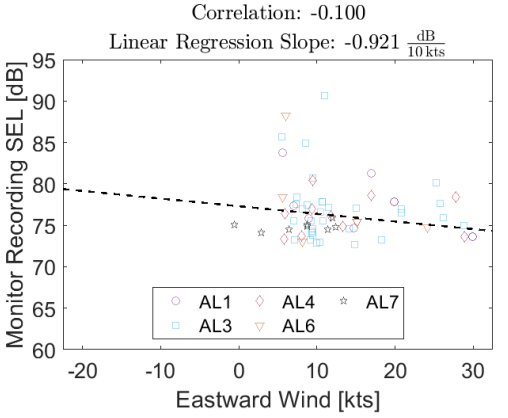

(h) Eastward wind (crosswind) impact, north far monitor. Eastward wind positive to the east

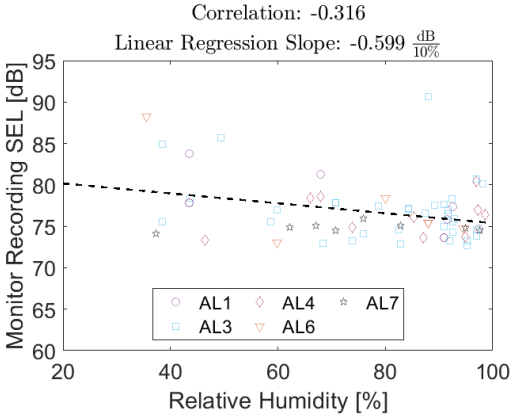

(i) Relative humidity wind impact, north far monitor

Figure 4-32: Trends for arriving Boeing 737NGs at the north far monitor

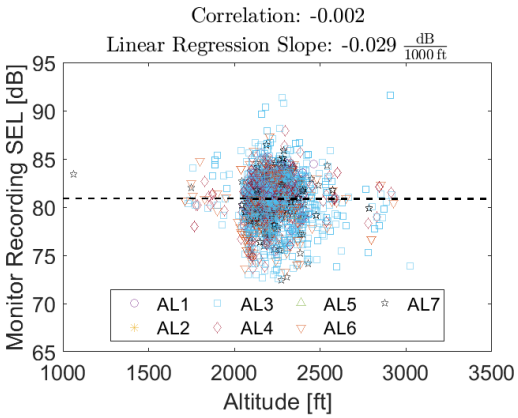

(a) Altitude impact, north mid monitor

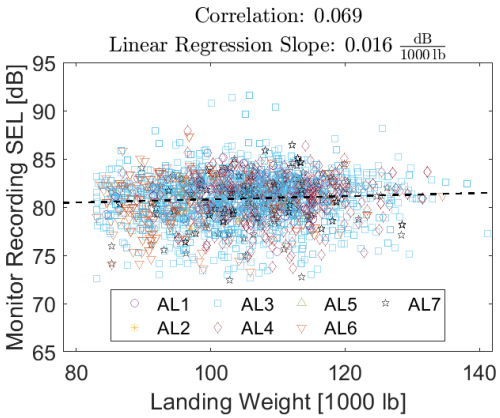

(b) Weight impact, north mid monitor

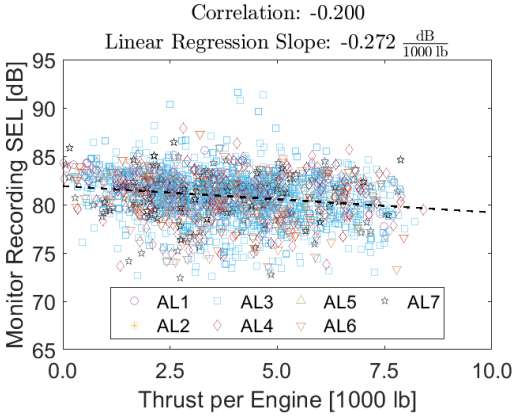

(c) Thrust impact, north mid monitor

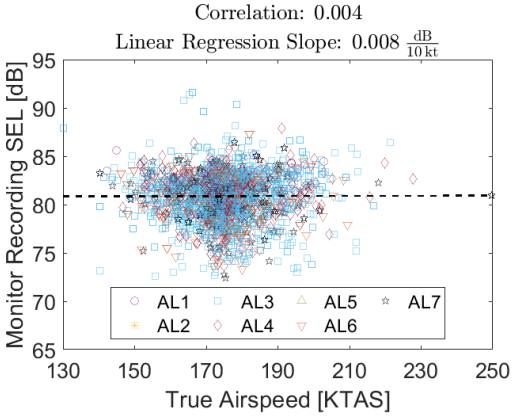

(d) True airspeed impact, north mid monitor

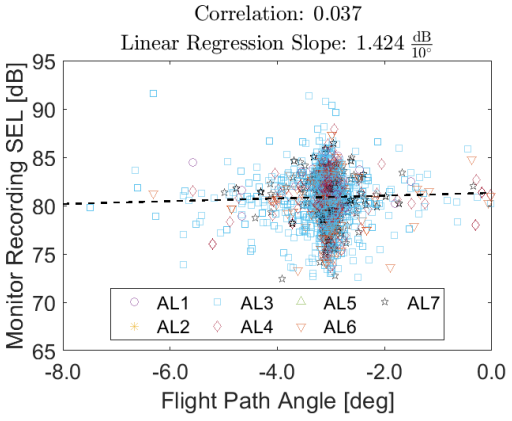

(e) Flight path angle impact, north mid monitor

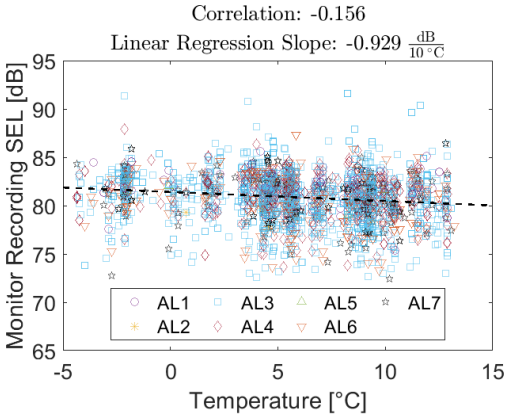

(f) Temperature impact, north mid monitor

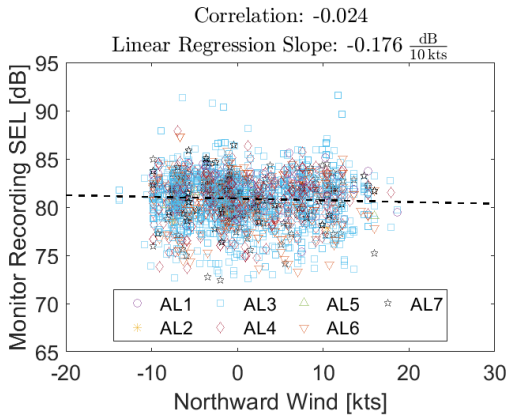

(g) Northward wind (headwind) impact, north mid monitor. Northward wind positive to the north

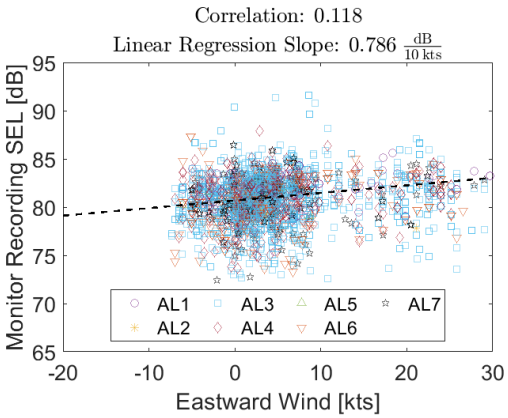

(h) Eastward wind (crosswind) impact, north mid monitor. Eastward wind positive to the east

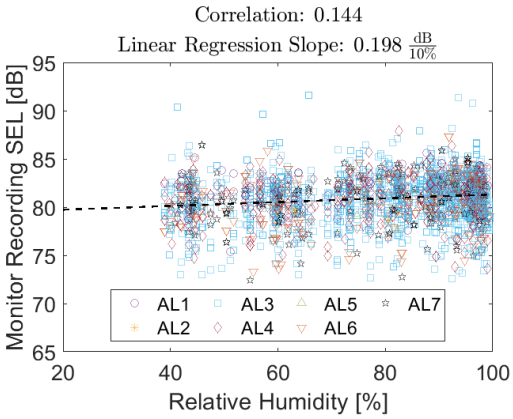

(i) Relative humidity wind impact, north mid monitor

Figure 4-33: Trends for arriving Boeing 737NGs at the north mid monitor

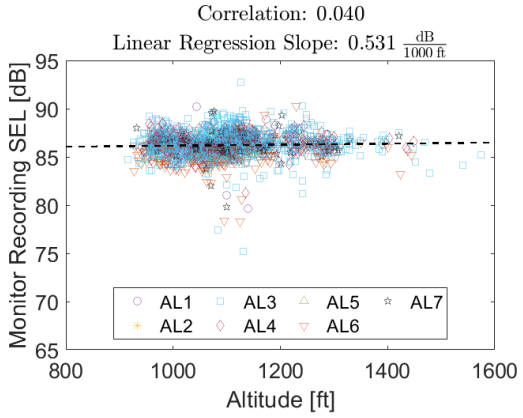

(a) Altitude impact, north close monitor

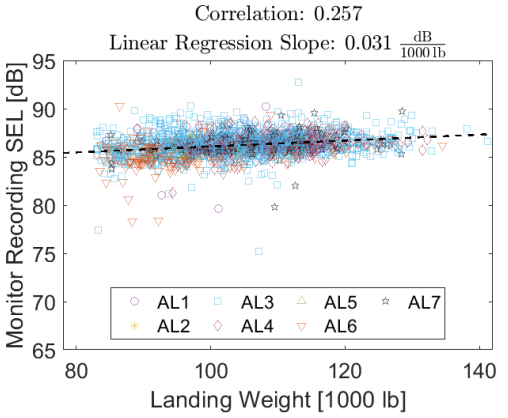

(b) Weight impact, north close monitor

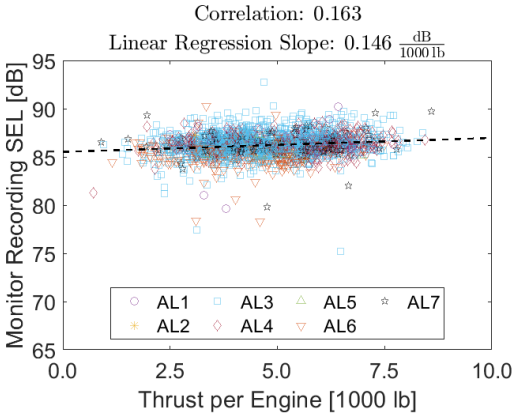

(c) Thrust impact, north close monitor

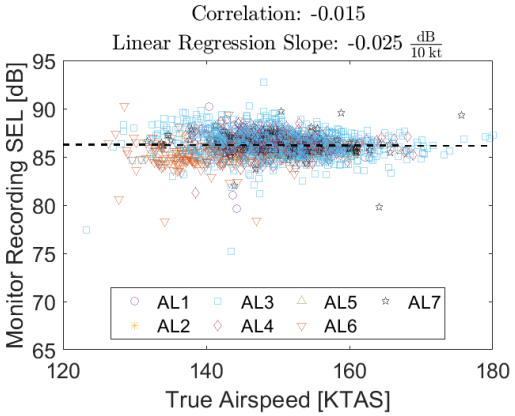

(d) True airspeed impact, north close monitor

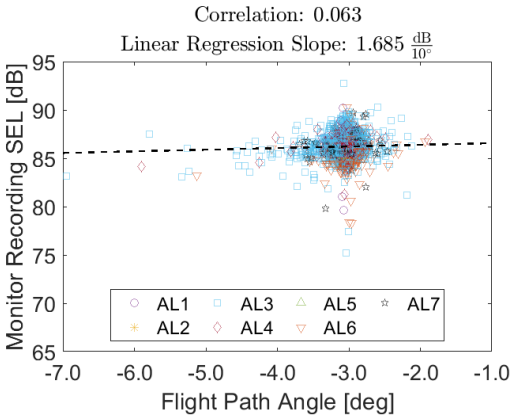

(e) Flight path angle impact, north close monitor

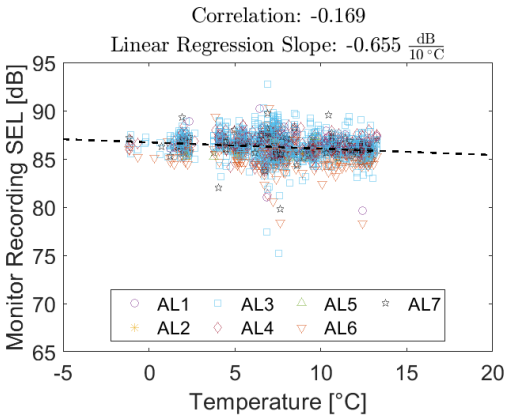

(f) Temperature impact, north close monitor

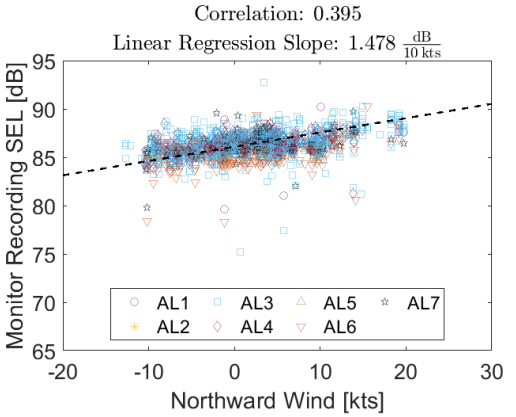

(g) Northward wind (headwind) impact, north close monitor. Northward wind positive to the north

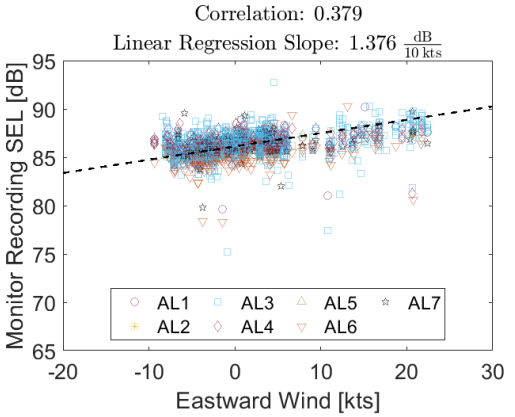

(h) Eastward wind (crosswind) impact, north close monitor. Eastward wind positive to the east

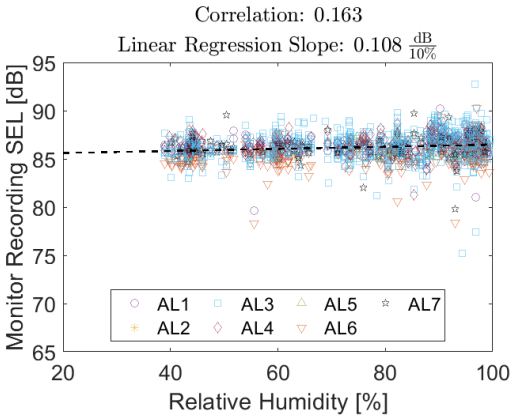

(i) Relative humidity wind impact, north close monitor

Figure 4-34: Trends for arriving Boeing 737NGs at the north close monitor

4.5.2 Analysis of Boeing 737NG Arrival Noise Trends

The variables correlating with arrival noise at all three monitor locations were examined in order of strongest impact to weakest impact. Impact was determined by averaging the absolute value of the correlation coefficients at the close, mid, and far monitors. The variable with the highest impact had the highest average correlation coefficient, and the variable with the lowest impact had the lowest average correlation coefficient.

Effect 1: Thrust

Thrust was observed to have the greatest impact on measured B737NG arrival noise as shown in Figure 4-35. Measured noise increased by up to 1.5 dB for each additional 1000 lb of increased thrust at the close and far monitors. Modeled thrust varied by approximately 5000 lb at these monitors. This meant that up to 0.75 dB variation in measured noise may have been attributed to variation in thrust, although there may have been confounding factors. This trend was expected because engine noise was previously known to correlate with thrust levels, all other factors constant. The opposite trend was observed at the mid monitor. This trend was likely observed because thrust was modeled as a function of assumed slat, flap, and landing gear

deployment schedules, potentially leading to unreliable thrust estimates in some cases. Had the actual deployment schedules been known, modeled thrust would have been less susceptible to modeling error.

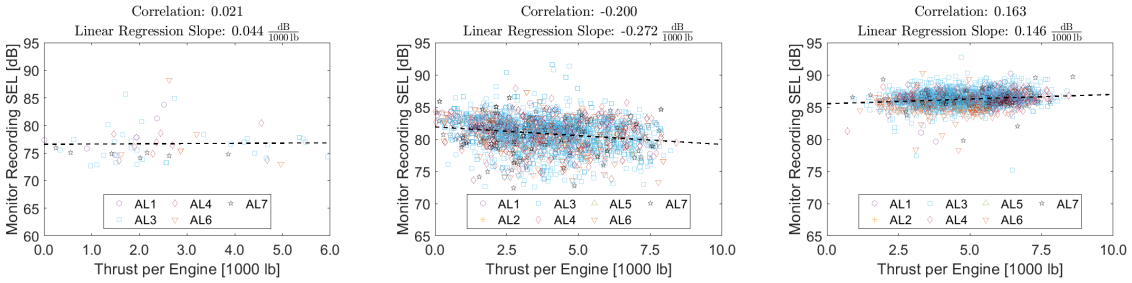

(a) North far monitor (b) North mid monitor (c) North close monitor

Figure 4-35: Thrust Impact on Noise from Arriving B737NG Aircraft

Effect 2: Landing Weight

Next, landing weight was observed to impact arrival noise as shown in Figure 4-36. Measured noise increased at the three monitor locations by up to 0.03 dB for each additional 1000 lb increase in landing weight. Landing weight varied by approximately 40,000 lb at the three monitor locations. This meant that up to 1.2 dB variation in measured noise may have been attributable to variation in landing weight, although there may have been confounding factors. The trend was weakest at the far monitor and became stronger at the mid and close monitors. This may be because heavier aircraft require higher slat and flap extension levels and more thrust to maintain approach speed, increasing airframe and engine noise. Note that even though heavier aircraft approach at faster approach speeds, the results from Figure 4-37 (upcoming) suggest that true airspeed only weakly impacts noise propagation for arrivals close to the airport.

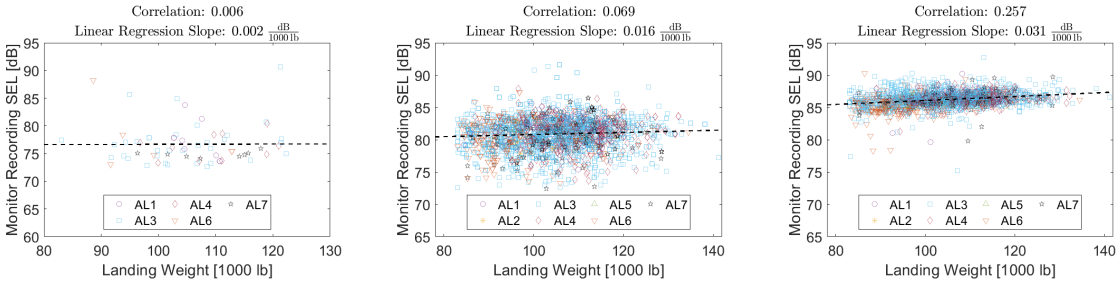

(a) North far monitor (b) North mid monitor (c) North close monitor

Figure 4-36: Weight Impact on Noise from Arriving B737NG Aircraft

Effect 3: True Airspeed

The impact of true airspeed on measured noise is shown in Figure 4-37. Measured noise was found to decrease by 0.2 dB for each additional 10 knots true airspeed at the far monitor. Airspeed was observed to vary by approximately 60 knots at the far monitor. This means that up to 1.2 dB variation in measured noise may have been attributable to variation in true airspeed. This finding was consistent with the delayed deceleration approach, which has been proposed to reduce noise at far distances from the airport. Aircraft performing delayed deceleration approaches fly faster approach speeds and remain cleanly configured for a longer duration of the approach, decreasing airframe noise and potentially engine noise due to lower thrust requirements. Measured noise was a weak function of airspeed at the mid and close monitors. At these monitors, aircraft were flying at airspeeds where flaps and slats were likely extended. The measured noise likely depended on the exact slat, flap, and landing gear positions, and the associated thrust.

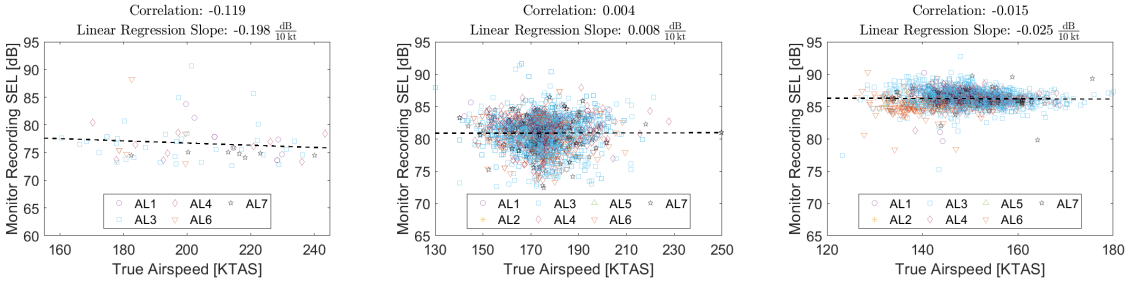

(a) North far monitor (b) North mid monitor (c) North close monitor

Figure 4-37: True Airspeed Impact on Noise from Arriving B737NG Aircraft

Effect 4: Altitude

The impact of altitude on measured noise is shown in Figure 4-38. Measured noise was observed to decrease by up to 0.7 dB at the far and mid monitors for each additional 1000 ft increase in altitude. Altitude was observed to vary by approximately 1000 ft at the far and mid monitors. This meant that approximately 0.7 dB variation in measured noise may have been attributable to variation in altitude, although there may have been confounding factors. Measured noise was observed to increase with altitude at the close monitor, but this effect was weak and may have been affected by factors such as variation in aircraft configuration close to the airport.

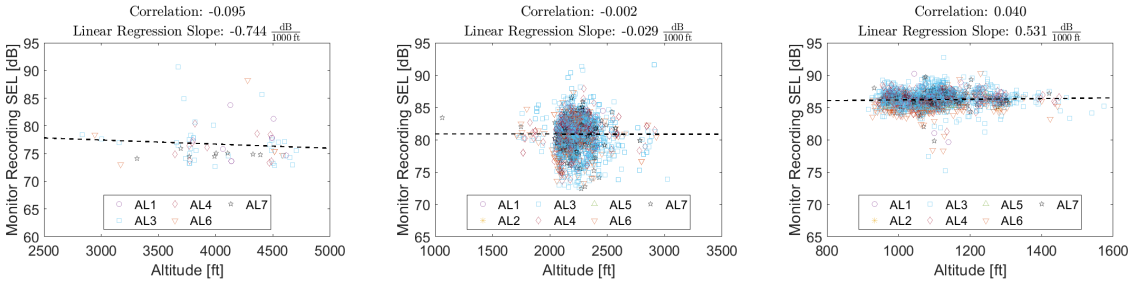

(a) North far monitor (b) North mid monitor (c) North close monitor

Figure 4-38: Altitude Impact on Noise from Arriving B737NG Aircraft

Effect 5: Flight Path Angle

Next, the impact of flight path angle on measured noise is shown in Figure 4-39. Measured noise increased by approximately 1.5 dB for each additional 10°increase in flight path angle at the mid and close monitors. Flight path angle was observed to vary by approximately 3°at the mid and close monitors. This meant that approximately 0.5 dB variation in measured noise may have been attributable to variation in flight path angle, although there may have been confounding factors. This trend was expected because aircraft approaching the runway at shallower approach angles would be expected to require more thrust to maintain airspeed. At the far monitor, measured noise was observed to decrease with flight path angle. This finding could have been caused by various factors that would require more data to validate. One possible explanation is that aircraft descending more steeply were more likely to do

so with spoilers or flaps extended, increasing airframe noise. However, flight data recorder data would be required to validate this hypothesis. More flyover data at the far monitor could also explain why the trend was reversed. It is possible that with more data at the north far monitor, the trend would be similar to those observed at the mid and close monitors.

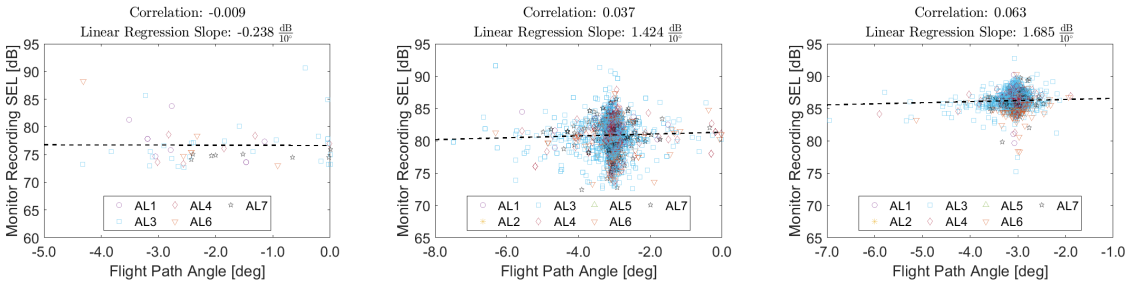

(a) North far monitor (b) North mid monitor (c) North close monitor

Figure 4-39: Flight Path Angle Impact on Noise from Arriving B737NG Aircraft

Next, the impact of environmental variables on measured noise was demonstrated at all three monitor locations. The environmental variables correlating with arrival noise at all three monitor locations were examined in order of strongest impact to weakest impact. Impact was determined by averaging the absolute value of the correlation coefficients at the close, mid, and far monitors. The environmental variable with the highest impact had the highest average correlation coefficient, and the variable with the lowest impact had the lowest average correlation coefficient.

Environmental Effect 1: Relative Humidity

As shown in Figure 4-40, measured noise increased by 0.1-0.2 dB for each additional 10% increase in relative humidity at the mid and close monitors. Relative humidity was observed to vary by approximately 60% at the two monitors. This meant that up to 1.2 dB variation in measured noise may have been attributable to variation in relative humidity, although there may have been confounding factors. This trend was consistent with the findings in [11], which demonstrates lower noise attenuation for increased relative humidity values above 20 percent. The opposite trend at the north far monitor was observed, but was possibly a result of the limited data set at the far

monitor.

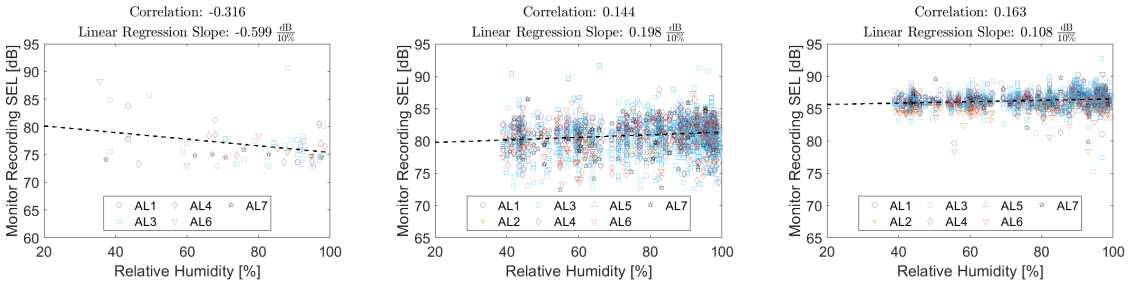

(a) North far monitor (b) North mid monitor (c) North close monitor

Figure 4-40: Relative Humidity Impact on Noise from Arriving B737NG Aircraft

Environmental Effect 2: Crosswind (Eastward Wind)

The impact of the crosswind (eastward) component at the three monitor locations is shown in Figure 4-41. Measured noise varied by up to 1.4 dB for each additional 10 knots of crosswind. The crosswind component was observed by vary by approximately 30 knots. This meant that up to 4.2 dB variation in measured noise may have been attributable to variation in the crosswind component, although there may have been confounding factors. This observation may be explained by advection. Noise advected towards or away from the monitors depending on the direction of the eastward wind and the location of the airplane relative to the monitor being examined.

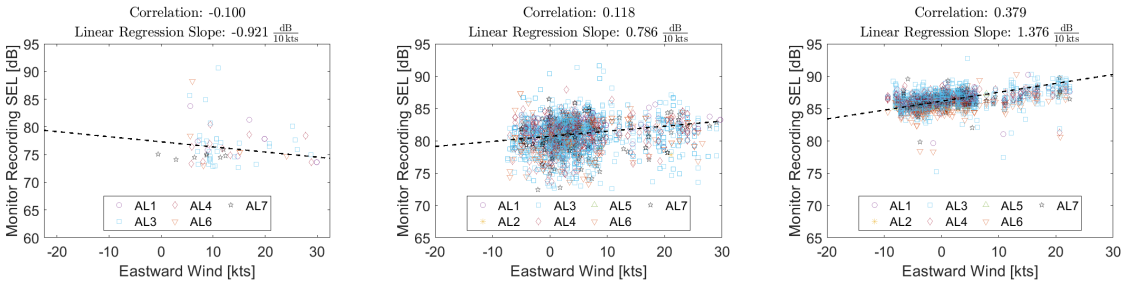

(a) North far monitor (b) North mid monitor (c) North close monitor

Figure 4-41: Eastward Wind (Crosswind) Impact on Noise from Arriving B737NG Aircraft

Environmental Effect 3: Temperature

The impact of temperature is shown in Figure 4-42. Measured noise correlated weakly with temperature. Measured noise was observed to vary by 0.7-0.9 dB for each additional 10°C increase in temperature at the three monitors. Temperature was observed to vary by approximately 20°C at each monitor. This meant that up to 1.8 dB variation in measured noise may have been attributable to variation in temperature, although there may have been confounding factors. Measured noise was observed to increase at the far monitor, and decrease at the mid and close monitors. Measured noise was expected to increase with temperature given that attenuation is known to decrease with temperature. The behavior observed at the mid and close monitors is consistent with the behavior observed for departures, but remains a source of uncertainty.

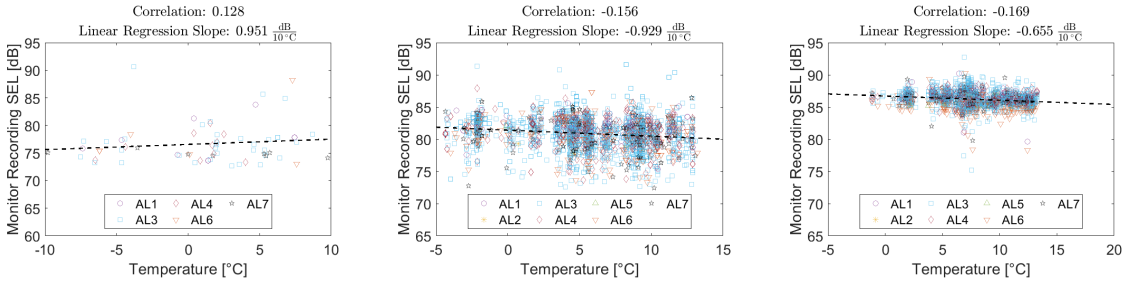

(a) North far monitor (b) North mid monitor (c) North close monitor

Figure 4-42: Temperature Impact on Noise from Arriving B737NG Aircraft

Environmental Effect 4: Headwind (Northward Wind)

The impact of headwind is shown in Figure 4-43. Measured noise was observed to correlate most strongly with northward wind at the close monitor, where a 10 knot change in headwind increased measured noise by up to 1.5 dB. Northward wind was observed to vary by 30 knots at the close monitor. This meant that up to 4.5 dB variation in measured noise may have been attributable to variation in headwind, although there may have been confounding factors. For arrivals, the headwind component was expected to impact noise by means of advection, since the improvement in climb performance associated with headwind was more relevant to departures than arrivals.

Therefore, the impact of headwind was expected to vary based on the location of the aircraft relative to the noise monitor at the point of closest approach.

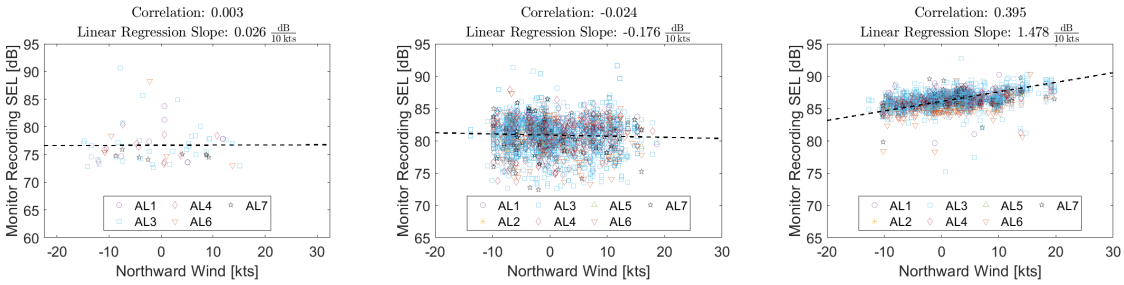

(a) North far monitor (b) North mid monitor (c) North close monitor

Figure 4-43: Northward Wind (Headwind) Impact on Noise from Arriving B737NG Aircraft

4.5.3 Impact of Airline-Specific Arrival Procedures on Measured B737NG Noise

Figure 4-44 shows how departure performance parameters for each airline varied relative to the average B737NG flyover. The difference between the average airline parameter and the average overall parameter was then normalized by the maximum difference so that all values fell between -1 and 1. Airlines that registered more than 10 noise measurements were included. The average performance parameter values for each airline are given in Appendix C.

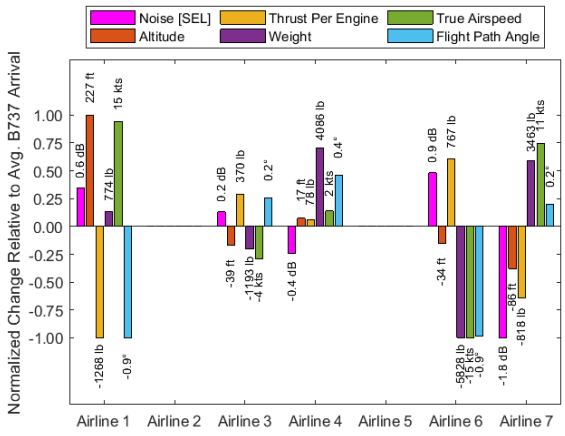

(a) North far monitor

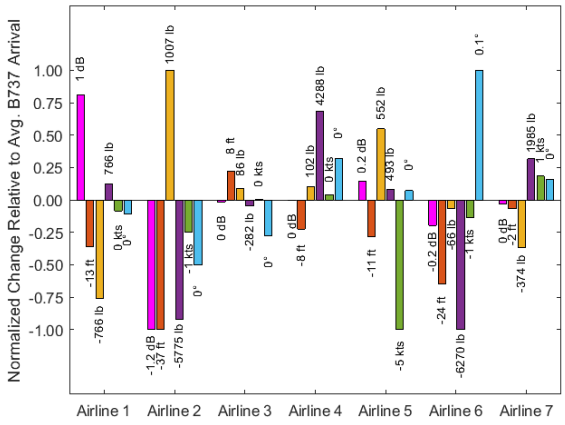

(b) North mid monitor

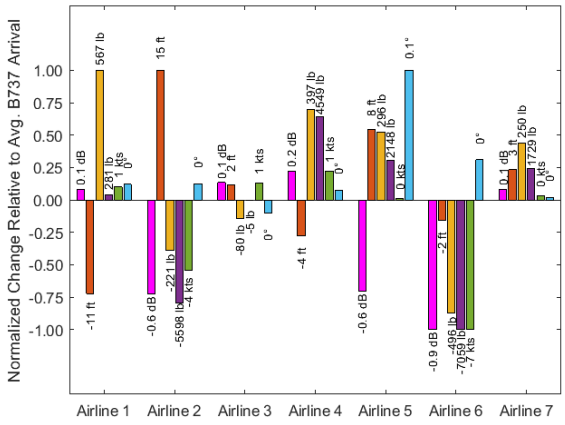

(c) North close monitor

Figure 4-44: B737NG Arrival Performance Parameter Averages by Airline Relative to Average B737NG Southbound Arrival

At the north far monitor, the aircraft operated by Airline 7 were observed to be the quietest on average by 1.8 dB. These aircraft overflew the north far monitor 11 kts faster and with approximately 800 lb less thrust per engine than the average B737NG. The next quietest airline was Airline 4, which was quieter than the average by 0.4 dB and overflew the monitor 2 kts faster than the average. These findings were consistent with the delayed deceleration approach concept, where delaying deceleration allows the aircraft to remain cleanly configured and at lower thrust until the final approach stabilization point. It is interesting that Airline 1, which was observed to overfly the north far monitor 15 knots faster and with approximately 1300 lb less thrust per engine than the average, was 0.4 dB louder than the average. The steeper-than-average flight path angle may suggest that the aircraft was descending with spoilers deployed, increasing airframe noise. However, this hypothesis must be validated using flight data recorder data.

4.5.4 Airbus A320 Arrival Noise Trends

Trends for the Airbus A320 follow at the far, mid, and close monitors follow in Figures 4-47, 4-46, and 4-45, respectively. Note that available data for aircraft arrivals was limited at the north far monitor.

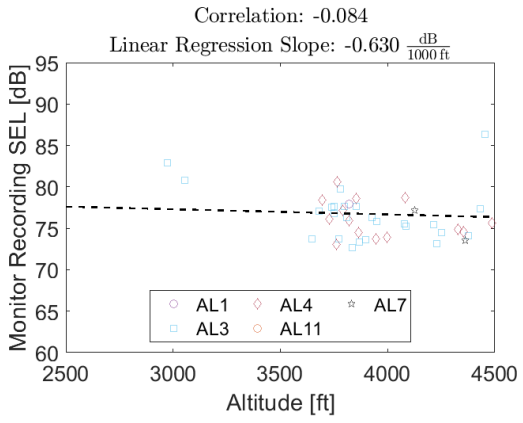

(a) Altitude impact, north far monitor

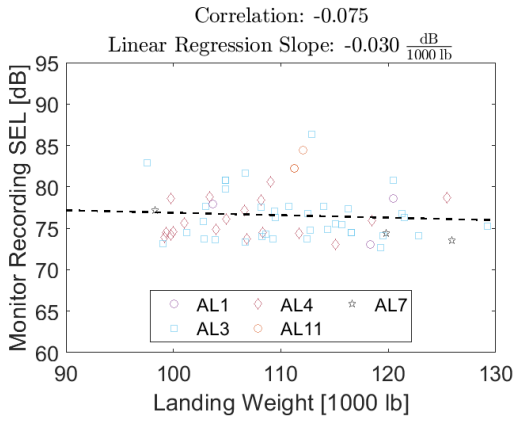

(b) Weight impact, north far monitor

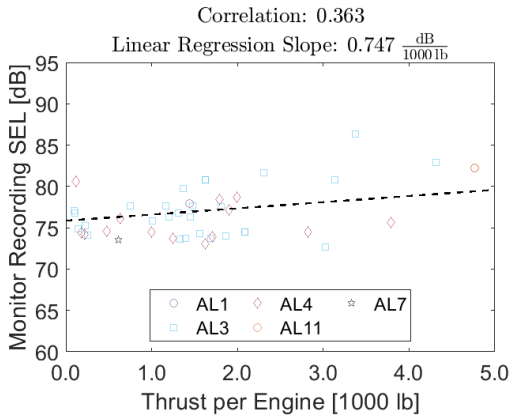

(c) Thrust impact, north far monitor

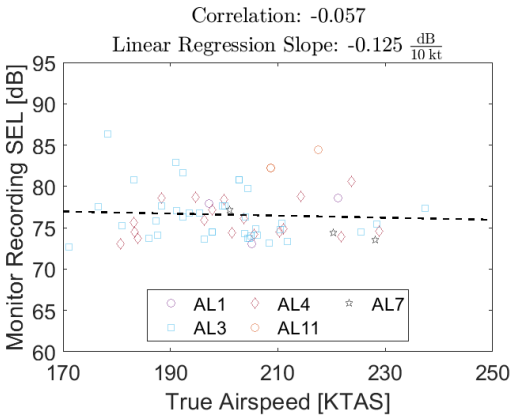

(d) True airspeed impact, north far monitor

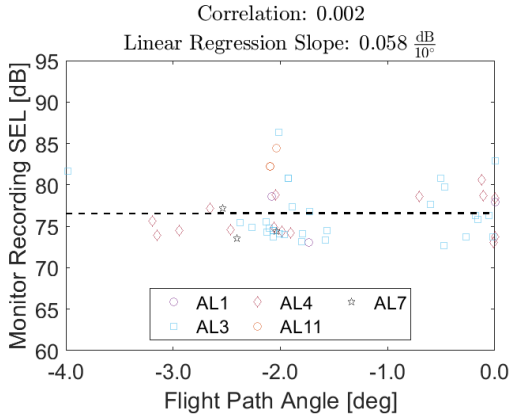

(e) Flight path angle impact, north far monitor

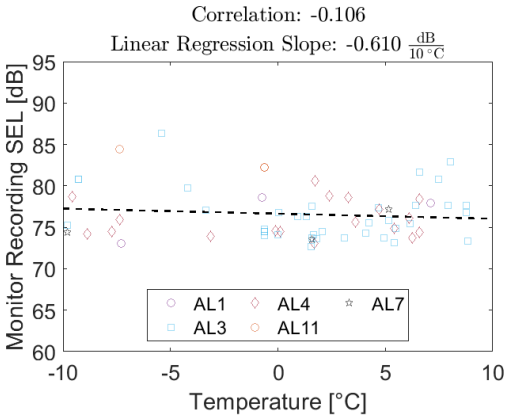

(f) Temperature impact, north far monitor

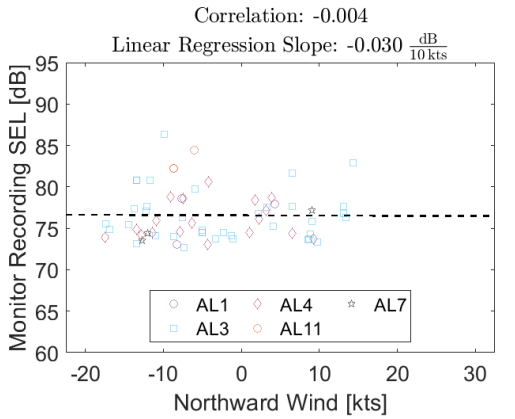

(g) Northward wind (headwind) impact, north far monitor. Northward wind positive to the north

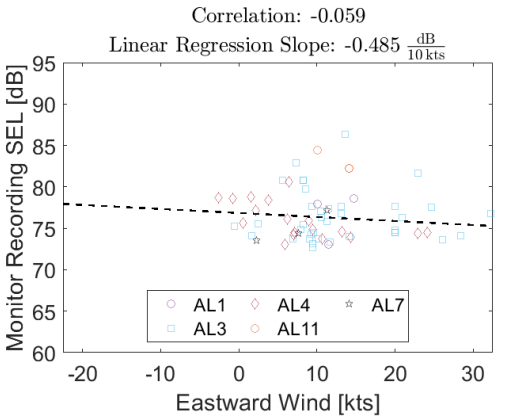

(h) Eastward wind (crosswind) impact, north far monitor. Eastward wind positive to the east

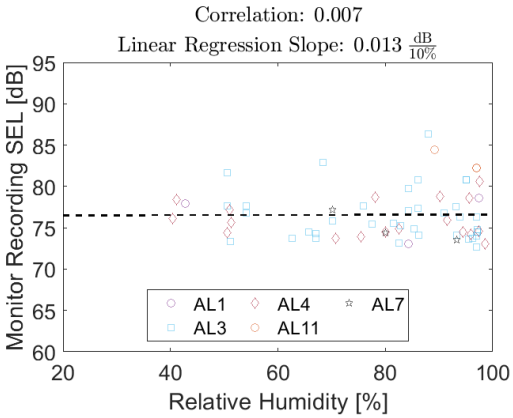

(i) Relative humidity wind impact, north far monitor

Figure 4-45: Trends for arriving Airbus A320s at the north far monitor

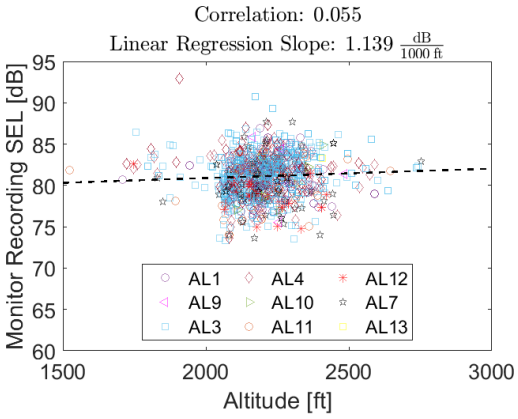

(a) Altitude impact, north mid monitor

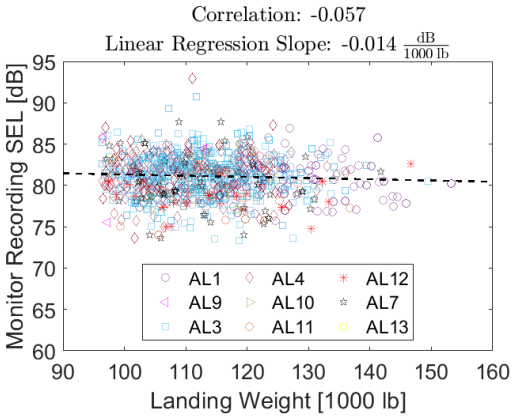

(b) Weight impact, north mid monitor

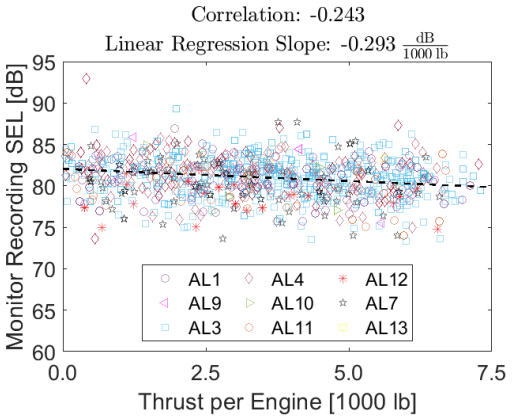

(c) Thrust impact, north mid monitor

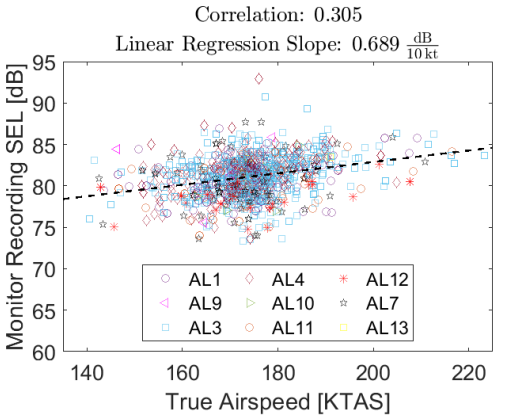

(d) True airspeed impact, north mid monitor

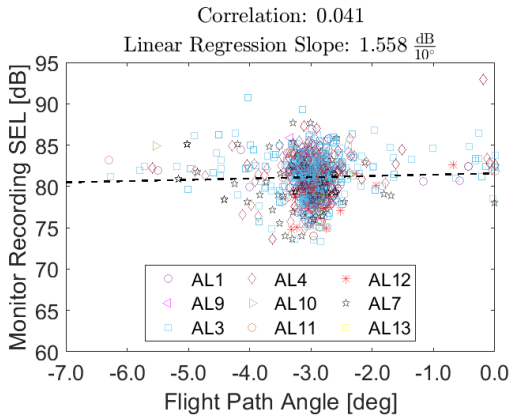

(e) Flight path angle impact, north mid monitor

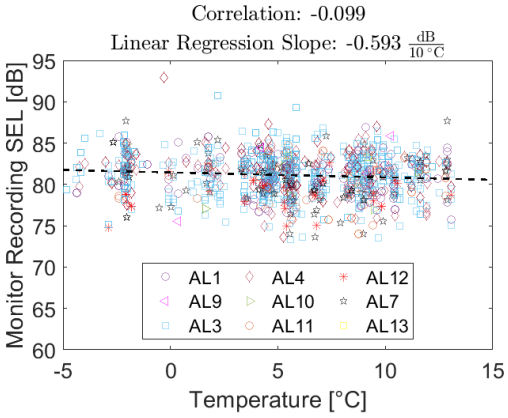

(f) Temperature impact, north mid monitor

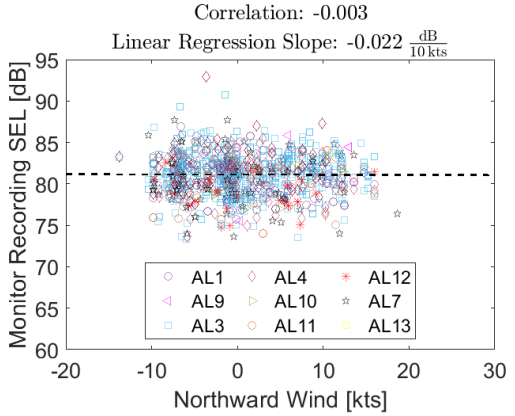

(g) Northward wind (headwind) impact, north mid monitor. Northward wind positive to the north

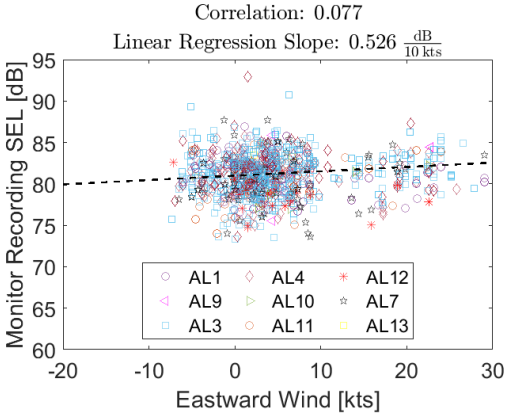

(h) Eastward wind (crosswind) impact, north mid monitor. Eastward wind positive to the east

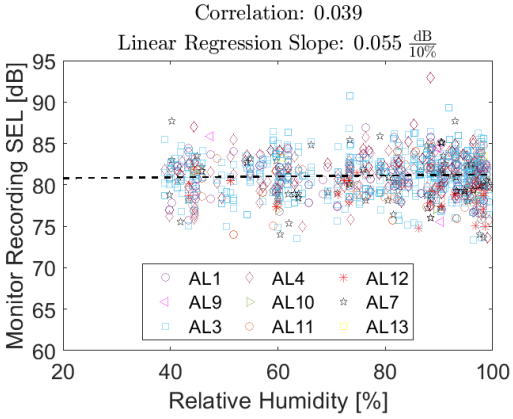

(i) Relative humidity wind impact, north mid monitor

Figure 4-46: Trends for arriving Airbus A320s at the north mid monitor

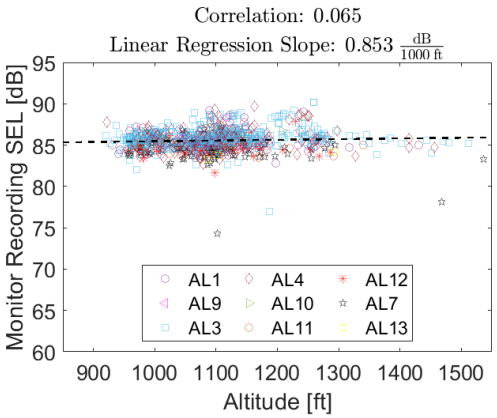

(a) Altitude impact, north close monitor

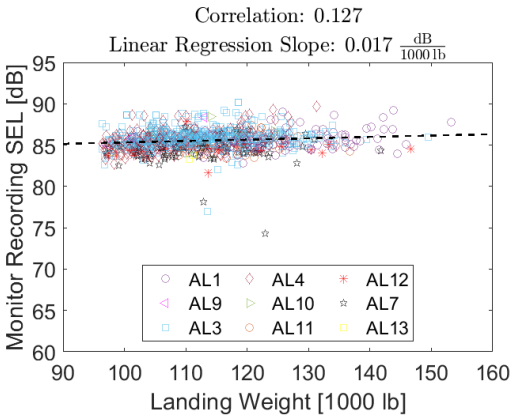

(b) Weight impact, north close monitor

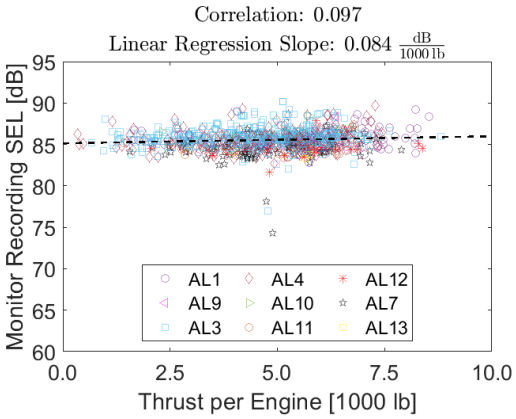

(c) Thrust impact, north close monitor

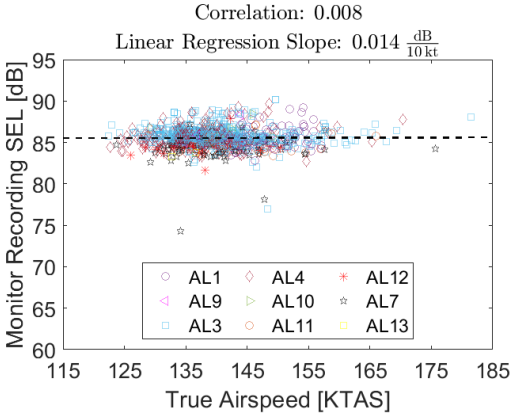

(d) True airspeed impact, north close monitor

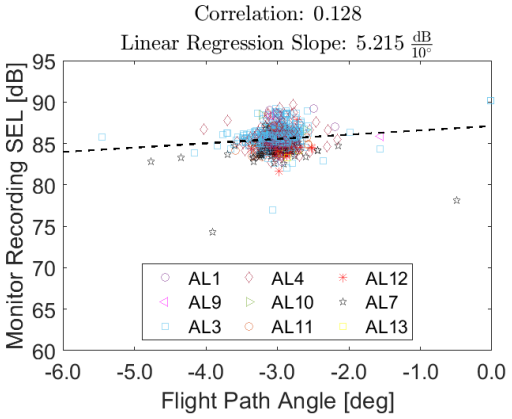

(e) Flight path angle impact, north close monitor

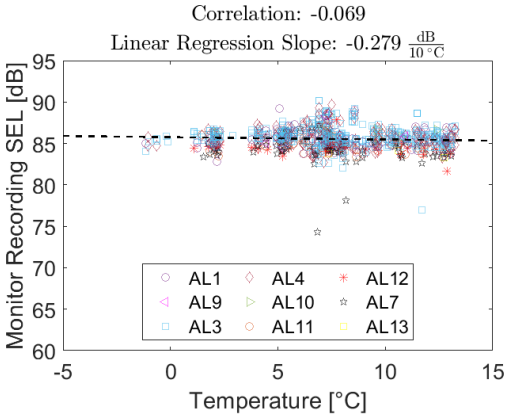

(f) Temperature impact, north close monitor

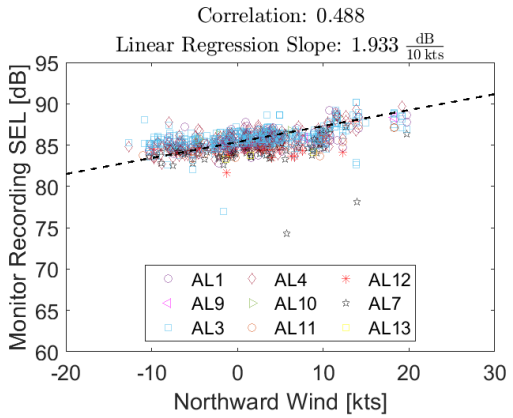

(g) Northward wind (headwind) impact, north close monitor. Northward wind positive to the north

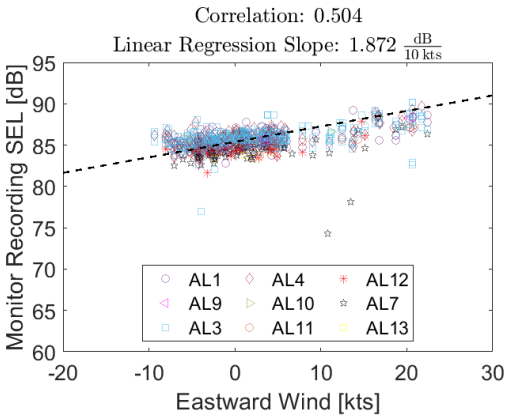

(h) Eastward wind (crosswind) impact, north close monitor. Eastward wind positive to the east

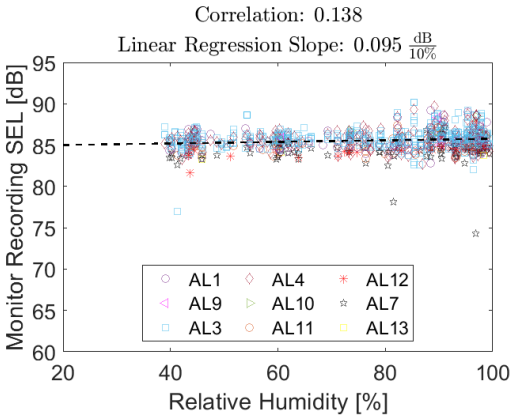

(i) Relative humidity wind impact, north close monitor

Figure 4-47: Trends for arriving Airbus A320s at the north close monitor

4.5.5 Analysis of Airbus A320 Arrival Noise Trends

The variables correlating with arrival noise at all three monitor locations were examined in order of strongest impact to weakest impact. Impact was determined by averaging the absolute value of the correlation coefficients at the close, mid, and far monitors. The variable with the highest impact had the highest average correlation coefficient, and the variable with the lowest impact had the lowest average correlation coefficient.

Effect 1: Thrust

Thrust was observed to have the greatest impact on measured A320 arrival noise as shown in Figure 4-48. Measured noise increased by up to 0.75 dB for each additional 1000 lb of increased thrust at the close and far monitors. Modeled thrust varied by approximately 5000 lb at these monitors. This meant that up to 3.8 dB variation in measured noise may have been attributed to variation in thrust, although there may have been confounding factors. This trend was expected because engine noise was previously known to correlate with thrust levels, all other factors constant. The opposite trend was observed at the mid monitor. This trend was likely observed because thrust was modeled as a function of assumed slat, flap, and landing gear deployment schedules, potentially leading to unreliable thrust estimates in some cases. Had the actual deployment schedules been known, modeled thrust would have been less susceptible to modeling error.

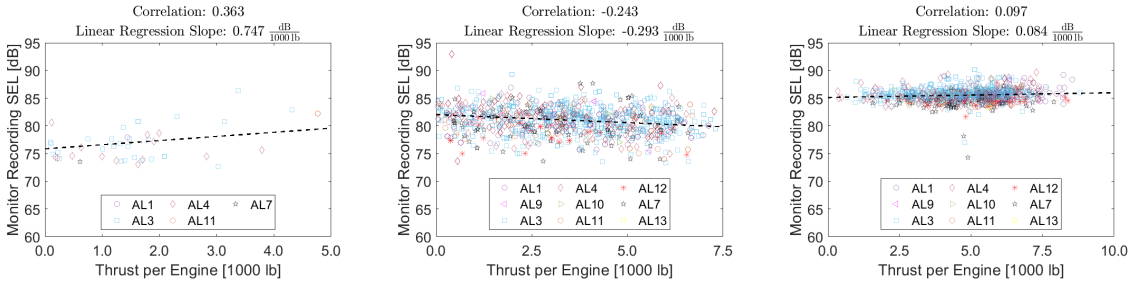

(a) North far monitor (b) North mid monitor (c) North close monitor

Figure 4-48: Thrust Impact on Noise from Arriving A320 Aircraft

Effect 2: True Airspeed

The impact of true airspeed on measured noise is shown in Figure 4-49. Measured noise was found to decrease by approximately 0.1 dB for each additional 10 knots true airspeed at the far monitor. Airspeed was observed to vary by approximately 60 knots at the far monitor. This means that up to 0.6 dB variation in measured noise may have been attributable to variation in true airspeed. This finding was consistent with the delayed deceleration approach, which has been proposed to reduce noise at far distances from the airport. Aircraft performing delayed deceleration approaches

fly faster approach speeds and remain cleanly configured for a longer duration of the approach, decreasing airframe noise and potentially engine noise due to lower thrust requirements. Measured noise was observed to increase with airspeed at the mid and close monitors. At these monitors, aircraft were flying at airspeeds where flaps and slats were likely extended, so flying at higher airspeeds would be expected to increase airframe noise at these monitors.

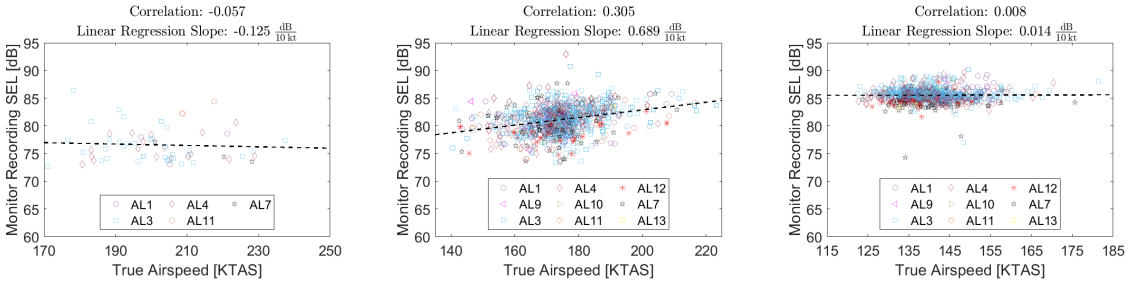

(a) North far monitor (b) North mid monitor (c) North close monitor

Figure 4-49: True Airspeed Impact on Noise from Arriving A320 Aircraft

Effect 3: Landing Weight

Next, landing weight was observed to impact arrival noise as shown in Figure 4-50. Measured noise was a weak function of landing weight, but was observed to correlate most strongly at the close monitor, where a 1000 lb increase in thrust increased measured noise by approximately 0.02 dB on average. Landing weight was observed to vary by approximately 50,000 lb at the north close monitor. This meant that up to 1 dB variation in measured noise may have been attributable to variation in landing weight at the north close monitor, although there may have been confounding factors. The opposite trend was observed at the far and mid monitors, although the correlation was weak. This behavior was not expected since heavier aircraft typically configure earlier and at higher airspeeds than light aircraft.

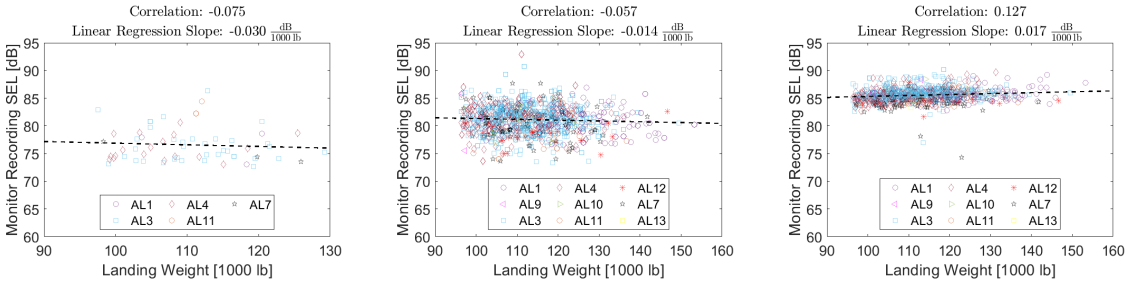

(a) North far monitor (b) North mid monitor (c) North close monitor

Figure 4-50: Weight Impact on Noise from Arriving A320 Aircraft

Effect 4: Altitude

The impact of altitude on measured noise is shown in Figure 4-51. Measured noise was observed to increase with altitude at the mid and close monitors. This trend was unexpected and may have been affected by factors such as variation in aircraft configuration close to the airport. At the far monitor, noise decreased by approximately 0.6 dB for each additional 1000 ft increase in altitude. Altitude was observed to vary by approximately 1000 ft at the far monitor. This meant that approximately 0.6 dB variation in measured noise was potentially attributable to variation in altitude at the far monitor, although there may have been confounding factors.

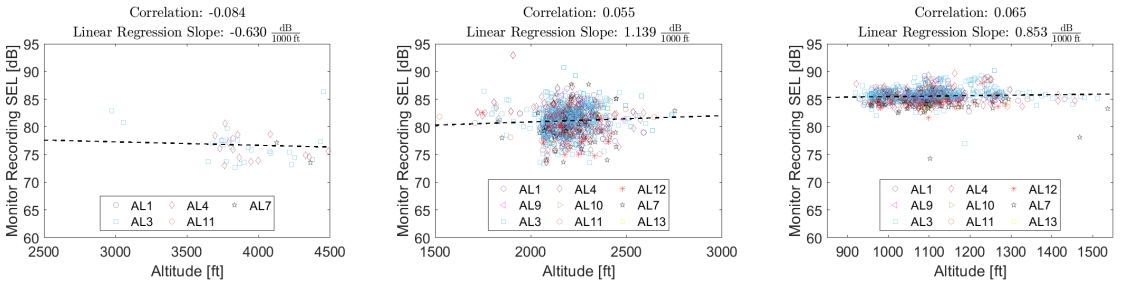

(a) North far monitor (b) North mid monitor (c) North close monitor

Figure 4-51: Altitude Impact on Noise from Arriving A320 Aircraft

Effect 5: Flight Path Angle

Next, the impact of flight path angle on measured noise is shown in Figure 4-52. Measured noise increased at each monitor by up to 5.2 dB for each additional 10°increase in flight path angle. Flight path angle was observed to vary by approximately 3°at

the mid and close monitors. This meant that approximately 1.5 dB variation in measured noise may have been attributable to variation in flight path angle, although there may have been confounding factors. This trend was expected because aircraft approaching the runway at shallower approach angles would be expected to require more thrust to maintain airspeed.

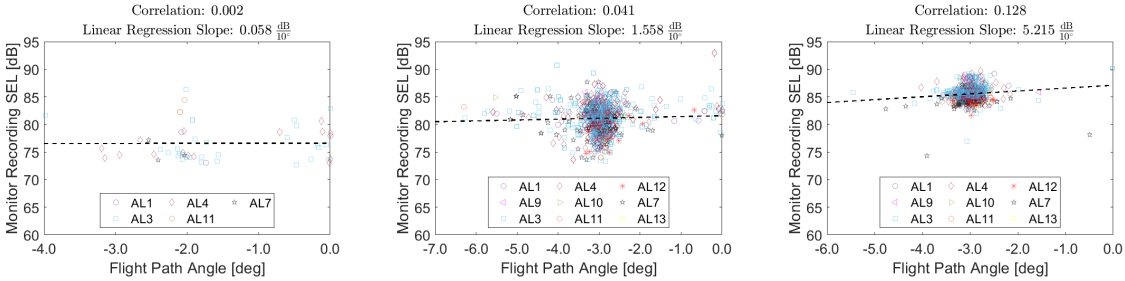

(a) North far monitor (b) North mid monitor (c) North close monitor

Figure 4-52: Flight Path Angle Impact on Noise from Arriving A320 Aircraft

Next, the impact of environmental variables on measured noise was demonstrated at all three monitor locations. The environmental variables correlating with arrival noise at all three monitor locations were examined in order of strongest impact to weakest impact. Impact was determined by averaging the absolute value of the correlation coefficients at the close, mid, and far monitors. The environmental variable with the highest impact had the highest average correlation coefficient, and the variable with the lowest impact had the lowest average correlation coefficient.

Environmental Effect 1: Crosswind (Eastward Wind)

The impact of the crosswind (eastward) component at the three monitor locations is shown in Figure 4-53. Measured noise varied by up to 1.9 dB for each additional 10 knots of crosswind. The crosswind component was observed by vary by approximately 30 knots. This meant that up to 5.7 dB variation in measured noise may have been attributable to variation in the crosswind component, although there may have been confounding factors. This observation may be explained by advection. Noise advected towards or away from the monitors depending on the direction of the eastward wind and the location of the airplane relative to the monitor being examined. Note that

the strongest correlation and steepest slope were observed at the close monitor. This trend was observed for the headwind component, which follows.

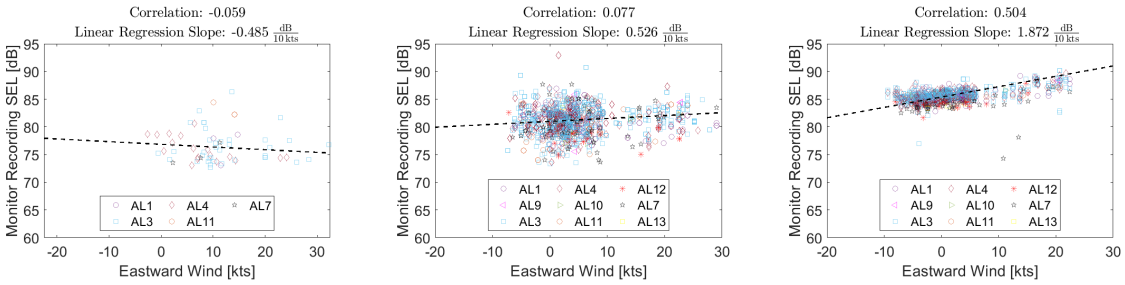

(a) North far monitor (b) North mid monitor (c) North close monitor

Figure 4-53: Eastward Wind (Crosswind) Impact on Noise from Arriving A320 Aircraft

Environmental Effect 2: Headwind (Northward Wind)

The impact of headwind is shown in Figure 4-54. Measured noise was observed to correlate most strongly with northward wind at the close monitor, where a 10 knot change in headwind increased measured noise by up to 1.9 dB. Northward wind was observed to vary by 30 knots at the close monitor. This meant that up to 5.7 dB variation in measured noise may have been attributable to variation in headwind, although there may have been confounding factors. For arrivals, the headwind component was expected to impact noise by means of advection, since the improvement in climb performance associated with headwind was more relevant to departures than arrivals. Therefore, the impact of headwind was expected to vary based on the location of the aircraft relative to the noise monitor at the point of closest approach. It is interesting that both the headwind and crosswind components had the strongest impact on measured noise for A320 arrivals at the close monitor. Similar behavior for both the headwind and crosswind components was observed for the B737NG arrivals at the close monitor as shown in Figures 4-41 and 4-43. This indicates that advection may have a stronger impact on arrival noise close to the airport.

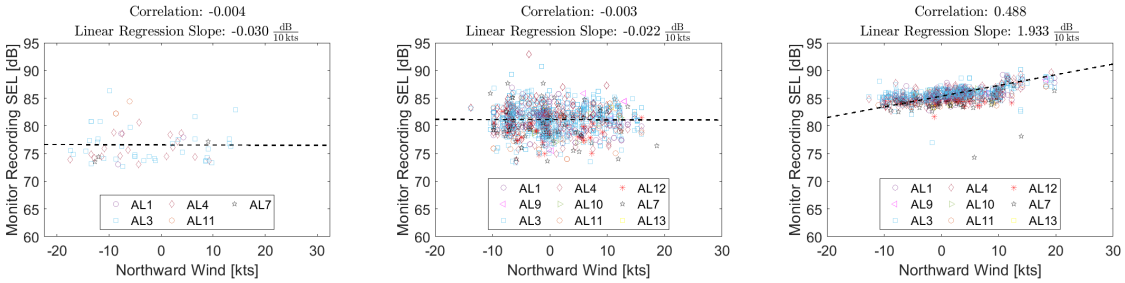

(a) North far monitor (b) North mid monitor (c) North close monitor

Figure 4-54: Northward Wind (Headwind) Impact on Noise from Arriving A320 Aircraft

Environmental Effect 3: Temperature

The impact of temperature is shown in Figure 4-55. Measured noise correlated weakly with temperature. Measured noise was observed to decrease by 0.3-0.6 dB for each additional 10°C increase in temperature at the three monitors. Temperature was observed to vary by approximately 15°C at each monitor. This meant that up to 0.5-0.9 dB variation in measured noise may have been attributable to variation in temperature, although there may have been confounding factors. Measured noise was expected to increase with temperature, given that attenuation decreases with temperature. This behavior remains a source of uncertainty.

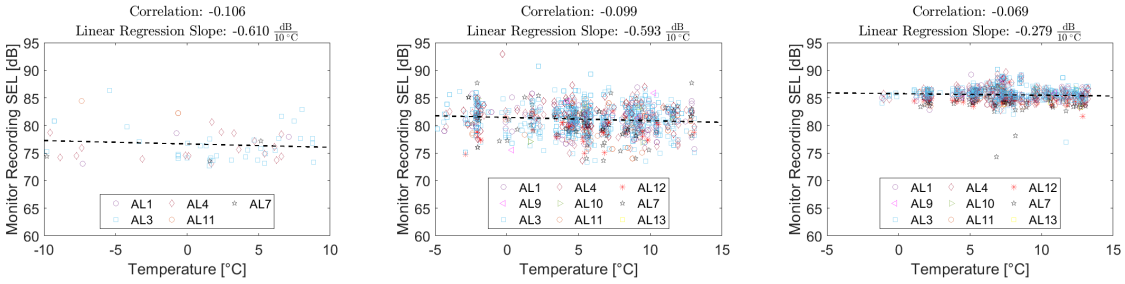

(a) North far monitor (b) North mid monitor (c) North close monitor

Figure 4-55: Temperature Impact on Noise from Arriving A320 Aircraft

Environmental Effect 4: Relative Humidity

As shown in Figure 4-56, measured noise increased by up to 0.1 dB for each additional 10% increase in relative humidity at the mid and close monitors. Relative humidity

was observed to vary by approximately 60% at the two monitors. This meant that up to 0.6 dB variation in measured noise may have been attributable to variation in relative humidity, although there may have been confounding factors. This trend was consistent with the findings in [11], which demonstrates lower noise attenuation for increased relative humidity values above 20 percent. The opposite trend at the north far monitor was observed, but was possibly a result of the limited data set at the far monitor.

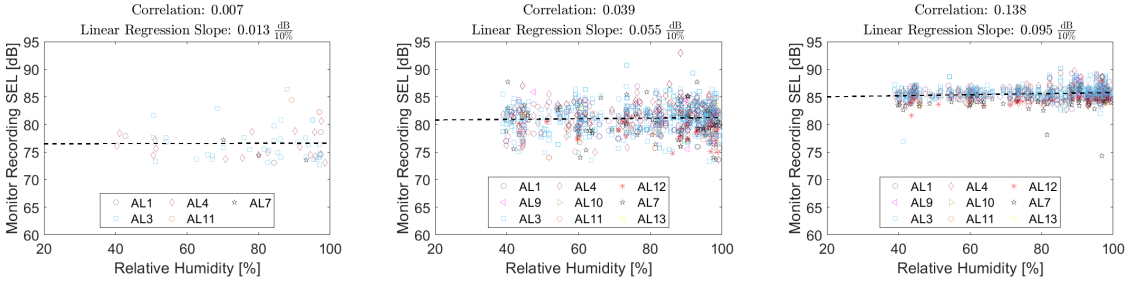

(a) North far monitor (b) North mid monitor (c) North close monitor

Figure 4-56: Relative Humidity Impact on Noise from Arriving A320 Aircraft

4.5.6 Impact of Airline-Specific Arrival Procedures on Measured A320 Noise

Figure 4-57 shows how departure performance parameters for each airline varied relative to the average A320 flyover. The difference between the average airline parameter and the average overall parameter was then normalized by the maximum difference so that all values fell between -1 and 1. The average performance parameter values for each airline are given in Appendix C.

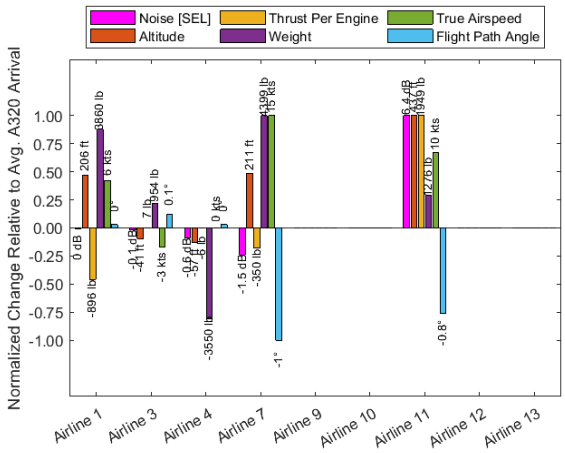

(a) North far monitor

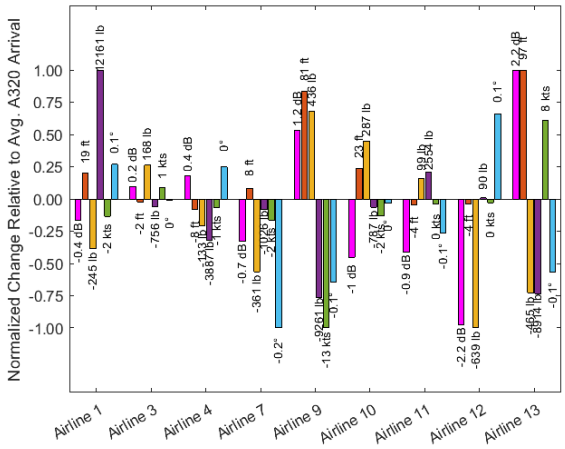

(b) North mid monitor

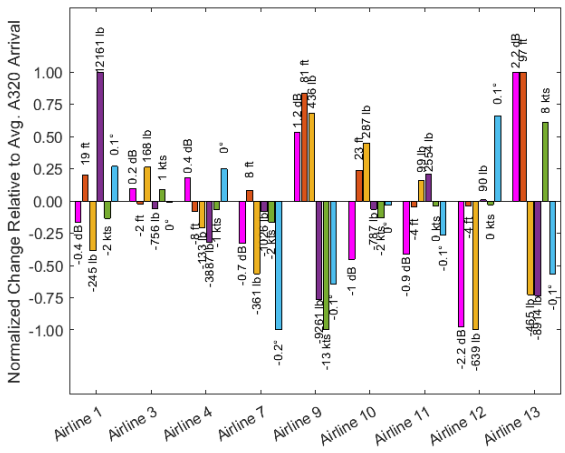

(c) North close monitor

Figure 4-57: A320 Arrival Performance Parameter Averages by Airline Relative to Average A320 Southbound Arrival

At the north far monitor, the aircraft operated by Airline 7 were observed to be the quietest on average by 1.5 dB. These aircraft overflew the north far monitor 15 kts faster and with approximately 350 lb less thrust per engine than the average A320. The next quietest airline was Airline 4, which was quieter than the average by 0.6 dB and overflew the monitor at the average airspeed. These aircraft were lighter than the average A320 by approximately 3500 lb. The finding for Airline 7 was consistent with the delayed deceleration approach concept, where delaying deceleration allows the aircraft to remain cleanly configured and at lower thrust until the final approach stabilization point. It is interesting that Airlines 4 and 7 were also observed to be the quietest airlines at the north far monitor for the B737NG. This may suggest that these airlines employ a procedure that delays deceleration far from the airport.

4.5.7 Arrival Noise Data Summary

Thrust and airspeed were shown to have the strongest effect on community noise exposure due to aircraft arrivals. At far monitors, measured noise was observed to decrease as true airspeed increased. This finding was consistent with the delayed deceleration approach. The delayed deceleration approach may require less thrust (and therefore, produce less engine noise) and produce less airframe noise by enabling the aircraft to fly in cleanly configured states for a longer duration of the approach. The delayed deceleration approach could be validated using flight data recorder data or by modeling noise due to aircraft flying at various approach speeds far from the airport. Environmental factors including ambient wind and relative humidity were shown to have impacts on climb performance (headwind), advection of noise (crosswind), and attenuation of noise (relative humidity). Model-based validations of the delayed deceleration approach and the community noise impacts of aircraft weight and ambient relative humidity follow in Chapter 5.

Chapter 5

Model-Based Validation of the Factors Contributing to Community Noise due to Aircraft Arrivals

The purpose of this chapter is to model the impacts of the variables found to correlate with aircraft noise in Chapter 4. First, the noise impacts of aircraft weight and relative humidity were modeled, since both were shown to impact noise due to departures and arrivals. Next, the noise from aircraft flying delayed deceleration approaches was modeled. Community noise due to arriving aircraft was shown in the data-driven exploration of Chapter 4 to vary inversely with true airspeed at the far monitor. This finding was consistent with the delayed deceleration approach concept, which has been shown to have community noise reduction potential far (> 8 nm) from the airport.

5.1 Modeled Impacts of Aircraft Weight and Relative Humidity on Community Noise Exposure

The impact of aircraft weight on noise exposure was modeled for arrivals. A reference Boeing 737-800 approach into Seattle, shown in Figure 5-1 (a), was modeled at

approach weights ranging from 70% Maximum Landing Weight (MLW) to MLW in 10% increments. 70% MLW was treated as a lower bound on weight for this study, since weights below this approach the Operating Empty Weight (OEW).

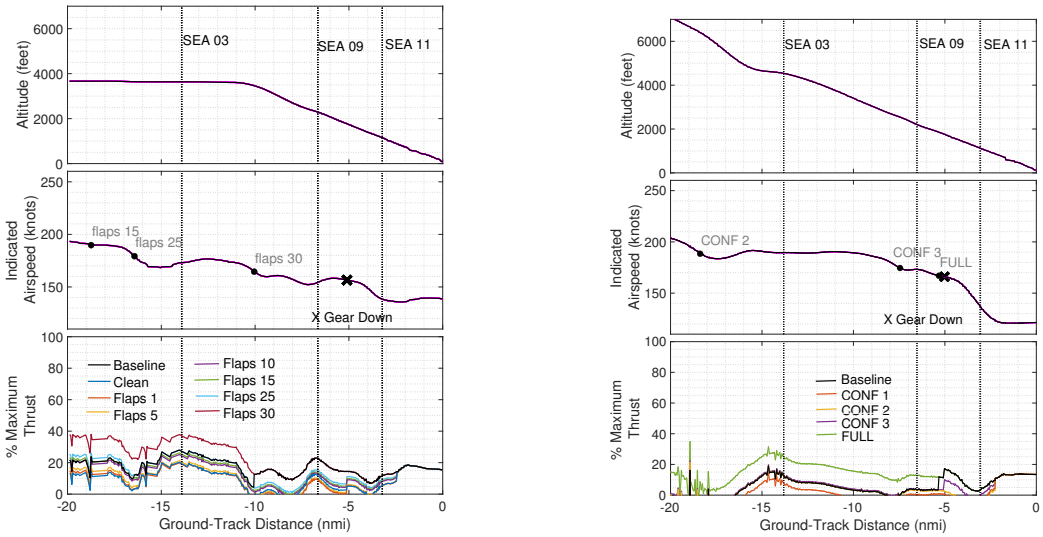

(a) Boeing 737-800 (b) Airbus A320

Figure 5-1: Example ADS-B velocity and altitude profiles and modeled thrust levels at different configuration settings

Each approach weight was modeled at each flap setting to determine the corresponding final approach noise. Sound exposure level (SEL) noise results at SEA11, whose location is shown in Figure 5-1, are given in Figure 5-2.

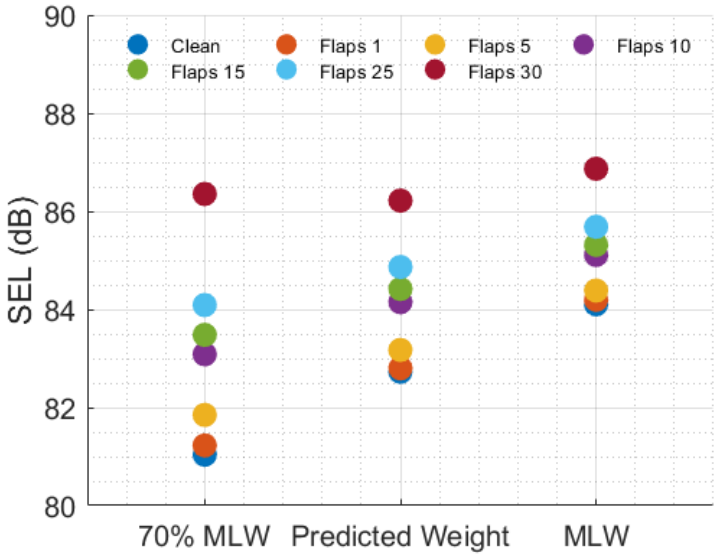

Figure 5-2: Variation in predicted noise with weight for a Boeing 737-800 reference approach into SEA

The results in Figure 5-2 demonstrate that approach weight has a measurable effect on noise at clean and lower flap settings (i.e., Flaps 1 - Flaps 5), but for higher flap settings (i.e., Flaps 25 and above) the effect of weight on noise is diminished. For the Boeing 737-800, there is a 2-3 dB difference in predicted noise between the 70% MLW and MLW cases for the Clean - Flaps 5 cases, while the difference is less than 1 dB for Flaps 30. This suggests that at lower flap settings, the increase in thrust associated with heavier landing weights increases predicted total noise by 2-3 dB. At higher flap settings, the airframe noise component is more significant, therefore changes in engine noise due to changes in thrust have less impact on overall noise than in the case where the airframe is clean. The modeled impact of weight on noise is consistent with the results of the data-driven approach of Chapter 4, which at the north close monitor reports the magnitude of the noise impact to be approximately 0.03 dB/1000 lb (note that SEA11 is placed near the north close monitor). For the 30% difference in MLW for the Boeing 737-800, this corresponds to a difference of 1.6 dB at the close and mid monitors. Therefore, estimating weight correctly is critical to generating realistic thrust and flap configuration estimates, which in turn contribute to plausible engine and airframe noise estimates, respectively.

Relative humidity was also shown to impact noise propagation. The impact of relative humidity was therefore modeled in ANOPP to determine whether modeled results are consistent with results from the data-driven study of Chapter 4. Attenuation due to relative humidity was modeled in ANOPP using the ANSI S1.26-2014 method [2]. To demonstrate the sensitivity of predicted noise to atmospheric conditions, noise from the baseline A320 flight from Figure 5-1(b) was modeled at SEA11 with the actual relative humidity and temperature recorded during that flight, as well as with relative humidity values of 20% and 100%, at two operating conditions. Variations in noise of up to 3 dB are predicted between the 20% and 100% relative humidity cases as shown in Figure 5-3 for the different altitude conditions. The modeled impact of relative humidity on noise is consistent with the results of the data-driven approach of Chapter 4, which at the north close monitor reports the magnitude of the noise impact to be approximately 0.35 dB/10%. For the 80% change in relative humidity modeled here, this corresponds to a 2.8 dB variation in noise. Note from the example data shown in Figure 3-4 that the relative humidity at 4000 ft varied between 80-85%, and that the relative humidity at 1000 ft was approximately 75%. Therefore, accounting for spatial and vertical variation in relative humidity is essential to generating reasonable aircraft noise estimates; incorrect assumptions could lead to noise estimates that vary from measured values by 3 dB.

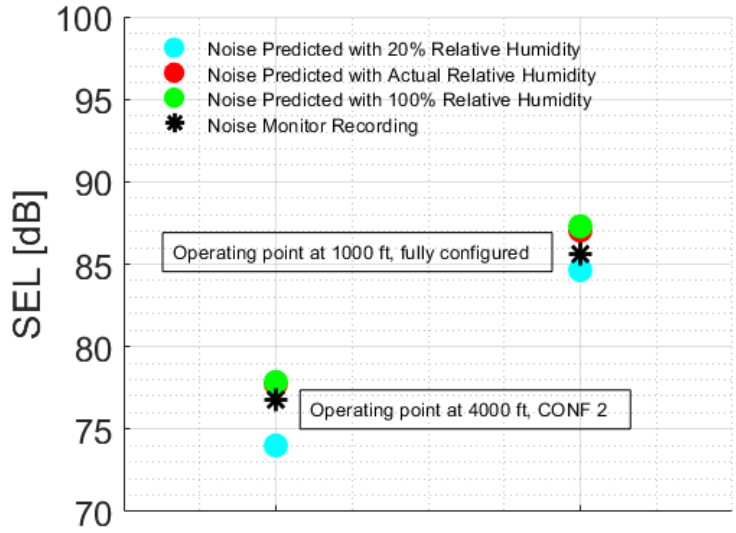

Figure 5-3: Example humidity impact on predicted noise for an Airbus A320 flight

5.2 Model-Based Validation of the Delayed Deceleration Approach

Delayed deceleration approaches (DDAs) have previously been identified as a potential arrival noise abatement procedure [24] [23]. This is consistent with the findings in the data-driven analysis of factors correlating with aircraft noise of Chapter 4. The delayed-deceleration approach concept is demonstrated in Figure 5-4, which shows Boeing 737-800s on approach into Boston Logan Airport (BOS) in 2017. As shown in Figure 5-4, velocity on approach varies before the final approach stabilization point, the point at which aircraft must be fully configured for landing. Factors including air traffic, weather, and airline operations can contribute to this variation in speed. The mean velocity profile and sample early-deceleration and delayed-deceleration approaches are highlighted. While flap and slat deployment can occur over a range of velocities, an aircraft that decelerates early will typically configure earlier than an aircraft that delays its deceleration. The markers in Figure 5-4 denote the locations where flaps and slats would be deployed on the early deceleration and delayed decel-

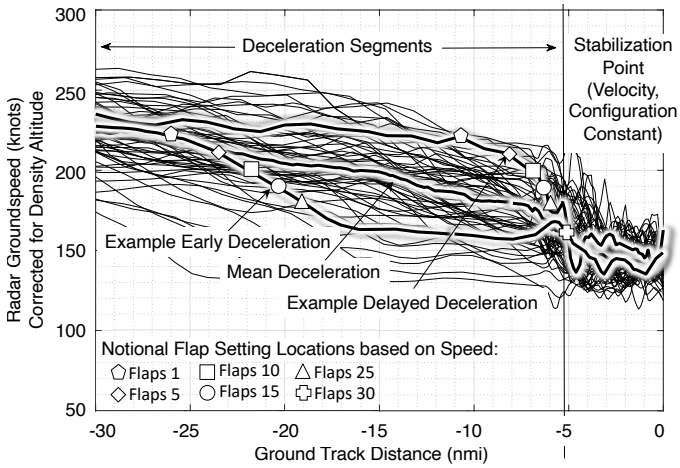

Figure 5-4: Radar velocity data and notional flap settings of example Boeing 737-800 approaches, indicating significant velocity variation prior to stabilization point. Adapted from Figure 1 of [23]

eration profiles if configuration deployment occurred at the same speed. In addition, aircraft that decelerate earlier in the approach will require more thrust to compensate for drag that arises from configuring the slats, flaps, and landing gear earlier [24] [23]. Reduced engine thrust due to delayed deceleration and flap deployment has been shown to yield fuel burn reductions [5][23].

The model-based validation was conducted for Boeing 737-800, Airbus A320, and Embraer E190 flights at Boston Logan International Airport in 2015 and 2016 [17] and Seattle Tacoma International Airport in 2019. Thrust was modeled based on weight predicted from final approach speed and assumed flap and slat settings as described in Chapter 3. Modeled noise for each flight was compared with the noise recorded by monitors. Measured noise levels for the different aircraft types at varying velocities were compared to examine potential correlations between the noise levels and deceleration profiles directly from the data.

5.3 Validation of Delayed Deceleration Approach Noise Modeling for Different Aircraft Types

The purpose of this section is to demonstrate the DDA noise modeling validation methodology at Boston Logan and Seattle-Tacoma International Airports. The noise monitors analyzed, in addition to the approach paths to the runways at each airport, are shown in Figure 5-5.

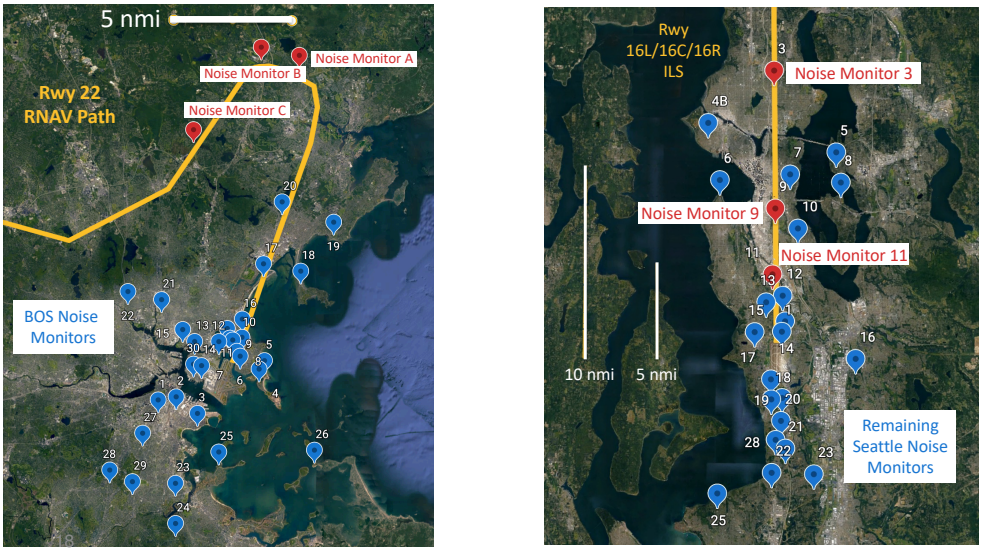

(a) BOS RNAV 22L (b) SEA ILS 16L/16C/16R

Figure 5-5: Noise Monitor Networks at (a) BOS and (b) SEA

The analysis of DDA procedures is implemented using operational flights from ASDE-X, ADS-B and ground monitor data taken from the two study airports. The potential noise benefit from delayed deceleration approaches occurs beyond 8 nautical miles from the runway ends. Noise monitors are not always available in the desired locations for validation. Seattle-Tacoma International Airport has noise monitors that are placed beyond 8 nautical miles from the runway ends as shown in Figure 5-5.

At Boston Logan International Airport, shown in Figure 5-5 (a), noise monitor installation locations (shown in blue) are not necessarily far enough from runway ends to address the region of concern for the procedures like the delayed deceleration

approach. Therefore, a separate monitoring campaign that ran between 2015 and 2016 was used to obtain data at Boston. ASDE-X was used to provide aircraft surveillance data, while noise monitor data was collected from three Brüel & Kjær (B&K) sentinel noise monitors placed under the runway 22L RNAV approach path as described in [17]. These monitors are labeled as Noise Monitor A, B, and C in Figure 5-5 (a). Aircraft in the dataset included Boeing 737-800s and Embraer E190s. Flights recorded by the monitors were converted into Sound Exposure Level and correlated to noise measurements. Altitude, groundspeed, and lateral track data from the Boston Logan ASDEX, and NOAA Rapid Refresh weather data at the three noise monitor locations, were gathered for each aircraft approaching runway 22L. Aggregate altitude and indicated airspeed profiles for the Boeing 737-800 and Embraer 190 are shown in Figure 5-6 and Figure 5-7, respectively. Aggregating flights as shown in these two figures makes clear the variation in altitude and airspeed for each approach to runway 22L. It is therefore of interest to identify flights that follow conventional deceleration profiles and aircraft that delay deceleration at the same altitude in order to isolate the effect of airspeed on the noise profiles generated by these flights.

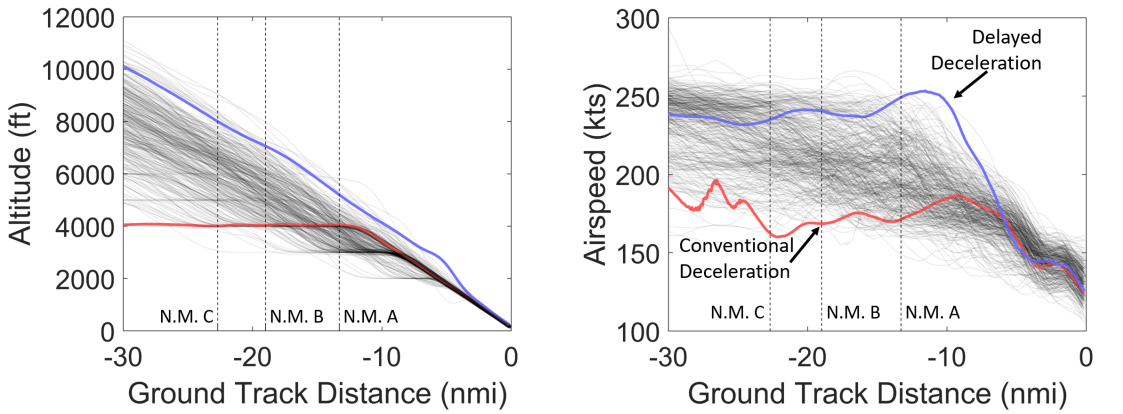

(a) Aggregate Altitude Profiles (b) Aggregate Indicated Airspeed Profiles

Figure 5-6: Operational Boeing 737-800 Arrival Profiles, BOS RWY 22L

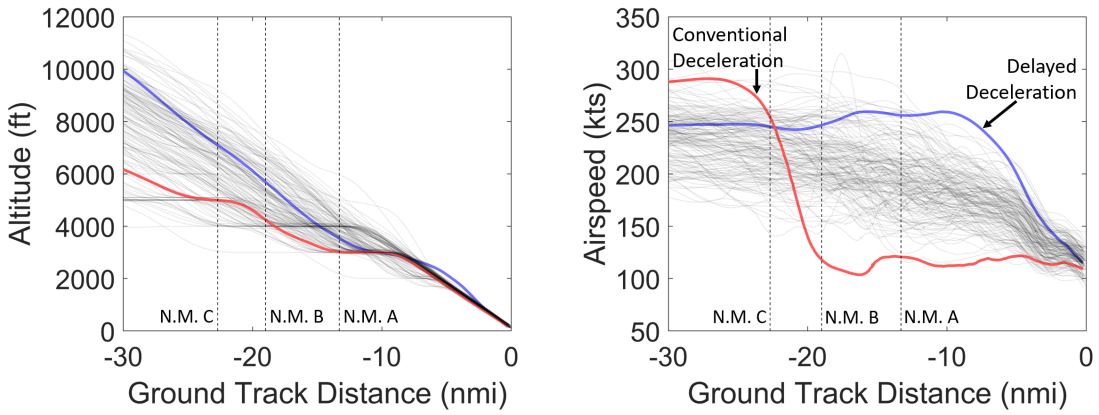

(a) Aggregate Altitude Profiles (b) Aggregate Indicated Airspeed Profiles

Figure 5-7: Operational Embraer E190 Arrival Profiles, BOS RWY 22L

In addition, noise monitor data collected by the Port of Seattle was gathered for this analysis. Seattle Tacoma Airport publishes noise recordings for monitors located up to 14 nmi from the runway ends. Noise recordings for approaches into runways 16L/16C/16R during November 2019 were gathered for this analysis. The associated operational flight profiles were obtained from the OpenSky ADS-B database [19] and included Boeing 737-800s and Airbus A320s. As with the Boeing 737-800s and Embraer 190s at Boston, altitude and indicated airspeed profiles were aggregated for A320 arrivals into runways 16L/16C/16L during the November 2019 period. Note that here, the number of total flights shown is less than the number shown for 737-800s and E190s at Boston because weather data from NOAA Rapid Refresh was less available for the time period of interest. Even with fewer aggregate overflights, there was enough variation in the indicated airspeed profiles given in Figure 5-8 to identify conventional and delayed deceleration approaches.

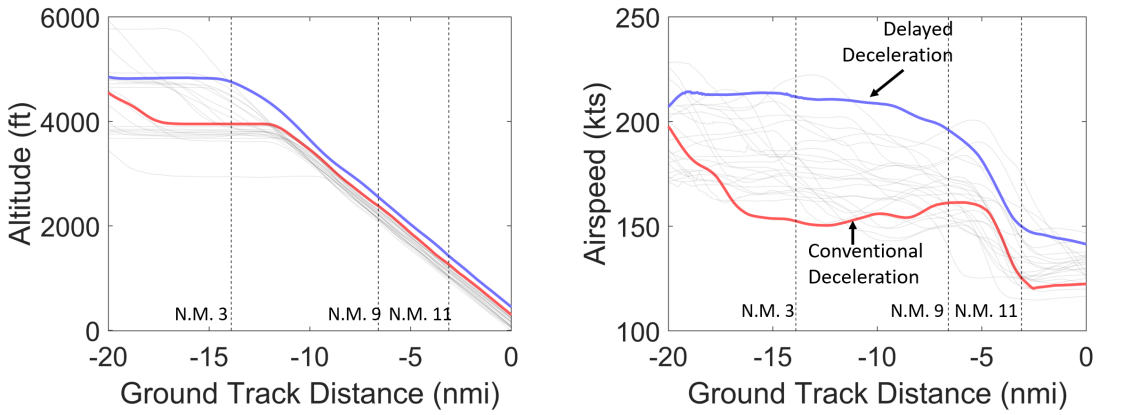

(a) Aggregate Altitude Profiles

(b) Aggregate Indicated Airspeed Profiles

Figure 5-8: Operational Airbus A320 Arrival Profiles, SEA RWY 16L/C/R

5.3.1 Flap Extension Assumptions

Flap settings were not known a priori from surveillance data sources such as ASDEX. Therefore, noise results were modeled for different flap settings for each flight.

The indicated airspeed profiles obtained from the operational ASDE-X data collection campaign were used to define reasonable flap extension locations for the three aircraft. Indicated airspeed was used as the basis for flap extension assumptions for two reasons. First, manufacturers publish flap speeds based on indicated airspeed, and pilots extend flaps using indicated airspeed as a primary reference. Second, using indicated airspeed ensured that winds aloft did not affect assumptions regarding flap extension.

Flap extension was assumed to occur 10 knots below the maximum published flap speed for each aircraft, which was included in BADA [6]. These extension speeds are summarized in Tables 5.1 - 5.3. Note that for the Embraer 190, Flaps 1 and Flaps 3 were omitted because drag data for these configurations was unavailable in BADA.

Table 5.1: B737-800 Flap Extension Speeds

Flap Setting	Flaps 1	Flaps 5	Flaps 10	Flaps 15	Flaps 25	Flaps 30
Extension Speed [KIAS]	230	210	200	190	180	165

Table 5.2: E190 Flap Extension Speeds

Flap Setting	Flaps 2	Flaps 4	Flaps Full
Extension Speed [KIAS]	205	170	155

Table 5.3: A320 Flap Extension Speeds

Flap Setting	CONF 1	CONF 2	CONF 3	FULL
Extension Speed [KIAS]	220	190	175	167

5.3.2 Comparison of Modeled and Measured Noise

An example of the noise validation analysis is shown in Figure 5-11, which depicts a 737-800 approaching Runway 22L at Boston Logan International Airport. The aircraft overflew monitors C, B, and A at 20, 15, and 14 nmi to touchdown, respectively. The velocities in this profile begin at 235 knots over Noise Monitor C, 210 knots over Noise Monitor B, and 190 knots over Noise Monitor A. The groundspeed was converted to true and indicated airspeed in the regions where noise was modeled. In addition, the wind, temperature, and pressure near the runway were used to obtain the final approach airspeed $V_{approach}$ for weight estimation as defined in Equation 3.1.

As mentioned in section 5.3.1, configuration deployment schedules were assumed for the thrust and weight predictions. Thrust and the resulting noise were modeled for each configuration setting. This is shown in Figure 5-9 (a), which shows the altitude, indicated airspeed, and modeled thrust profiles for this flight over the various configuration settings. The indicated airspeed profile also shows in gray the locations where each configuration change would have been made if deployment were to have occurred at 10 knots below the maximum flap speed for each setting. Landing gear was assumed to be retracted over the three noise monitors. Finally, the modeled thrust profiles for each of the flap setting assumptions are shown for reference.

Figure 5-9 (b) shows modeled noise results for each flap setting assumption in terms of Sound Exposure Level (SEL) in dB plotted with the measured noise at each

monitor location. Each dot represents the modeled noise for each configuration from clean to Flaps 25, and the actual monitor readings are denoted by the black asterisk.

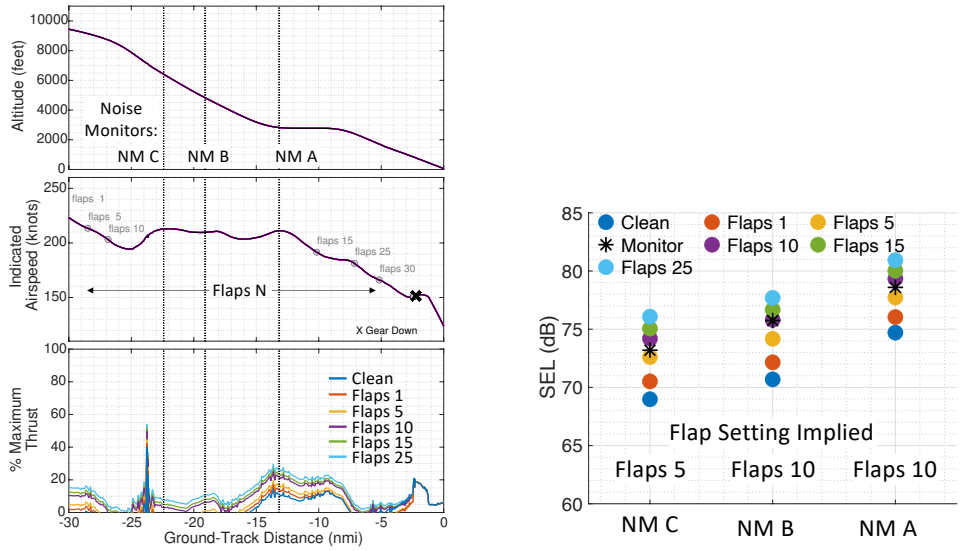

(a) Flight profiles

(b) Modeled and measured noise

Figure 5-9: Boeing 737-800 early deceleration flight profile and noise modeling results compared to measured ASDE-X data

Figure 5-9 shows that there is a variation in the modeled noise of up to 7 dB SEL for a given location depending on the configuration setting assumed, suggesting that configuration deployment can account for some of the variation seen typically seen in noise monitor data. In addition, the modeled results appear to be consistent with the measured data when flap and slat changes are considered, and flap settings implied for a given location appear to be reasonable based on the expected setting for the velocity in that region. More specifically, the noise measurements and model results imply that the aircraft was configured with Flaps 5 or 10 over noise monitor C, which is expected given the early deceleration. Likewise the results imply that the aircraft was at Flaps 10 over noise monitors B and A.

This trend is observed for various velocity profiles. An example of this analysis for a Boeing 737-800 that flew a delayed deceleration profile is shown in Figure 5-10 and an additional conventional, or intermediate, deceleration profile is shown in Figure 5-11.

The velocity profile in Figure 5-10 (a) shows the aircraft maintained a velocity of 215 knots over noise monitors C, B, and A before continuing its deceleration to the final approach speed during the 3,000 ft level segment. The noise results in Figure 5-10 (b) imply that a clean flap setting was maintained over all three monitors when compared to the measured noise results, which is consistent with the constant 215-knot velocity held over each monitor.

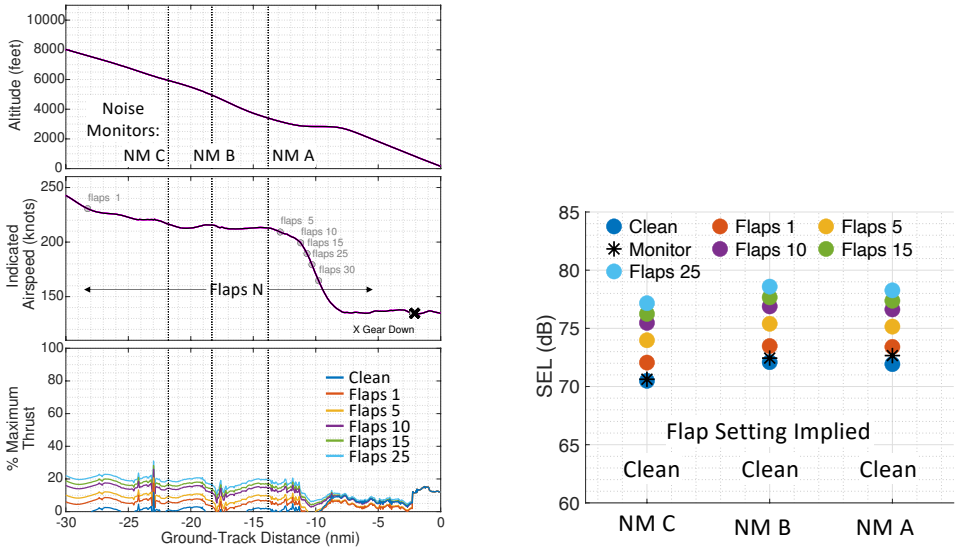

(a) Flight profiles

(b) Modeled and measured noise

Figure 5-10: Boeing 737-800 delayed deceleration flight profile and noise modeling results compared to measured ASDE-X data

The velocity profile in Figure 5-11 (a) shows the aircraft overflew noise monitor C at 230 knots before decelerating to 210 knots and 190 knots over monitors B and A, respectively. The noise results in Figure 5-11 (b) imply that the aircraft overflew noise monitor C in a clean configuration, and that the aircraft overflew monitors B and A with Flaps 5 deployed. These results are consistent with the velocities over each monitor.

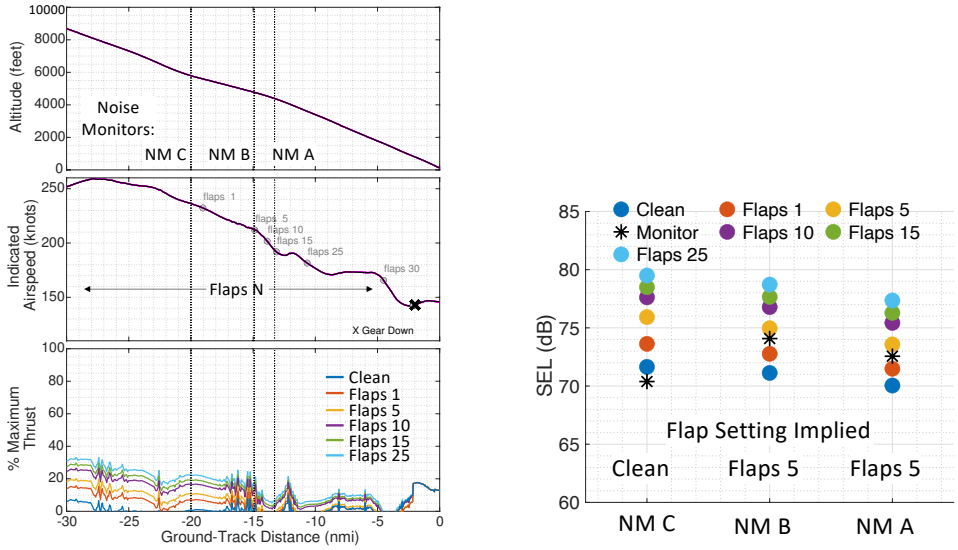

(a) Flight profiles

(b) Modeled and measured noise

Figure 5-11: Boeing 737-800 intermediate deceleration flight profile and noise modeling results compared to measured ASDE-X data

Measured and modeled noise were compared for the Embraer E190 using data at Boston Logan International Airport. Figure 5-12 (a) shows altitude and velocity ASDE-X data and modeled thrust of example conventional and delayed deceleration profiles that flew into runway 22L. Representative configuration deployment locations based on the flap deployment assumptions from Table 5.2 are shown in grey, along with the modeled thrust for those assumptions. Figure 5-12 (b) and (c) show the associated modeled and measured noise over each monitor. For the conventional deceleration case, the noise results for Flaps 2 were consistent with the monitor C and B readings, while the noise results for Flaps 4 were consistent with the monitor A reading. These in turn were is consistent with the velocity profile. For the delayed deceleration case, the velocity was about 230 knots as the aircraft overflew each monitor. In this case, the noise results for the clean configuration were consistent with the monitor readings, which is also consistent with the velocity profile.

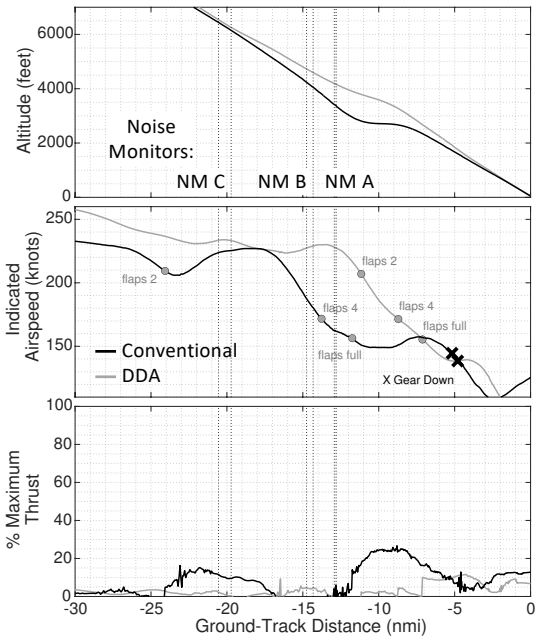

(a) Altitude and velocity data and modeled thrust

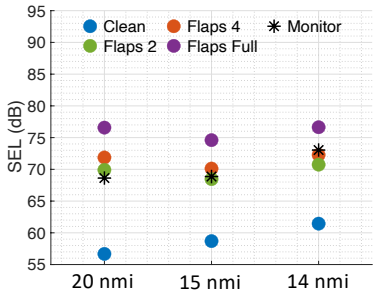

(b) Conventional modeled and measured noise

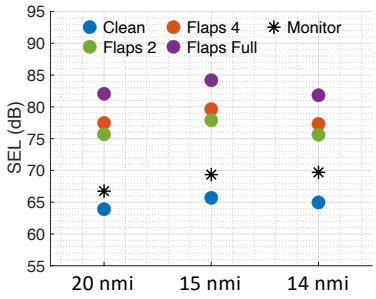

(c) DDA modeled and measured noise

Figure 5-12: Embraer E190 flight profile and noise modeling results compared to measured ASDE-X data

Measured and modeled noise were compared for Airbus A320. Example A320 altitude and velocity data for conventional and delayed deceleration approaches to Runway 16 at SEA were used and are shown in Figure 5-13 (a), along with representative configuration deployment assumptions from Table 5.3 and modeled thrust. The associated modeled and measured noise over monitors 3, 9, and 11 are shown in Figure 5-13 (b) and (c). For the conventional deceleration case, the noise results for CONF 2, CONF 3, and FULL were consistent with the monitor 3, 9, and 11 readings respectively which were consistent with the velocity profile. For the delayed deceleration case, the velocity was about 215 knots as the aircraft overflew Noise Monitor 3 and then decelerated to a similar profile to the conventional case over monitors 9 and 11. In this case, the noise results for CONF 1 were consistent with the Noise Monitor 3 reading.

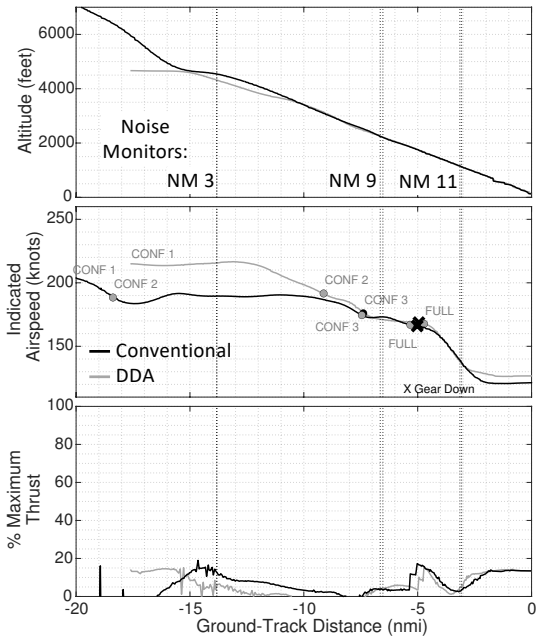

(a) Altitude and velocity data and modeled thrust

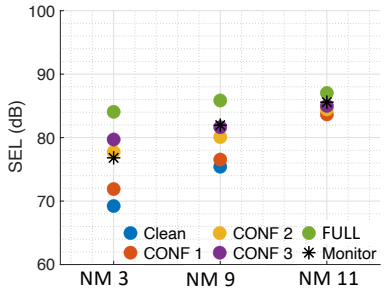

(b) Conventional modeled and measured noise

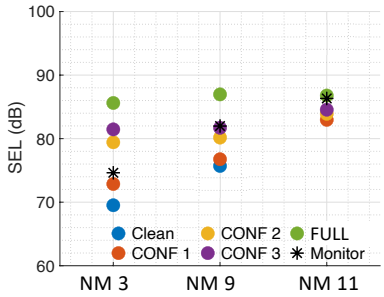

(c) DDA modeled and measured noise

Figure 5-13: Airbus A320 flight profile and noise modeling results compared to measured ADS-B data

Results for these analyses suggest that modeled noise from ASDE-X and ADS-B observations corrected for atmospheric conditions were consistent with noise monitor readings under reasonable flap setting assumptions for most cases. In addition, the modeled results suggest that there is noise reduction potential for delayed deceleration approach procedures compared to approaches that decelerate and configure early, the study of which is the objective for the next section.

5.4 Delayed Deceleration Approach Noise Impacts on Measured Data

The purpose of this section is to use noise monitor data to demonstrate that aircraft flying at the same altitude may generate different noise signatures by flying at different velocities. Data-observed relations between speed, configuration, and noise can be applied to the design of procedures like delayed deceleration approaches.

Surveillance and noise monitor data from the two study airports were used in this examination. There may be significant variation in noise monitor readings due to flap, thrust, and weather effects. Therefore, flights that overflew noise monitors at the same altitude but with enough variation in velocity profiles to imply different flap settings were isolated. At Boston Logan International Airport, flights over Noise Monitor A had the greatest variation in speed profiles, while at Seattle Tacoma International Airport, flights overflying Noise Monitor 3 had the greatest variation in speed profiles. The flap velocities from tables 5.1-5.3 were used to infer potential flap settings for different velocities.

First, various Boeing 737-800 approaches into Boston and Seattle are shown. The comparison was performed between flights with velocities greater than 220 knots and flights below 220 knots. Aircraft flying faster than 220 knots were likely cleanly configured, while aircraft flying below 220 knots were likely to have deployed flaps. Boeing 737-800s flying below the 220-knot DDA threshold before the monitor were expected to overfly with Flaps 5 or greater deployed. The collection of Boeing 737-800 flight profiles with altitudes within 100 feet of each other when the aircraft overflew noise monitors is shown in Figure 5-14. Flights with velocity greater than 220 knots prior to flying over Boston Noise Monitor A and Seattle Noise Monitor 3 were designated as delayed deceleration approaches and were colored grey. Flights with velocities less than 220 knots prior to flying over these noise monitors were colored black.

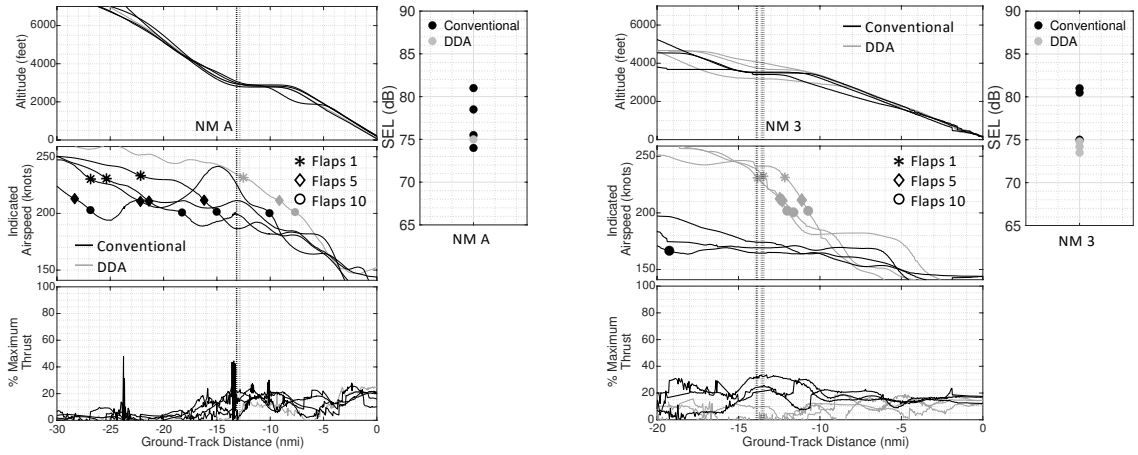

(a) BOS, 3000 ft

(b) SEA, 4000 ft

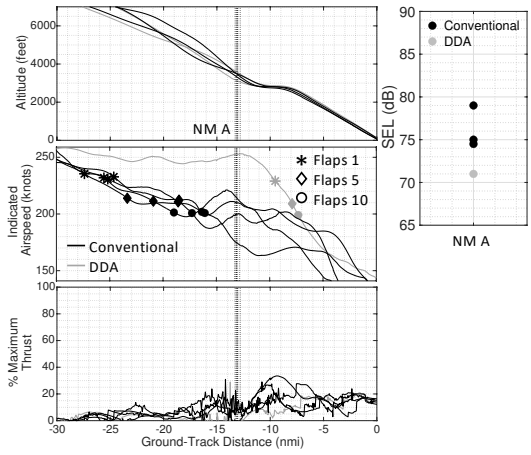

(c) BOS, 3500 ft

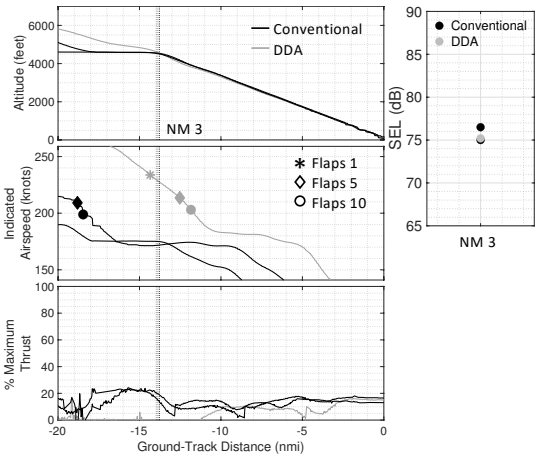

(d) SEA, 5000 ft

Figure 5-14: Boeing 737-800 surveillance data and measured noise over monitors at BOS and SEA for different velocity profiles

Although the overflight altitudes were similar in these examples, variations in the atmospheric conditions were expected to result in variations to the recorded noise for the same operational setting. However, the data presented indicates higher average noise when the aircraft flew below the 220-knot DDA threshold compared to the cases where the aircraft overflew the monitors above the 220 knot threshold. The average difference between the loudest early deceleration approaches and quietest delayed deceleration approaches was 6.5 dB. The quietest (71.0 dB) overflight, which occurred at Boston over noise monitor A (Figure 5-14 c), was a delayed deceleration approach, while the loudest (81.0 dB) overflight, which also occurred at Boston noise

monitor A (Figure 5-14 a), was an early deceleration approach.

Next, Airbus A320 approaches into Seattle are shown. The collection of A320 flight profiles with altitudes within 100 feet of each other when the aircraft overflew noise monitor 3 is shown in Figure 5-15. For the Airbus A320 profiles shown in Figure 5-15, 200 knots was identified as the DDA threshold. Aircraft that flew below the 200-knot DDA threshold prior to the noise monitor were expected to have been configured with CONF 1 or greater. Flights with velocities greater than 200 knots when they overflew Seattle noise monitor 3 were designated as delayed deceleration approaches and were colored grey. Flights with velocities less than 200 knots prior to flying over the noise monitors were colored black.

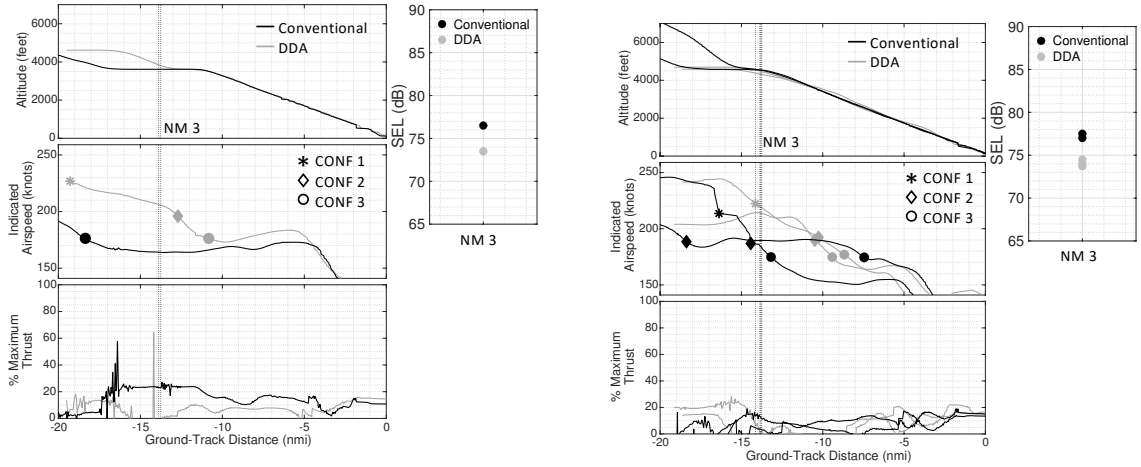

(a) SEA, 4000 ft

(b) SEA, 5000 ft

Figure 5-15: A320-200 ADS-B data and measured noise over monitors at SEA for different velocity profiles

Like with the Boeing 737-800, the data presented indicates higher average noise when the aircraft flew below the 200-knot DDA threshold compared to the cases where the aircraft overflew the monitors above the 200-knot threshold. The average difference between the loudest early deceleration approaches and quietest delayed deceleration approaches was 3.0 dB. Although the magnitude of this difference was 4.0 dB less than the average difference presented for the Boeing 737-800, note that the profiles shown in Figure 5-15 predict that the DDAs overflew noise monitor 3 with flaps set to CONF 1, while all DDA overflights for the Boeing 737-800 occurred

when the aircraft was flying in a clean configuration. Hence, a truly impactful DDA procedure would set a speed restriction such that aircraft approach the airport with a clean configuration over the noise abatement areas. The quietest (73.5 dB) overflight was a delayed deceleration approach, while the loudest (76.5 dB) overflight was an early deceleration approach.

Finally, Embraer E190 approaches into Boston are shown. The collection of E190 flight profiles with altitudes within 100 feet of each other when the aircraft overflew Boston noise monitor A is shown in Figure 5-16. For the profiles shown in Figure 5-16, 205 knots was identified as the DDA threshold. Aircraft flying below the 205-knot DDA threshold prior to the monitor were expected to be configured with Flaps 2 or greater. Flights with velocity greater than 205 knots when they overflew Seattle noise monitor 3 were designated as delayed deceleration approaches and were colored grey. Flights with velocities less than 205 knots prior to flying over the noise monitor were colored black.

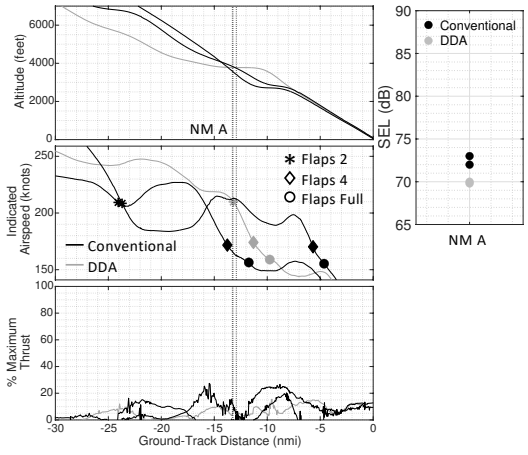

Figure 5-16: Embraer E190 ASDE-X data and measured noise over monitors at BOS for different velocity profiles

The Embraer E190 overflights generated higher average noise when the aircraft flew below the 205-knot DDA threshold compared to the cases where the aircraft overflew the monitors above the 205 knot threshold. The average difference between the loudest early deceleration approaches and quietest delayed deceleration approaches was 3.0 dB. Note again that for all flyovers, the aircraft was assumed to be configured

with Flaps 2. Hence, it is of interest to design delayed deceleration procedures such that aircraft overfly the noise abatement area with a completely clean configuration. Had the DDA shown in Figure 5-16 been predicted to have flown with a clean configuration, the magnitude of this average difference would likely be greater. Like with the 737-800 and A320, the quietest (70.0 dB) overflight was a delayed deceleration approach, while the loudest (73.0 dB) overflight was an early deceleration approach.

On average across the different aircraft types, cases for which overflights occurred above the DDA thresholds resulted in quieter noise recordings than those of aircraft that were below the DDA threshold prior to the monitors. These results indicate potential noise benefits for delayed deceleration approaches compared to procedures where aircraft decelerate and deploy flaps earlier due to the delay in the onset of flap noise.

Chapter 6

Conclusion and Future Work

This thesis presented a framework to model aircraft noise using open-source surveillance data, performed a data-based exploration of the factors that correlate with departure and arrival noise, and performed a model-based validation of the factors correlating with noise for arrivals.

The aircraft noise modeling framework demonstrated that readily-available surveillance and noise monitoring data can be used to model aircraft performance and community noise exposure. This measurement comparison can be developed into a large dataset. With a large dataset, the analytical methods presented can be used to identify potential noise sources not yet identified by the models. Furthermore, noise models can be developed using data mining techniques.

The data-driven exploration of factors correlating with noise demonstrated that variation in departure noise can be attributed to operator-specific climb procedures, aircraft weight, and environmental factors. Altitude was shown to have the strongest effect on community noise exposure. Airline-specific procedures with higher thrust and higher initial climb gradients were observed to have lower noise exposure. This finding may help inform the development of new noise abatement departure procedures. For arrivals, aircraft flying at higher true airspeeds far from the airport were found to generate less community noise in some cases. Future validation studies may examine the impact of specific airline standard operating procedures on aircraft noise. Data from flight data recorders can also be used to obtain precise configuration and

weight data. Finally, environmental factors including ambient wind and relative humidity were shown to have impacts on climb performance (headwind), advection of noise (crosswind), and attenuation of noise (relative humidity).

The model-based validation of delayed deceleration approach procedures flown by Boeing 737-800, Airbus A320, and Embraer E190 demonstrated that modeled results were consistent with recorded monitor data when the weight, weather, and configuration settings were modeled. The results demonstrated significant variation in the noise depending on the configuration setting assumed, and that lower noise levels were achieved when the aircraft was maintained in a clean configuration for a longer duration of the procedure. In the future, a model-based validation of the departure procedure identified in the data-driven exploration can be conducted. The modeled noise from aircraft with steep climb gradients would be expected to be lower than the noise from aircraft with shallower climb gradients.

Notably, the analysis in this thesis was conducted using only Boston ASDE-X and Seattle ADS-B data. While flight data recorder data would help verify assumptions about flap setting, weight, and thrust, it is not necessary for noise prediction. When combined with atmospheric corrections, easily obtainable ASDE-X or ADS-B data can be used for future noise validation efforts.

Appendix A

Boeing 737NG Departure Noise Trends at Seattle North Monitors

North Close Monitor

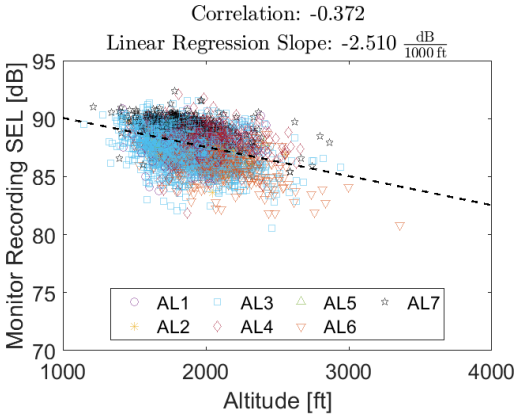

(a) Altitude impact, north close monitor

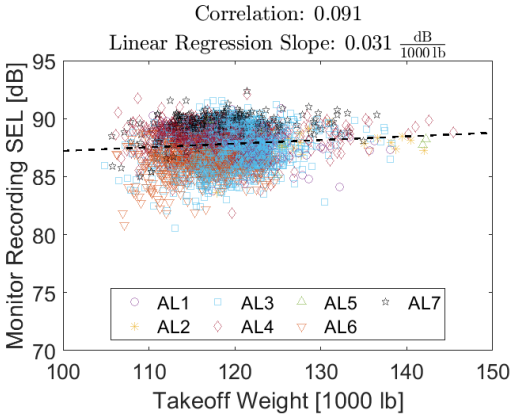

(b) Weight impact, north close monitor

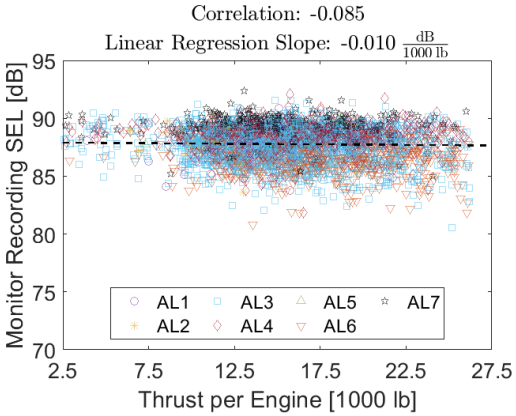

(c) Thrust impact, north close monitor

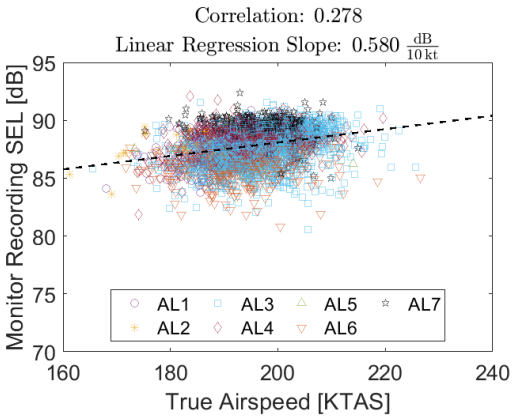

(d) True airspeed impact, north close monitor

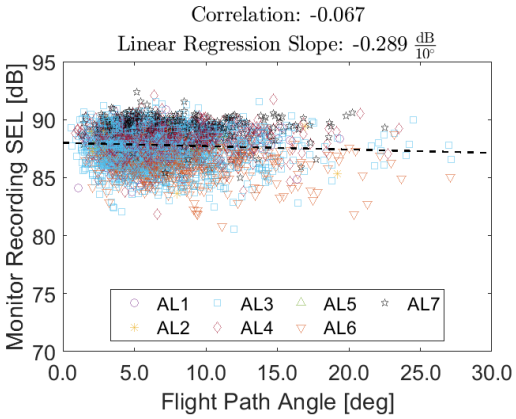

(e) Flight path angle impact, north close monitor

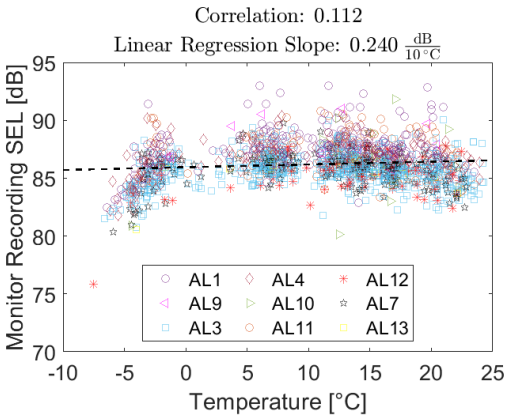

(f) Temperature impact, north close monitor

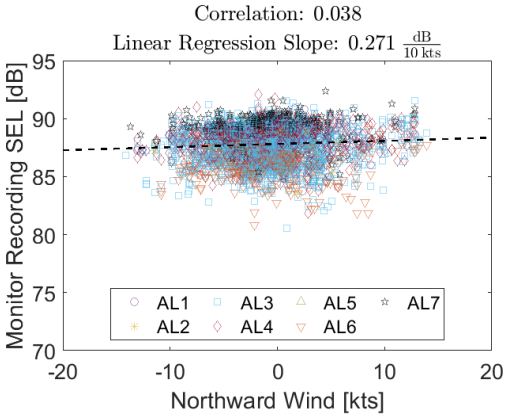

(g) Northward wind (tailwind) impact, north close monitor. Northward wind positive to the north

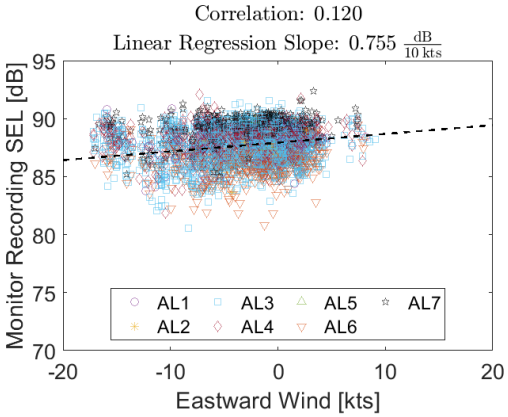

(h) Eastward wind (crosswind) impact, north close monitor. Eastward wind positive to the east

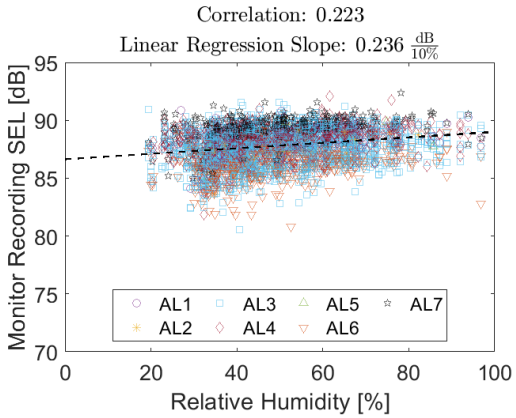

(i) Relative humidity wind impact, north close monitor

Figure A-1: Trends for the Boeing 737NG at the north close monitor

North Mid Monitor

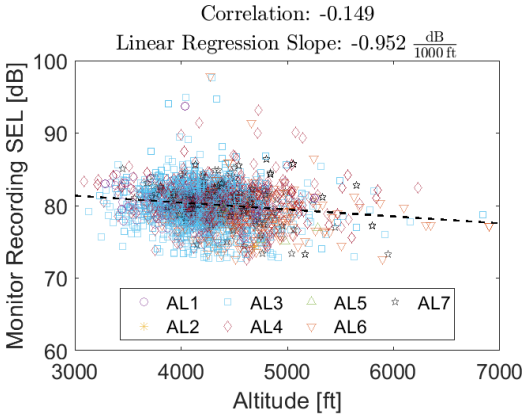

(a) Altitude impact, north mid monitor

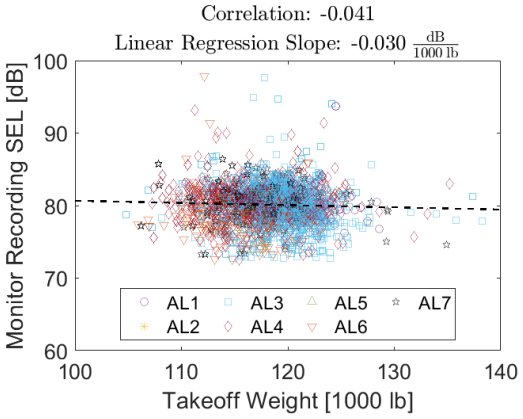

(b) Weight impact, north mid monitor

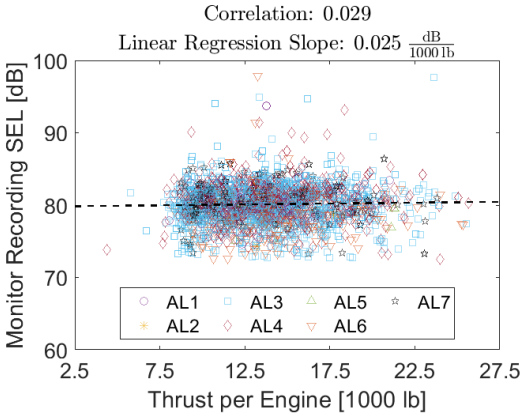

(c) Thrust impact, north mid monitor

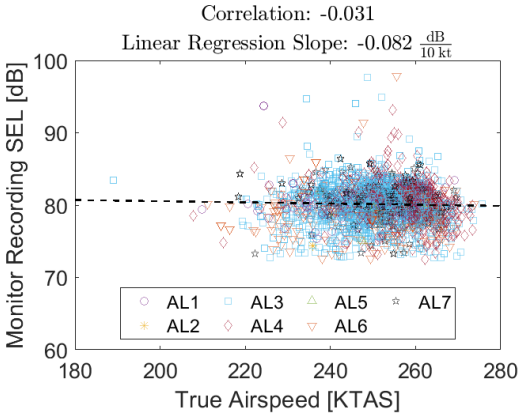

(d) True airspeed impact, north mid monitor

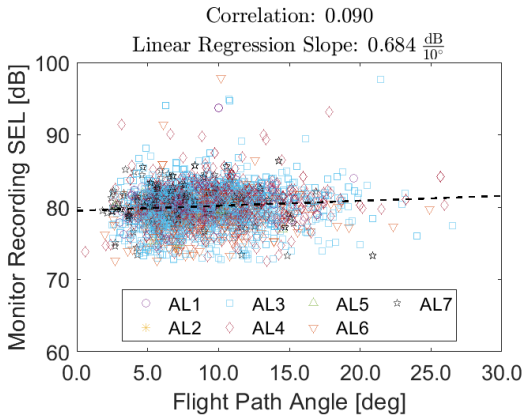

(e) Flight path angle impact, north mid monitor

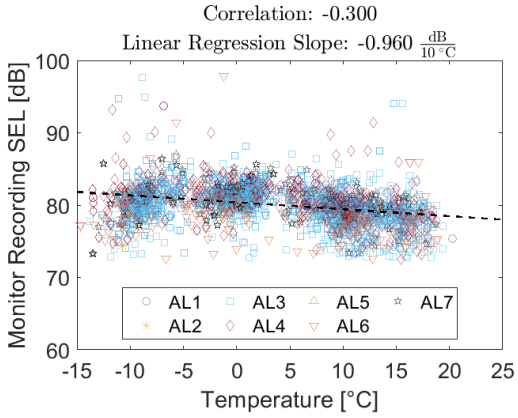

(f) Temperature impact, north mid monitor

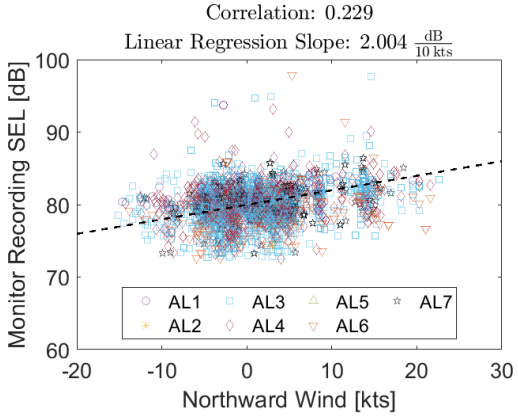

(g) Northward wind (tailwind) impact, north mid monitor. Northward wind positive to the north

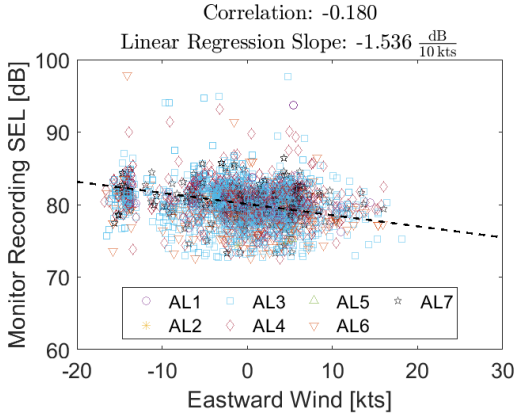

(h) Eastward wind (crosswind) impact, north mid monitor. Eastward wind positive to the east

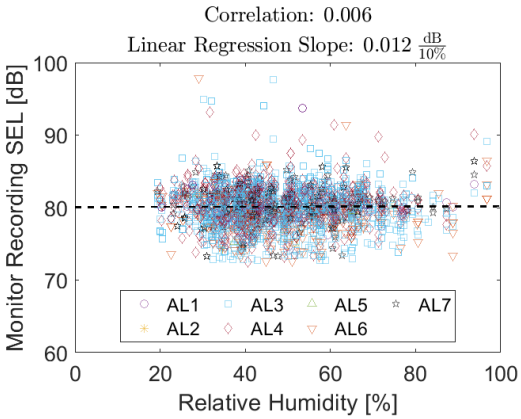

(i) Relative humidity wind impact, north mid monitor

Figure A-2: Trends for the Boeing 737NG at the north mid monitor

North Far Monitor

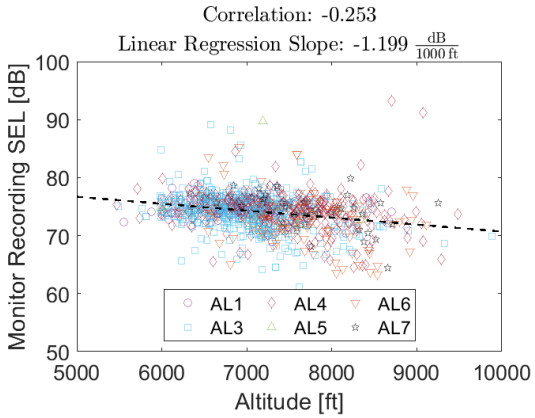

(a) Altitude impact, north far monitor

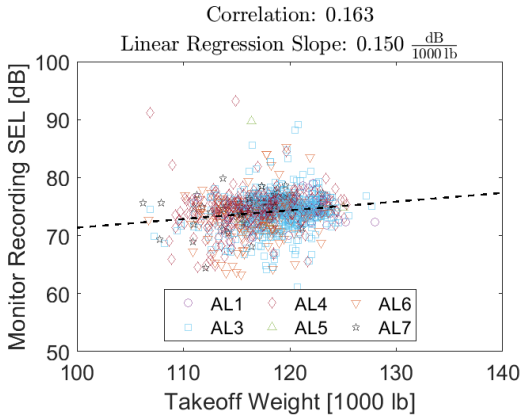

(b) Weight impact, north far monitor

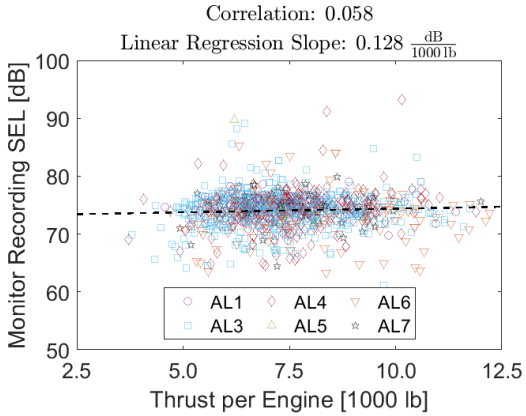

(c) Thrust impact, north far monitor

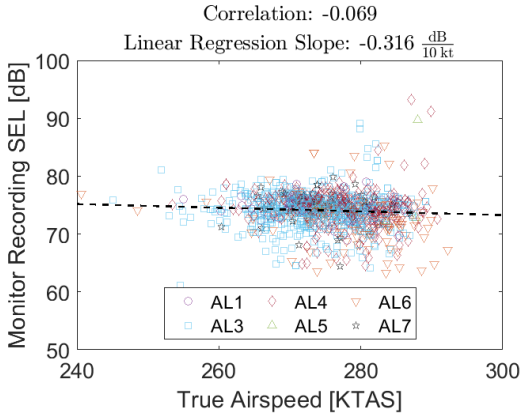

(d) True airspeed impact, north far monitor

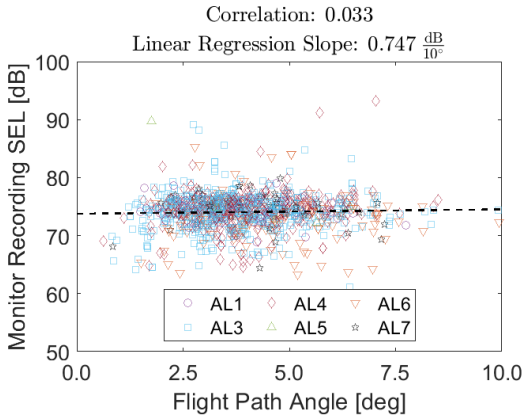

(e) Flight path angle impact, north far monitor

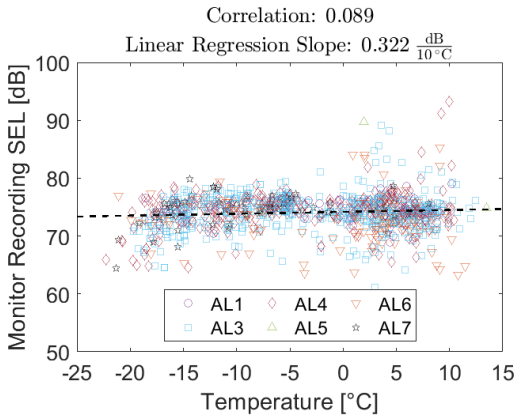

(f) Temperature impact, north far monitor

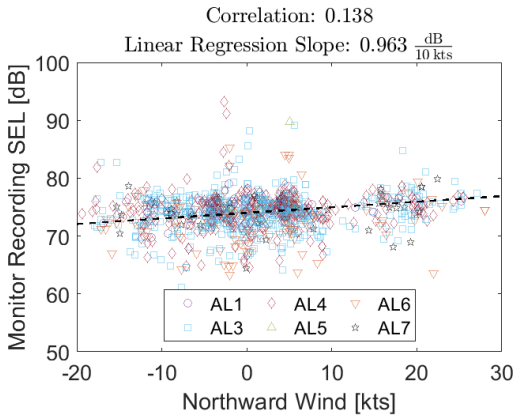

(g) Northward wind (tailwind) impact, north far monitor. Northward wind positive to the north

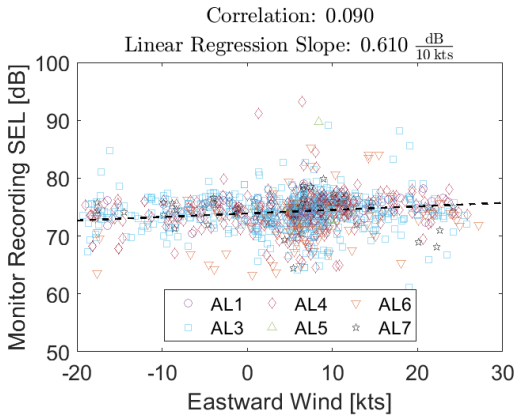

(h) Eastward wind (crosswind) impact, north far monitor. Eastward wind positive to the east

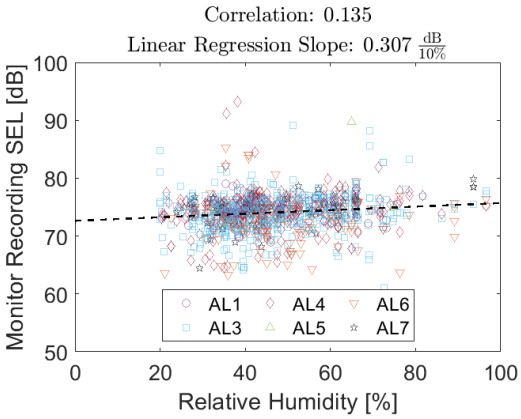

(i) Relative humidity wind impact, north far monitor

Figure A-3: Trends for the Boeing 737NG at the north far monitor

Appendix B

Airbus A320 Departure Noise Trends at Seattle North Monitors

North Close Monitor

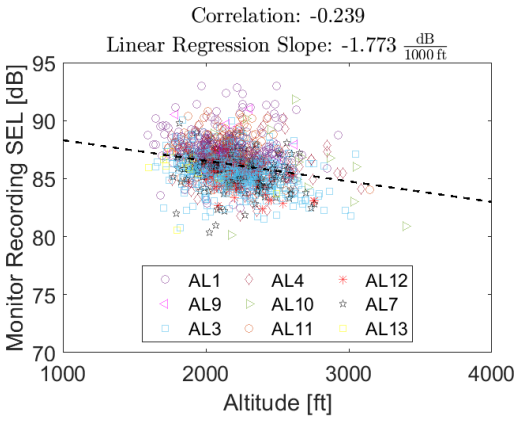

(a) Altitude impact, north close monitor

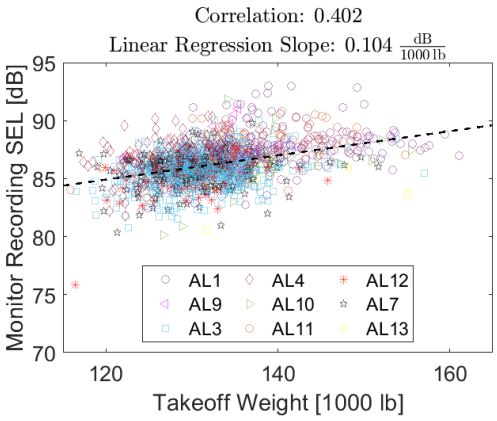

(b) Weight impact, north close monitor

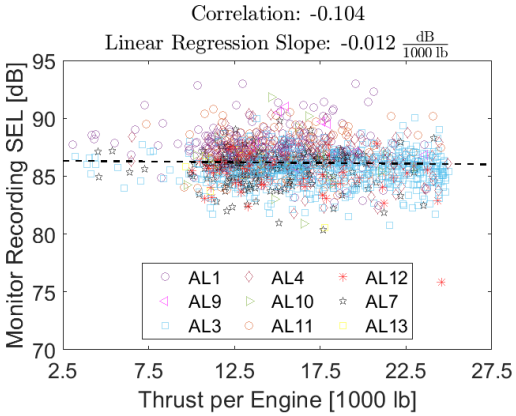

(c) Thrust impact, north close monitor

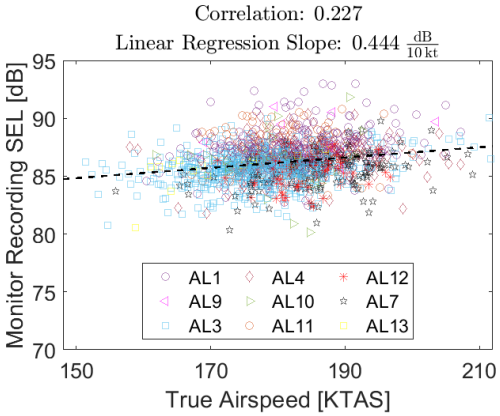

(d) True airspeed impact, north close monitor

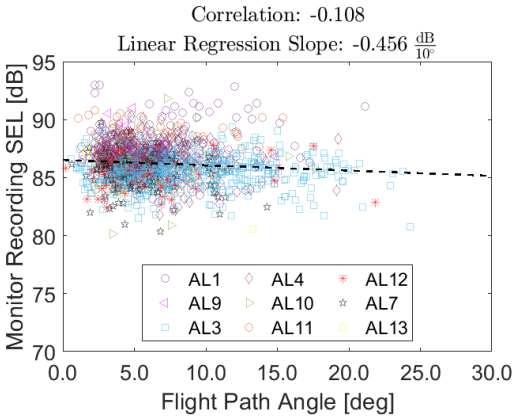

(e) Flight path angle impact, north close monitor

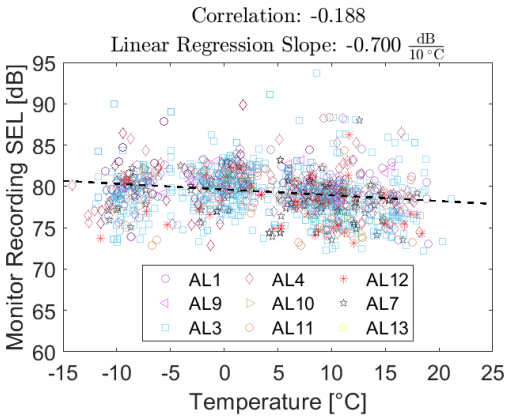

(f) Temperature impact, north close monitor

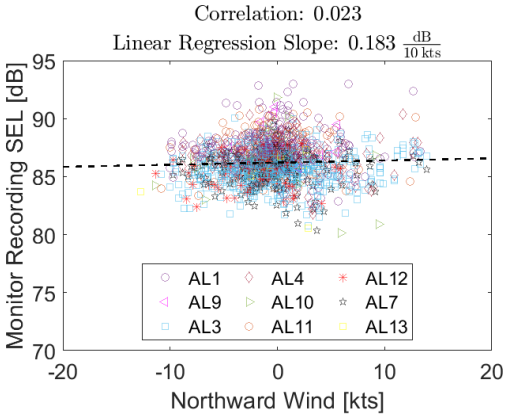

(g) Northward wind (tailwind) impact, north close monitor. Northward wind positive to the north

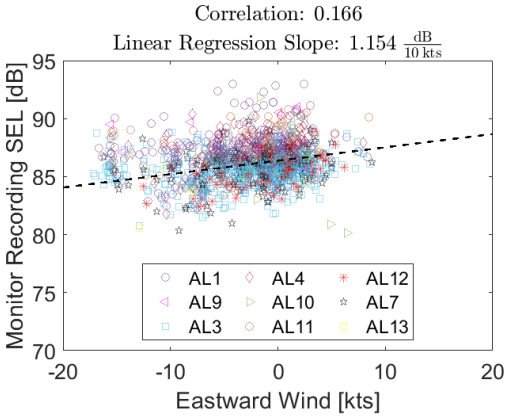

(h) Eastward wind (crosswind) impact, north close monitor. Eastward wind positive to the east

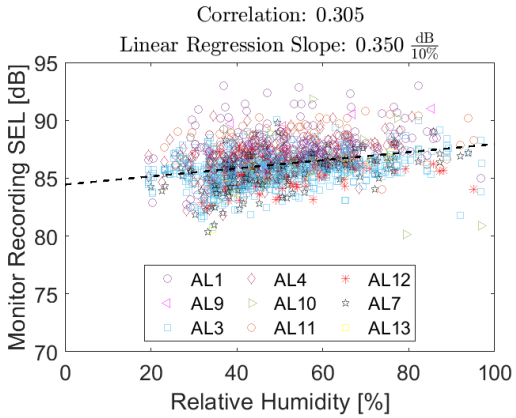

(i) Relative humidity wind impact, north close monitor

Figure B-1: Trends for the Airbus A320 at the north close monitor

North Mid Monitor

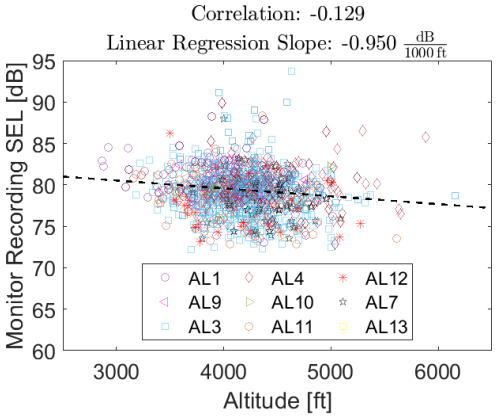

(a) Altitude impact, north mid monitor

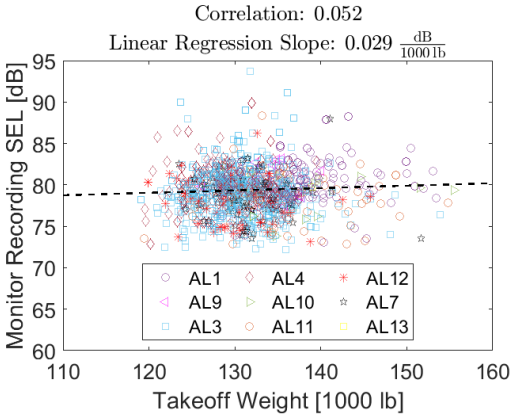

(b) Weight impact, north mid monitor

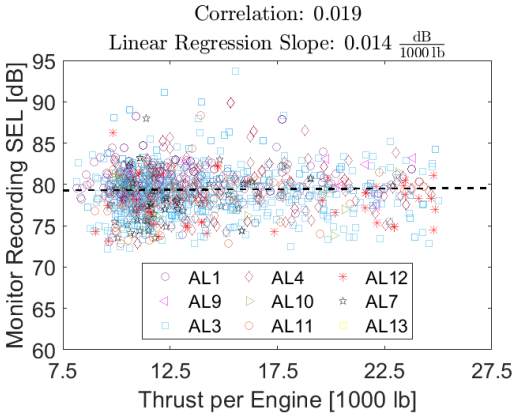

(c) Thrust impact, north mid monitor

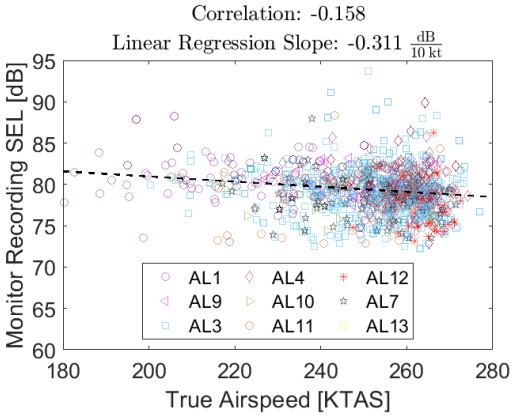

(d) True airspeed impact, north mid monitor

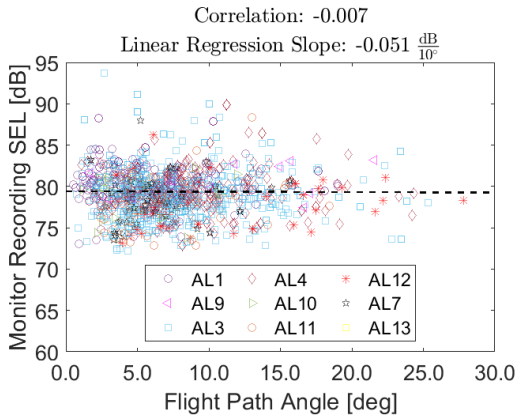

(e) Flight path angle impact, north mid monitor

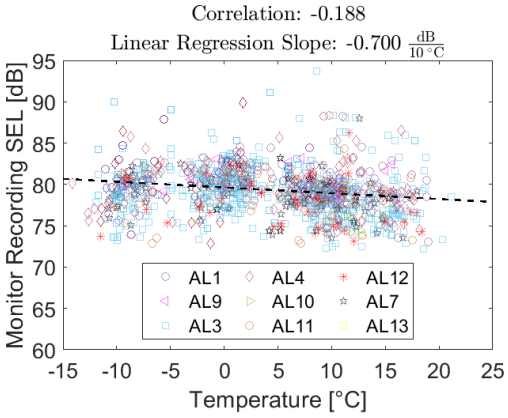

(f) Temperature impact, north mid monitor

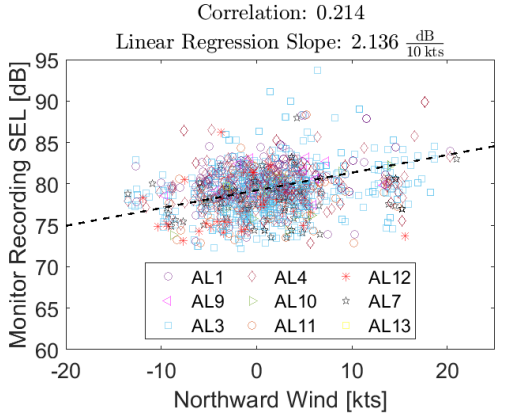

(g) Northward wind (tailwind) impact, north mid monitor. Northward wind positive to the north

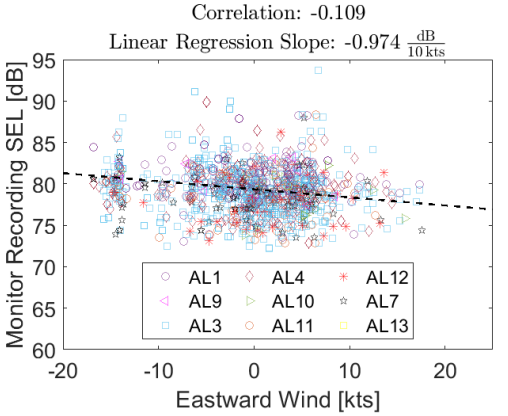

(h) Eastward wind (crosswind) impact, north mid monitor. Eastward wind positive to the east

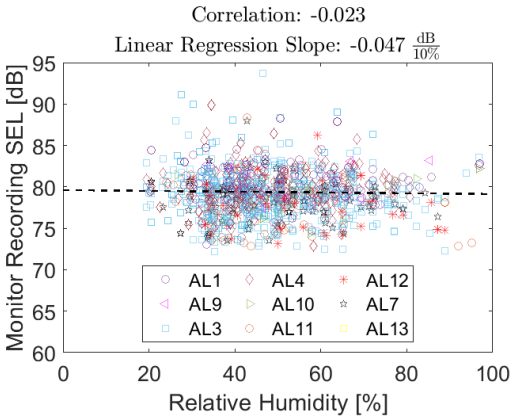

(i) Relative humidity wind impact, north mid monitor

Figure B-2: Trends for the Airbus A320 at the north mid monitor

North Far Monitor

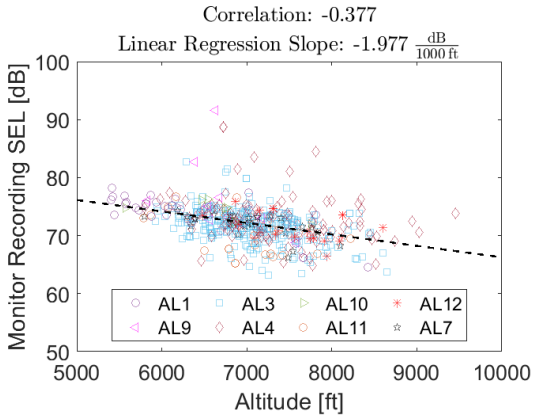

(a) Altitude impact, north far monitor

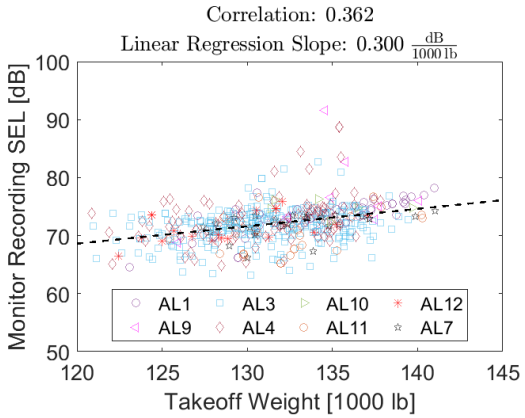

(b) Weight impact, north far monitor

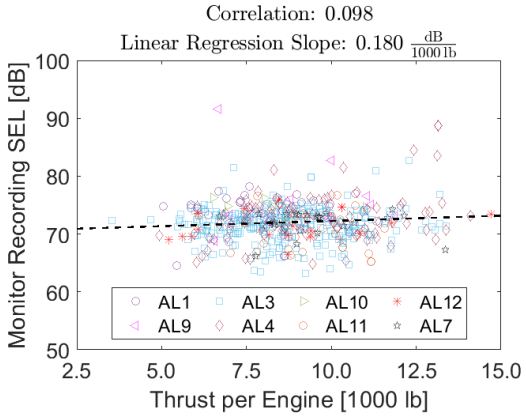

(c) Thrust impact, north far monitor

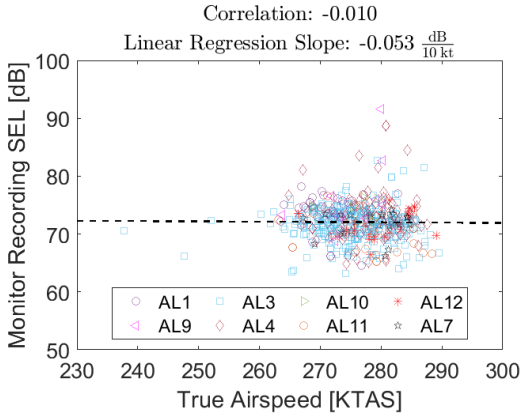

(d) True airspeed impact, north far monitor

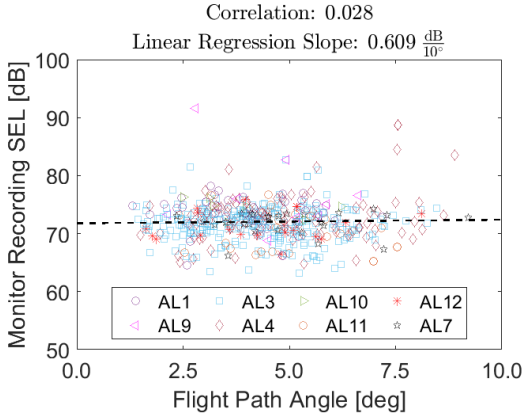

(e) Flight path angle impact, north far monitor

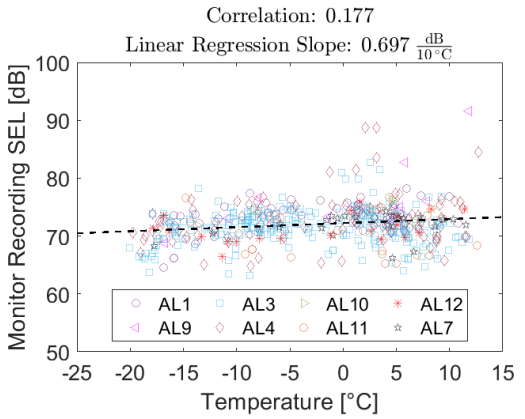

(f) Temperature impact, north far monitor

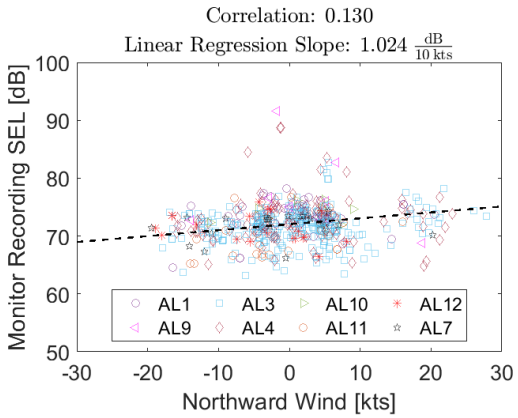

(g) Northward wind (headwind) impact, north far monitor. Northward wind positive to the north

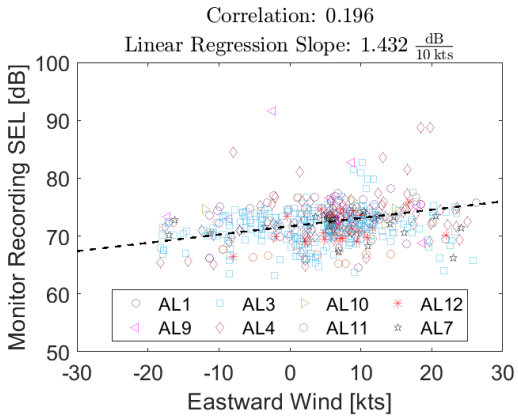

(h) Eastward wind (crosswind) impact, north far monitor. Eastward wind positive to the east

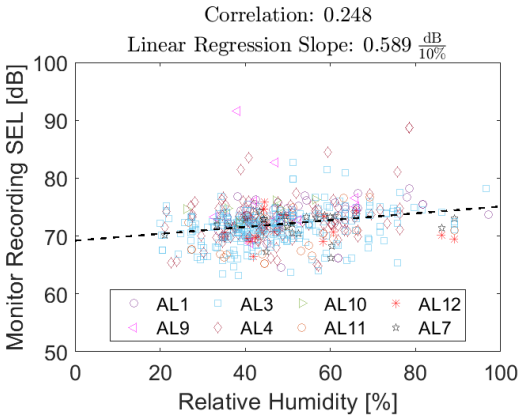

(i) Relative humidity wind impact, north far monitor

Figure B-3: Trends for the Airbus A320 at the north far monitor

Appendix C

Airline Performance Parameter Averages

B737NG Departures

Average departure performance parameters for the B737NG at the south close, mid, and far monitors are summarized for each airline in Tables C.1, C.2, and C.3, respectively.

Table C.1: B737NG Departure Performance Parameter Averages by Airline, South Close Monitor.

Airline	SEL [dB]	Altitude [ft]	Thrust Per Eng. [lb]	Weight [lb]	Airspeed [KTAS]	Flight Path Angle [deg]
AL1	88.1	2026	9781	124584	195	3.3
AL3	88.1	1980	10278	124989	204	3.1
AL4	88.6	2044	9960	123929	203	3.0
AL6	86.3	2160	10982	123248	200	4.0
AL7	89.4	1877	10225	122262	205	3.7

Table C.2: B737NG Departure Performance Parameter Averages by Airline, South Mid Monitor

Airline	SEL [dB]	Altitude [ft]	Thrust Per Eng. [lb]	Weight [lb]	Airspeed [KTAS]	Flight Path Angle [deg]
AL1	84.7	2615	10306	124491	215	3.9
AL3	84.2	2473	10707	124838	228	4.2
AL4	85.0	2546	10426	124039	227	3.9
AL6	82.0	2788	10985	123310	218	5.8
AL7	85.2	2606	10509	122288	221	5.9

Table C.3: B737NG Departure Performance Parameter Averages by Airline, South Far Monitor

Airline	SEL [dB]	Altitude [ft]	Thrust Per Eng. [lb]	Weight [lb]	Airspeed [KTAS]	Flight Path Angle [deg]
AL1	82.6	3709	10698	124335	258	7.8
AL3	81.4	3932	10401	125539	255	5.9
AL4	82.1	4077	10586	123818	258	6.3
AL6	78.3	4511	11533	122709	254	6.0
AL7	80.6	4578	11307	120706	254	5.4

A320 Departures

Average departure performance parameters for the Airbus A320 at the south close, mid, and far monitors are summarized for each airline in Tables C.1, C.2, and C.3, respectively.

Table C.4: A320 Departure Performance Parameter Averages by Airline, South Close Monitor

Airline	**SEL [dB]**	**Altitude [ft]**	**Thrust Per Eng. [lb]**	**Weight [lb]**	**Airspeed [KTAS]**	**Flight Path Angle [deg]**
AL1	88.2	2299.2	10586	141932	187	3.7
AL3	86.1	2199.1	11233	137469	185	3.3
AL4	86.9	2382.6	11299	134457	190	3.5
AL7	86.4	2195.1	11067	136489	194	3.3
AL9	88.0	2049.3	10407	138166	191	2.2
AL10	86.3	2389.3	10266	139852	183	3.0
AL11	88.1	2324.6	11364	139996	188	3.5
AL12	85.5	2335.4	10627	137139	184	3.0

Table C.5: A320 Departure Performance Parameter Averages by Airline, South Mid Monitor

Airline	**SEL [dB]**	**Altitude [ft]**	**Thrust Per Eng. [lb]**	**Weight [lb]**	**Airspeed [KTAS]**	**Flight Path Angle [deg]**
AL1	84.3	2839	9792	141898	200	2.8
AL3	83.5	2713	11041	137751	208	3.0
AL4	84.6	2931	11696	134359	218	3.7
AL7	83.6	2780	11109	136608	215	4.4
AL9	84.5	2990	11245	136723	205	3.5
AL10	83.0	2854	10415	140005	200	2.8
AL11	84.4	2839	10503	139776	207	3.1
AL12	83.0	2802	10737	137265	208	3.2

Table C.6: A320 Departure Performance Parameter Averages by Airline, South Far Monitor

Airline	SEL [dB]	Altitude [ft]	Thrust Per Eng. [lb]	Weight [lb]	Airspeed [KTAS]	Flight Path Angle [deg]
AL3	84.3	2839	9792	141898	200	2.8
AL4	80.5	4676	12836	133496	262	7.9
AL7	79.7	4516	13576	135702	257	6.4
AL11	80.6	4204	14014	136580	263	8.5

B737NG Arrivals

Average arrival performance parameters for the B737NG at the three monitors are summarized for each airline in Tables C.9, C.8, and C.7, respectively.

Table C.7: B737NG Arrival Performance Parameter Averages by Airline, North Far Monitor

Airline	SEL [dB]	Altitude [ft]	Thrust Per Eng. [lb]	Weight [lb]	Airspeed [KTAS]	Flight Path Angle [deg]
AL1	77.3	4263	987	106414	217	-2.5
AL3	76.9	3997	2625	104447	198	-1.3
AL4	76.2	4052	2334	109725	204	-1.1
AL6	77.6	4001	3023	99812	187	-2.5
AL7	74.9	3949	1438	109103	213	-1.4

Table C.8: B737NG Arrival Performance Parameter Averages by Airline, North Mid Monitor

Airline	SEL [dB]	Altitude [ft]	Thrust Per Eng. [lb]	Weight [lb]	TAS [KIAS]	Flight Path Angle [deg]
AL1	81.8	2219	3050	105121	174	-3.1
AL2	79.7	2196	4824	98581	174	-3.1
AL3	80.9	2241	3903	104073	175	-3.1
AL4	80.9	2224	3919	108644	175	-3.0
AL5	81.0	2222	4369	104849	169	-3.1
AL6	80.6	2209	3751	98086	174	-3.0
AL7	80.8	2230	3443	106341	176	-3.1

Table C.9: B737NG Arrival Performance Parameter Averages by Airline, North Close Monitor

Airline	SEL [dB]	Altitude [ft]	Thrust Per Eng. [lb]	Weight [lb]	TAS [KIAS]	Flight Path Angle [deg]
AL1	86.3	1087	5373	104659	150	-3.0
AL2	85.6	1113	4585	98780	145	-3.0
AL3	86.3	1099	4726	104373	150	-3.1
AL4	86.4	1094	5203	108927	150	-3.1
AL5	85.6	1106	5102	106525	149	-2.9
AL6	85.4	1095	4310	97319	142	-3.0
AL7	86.3	1101	5056	106107	149	-3.1

A320 Arrivals

Average arrival performance parameters for the A320 at the three monitors are summarized for each airline in Tables C.12, C.11, and C.10, respectively.

Table C.10: A320 Arrival Performance Parameter Averages by Airline, North Far Monitor

Airline	SEL [dB]	Altitude [ft]	Thrust Per Eng. [lb]	Weight [lb]	TAS [KIAS]	Flight Path Angle [deg]
AL1	76.5	4364	71	114126	208	-1.3
AL3	76.5	4117	973	111219	199	-1.2
AL4	76.0	4101	960	106715	202	-1.3
AL7	75.0	4369	616	114664	217	-2.3
AL11	82.9	4595	2915	111541	212	-2.1

Table C.11: A320 Arrival Performance Parameter Averages by Airline, North Mid Monitor

Airline	SEL [dB]	Altitude [ft]	Thrust Per Eng. [lb]	Weight [lb]	TAS [KIAS]	Flight Path Angle [deg]
AL1	80.8	2224	2904	125625	173	-2.9
AL3	81.3	2202	3317	112709	176	-3.0
AL4	81.5	2197	3016	109577	174	-2.9
AL7	80.4	2212	2788	112439	172	-3.1
AL9	82.3	2286	3585	104204	161	-3.1
AL10	80.1	2228	3436	112678	173	-3.0
AL11	80.2	2200	3248	116019	174	-3.0
AL12	78.9	2201	2510	113555	174	-2.8
AL13	83.4	2302	2684	104551	182	-3.1

Table C.12: A320 Arrival Performance Parameter Averages by Airline, North Close Monitor

Airline	**SEL [dB]**	**Altitude [ft]**	**Thrust Per Eng. [lb]**	**Weight [lb]**	**TAS [KIAS]**	**Flight Path Angle [deg]**
AL1	85.5	1098	5712	124975	147	-3.0
AL3	85.8	1091	4615	112614	141	-3.0
AL4	85.6	1095	4794	109776	137	-3.0
AL7	84.2	1104	4706	111949	140	-3.0
AL9	86.4	1099	5627	103797	139	-2.5
AL10	86.5	1117	4906	113943	140	-3.0
AL11	84.8	1083	4921	115871	144	-3.0
AL12	84.5	1110	5356	113574	137	-2.9
AL13	83.7	1161	5116	106572	135	-2.8

Bibliography

[1] FAA Airport Diagrams. https://www.faa.gov/airports/runway_safety/diagrams/. Accessed: 2022-05-39.

[2] American National Standard Method for the Calculation of the Absorption of Sound by the Atmosphere. Technical Report ANSI S1.26-2014 American Natl. Stand. Inst., Inc., 2014.

[3] Stanley G. Benjamin, Stephen S. Weygandt, John M. Brown, Ming Hu, Curtis R. Alexander, Tatiana G. Smirnova, Joseph B. Olson, Eric P. James, David C. Dowell, Georg A. Grell, Haidao Lin, Steven E. Peckham, Tracy Lorraine Smith, William R. Moninger, Jaymes S. Kenyon, and Geoffrey S. Manikin. A North American Hourly Assimilation and Model Forecast Cycle: The Rapid Refresh. *Monthly Weather Review*, 144(4):1669–1694, 2016.

[4] M. Drela. Transport Aircraft System OPTimization, Technical Description. In *Massachusetts Institute of Technology*, Cambridge, MA, 2010.

[5] Jean-Marie Dumont. Fuel Burn Reduction Potential from Delayed Deceleration Approaches. Master's Thesis, Massachusetts Institute of Technology, 2012. Massachusetts Institute of Technology.

[6] EUROCONTROL. Introducing Performance Based Navigation (PBN) and Advanced RNP (A-RNP) 21. Technical report, 2013.

[7] Federal Aviation Administration. AEDT Standard Input File (ASIF) Reference Guide. Technical report, 2015.

[8] Martin Fink. Airframe Noise Prediction Method. Technical Report FAA-FRD-77-29, Washington, D.C., 1977.

[9] Yueping Guo. Empirical Prediction of Aircraft Landing Gear Noise. Technical Report NASA/CR-2005-213780, Boeing Phantom Works, Long Beach, CA, 2005.

[10] Yueping Guo. An Improved Landing Gear Noise Prediction Scheme. Technical Report NASA/CR-NAS1-NNL04AA11B, The Boeing Company, Huntington Beach, CA, 2006.

[11] Cyril M. Harris. Absorption of sound in air versus humidity and temperature. *The Journal of the Acoustical Society of America*, 40(1), 1966.

[12] M. Heidmann. Interim Prediction Method for Fan and Compressor Source Noise. Technical Report NASA-TM-71763, Lewis Research Center, Cleveland, OH, 1979.

[13] F. Jane. *All the World's Aircraft*. London, 1912.

[14] Jack L. Kerrebrock. Aircraft Engines and Gas Turbines. page 347–364. MIT Press, Cambridge, Massachusetts, 2nd edition, 1992.

[15] Ara Mahseredjian, Jacqueline Thomas, and John Hansman. Advanced Procedure Noise Model Validation using Airport Noise Monitor Networks. In *50th International Congress and Exposition on Noise Control Engineering*, Virtual Event, 2021.

[16] A. Nuic. User Manual for the Base of Aircraft Data (BADA) Revision 3.12. Technical Report 12/11/22-58, Eurocontrol, 2013.

[17] Tom Reynolds, Melanie Sandberg, Jacqueline Thomas, and R John Hansman. Delayed Deceleration Approach Noise Assessment. In *16th AIAA Aviation Technology, Integration, and Operations Conference*, Reston, VA, 2016.

[18] Sandro Salgueiro, Jacqueline L Huynh, and R. John Hansman. Aircraft Takeoff and Landing Weight Estimation from Surveillance Data. In *AIAA Science and Technology Forum*, San Diego, CA, 2022.

[19] M Schäfer, L Strohmeier, I Martinovic, and M Wilhelm. Bringing Up OpenSky: A Large-scale ADS-B Sensor Network for Research. In *Proceedings of the 13th IEEE/ACM International Symposium on Information Processing in Sensor Networks (IPSN)*, Berlin, 2014.

[20] Michael J. T. Smith. *Aircraft Noise*. Cambridge University Press, Cambridge, 1989.

[21] J. R. Stone and F. J. Montegani. An Improved Prediction Method for the Noise Generated in Flight by Circular Jets. Technical Report NASA-TM-81470, Atlanta, Georgia, 1980.

[22] Jacqueline Thomas. *Systems Analysis of Community Noise Impacts of Advanced Flight Procedures for Conventional and Hybrid Electric Aircraft*. PhD dissertation, Massachusetts Institute of Technology, Department of Aeronautics and Astronautics, June 2020.

[23] Jacqueline Thomas and Robert J Hansman. Modeling of Delayed Deceleration Approaches for Community Noise Reduction. *Journal of Air Transportation*, 0(0):1–10, 2021.

[24] Jacqueline Thomas, Alison Yu, Clement Li, Pedro Manuel Maddens Toscano, and R. John Hansman. Advanced Operational Procedure Design Concepts for Noise Abatement. In *Thirteenth USA/Europe Air Traffic Management Research and Development Seminar*, Paper ID 49, Vienna, 2019.

[25] Christopher D. Wickens, John Lee, Yili Liu, and Sallie Gordon-Becker. *An Introduction to Human Factors Engineering*, chapter 4. Pearson Education Limited, 2014.

[26] William E Zorumski. Aircraft Noise Prediction Program (ANOPP) Theoretical Manual. Technical Report NASA-TM-83199, National Aeronautics and Space Administration, Hampton, VA, 1982.